5-1-2008

Elucidation of reaction pathways for catalytically cracked unsaturated lipids

Tracy John Benson

ELUCIDATION OF REACTION PATHWAYS FOR CATALYTICALLY CRACKED UNSATURATED LIPIDS

By

Tracy John Benson

A Dissertation
Submitted to the Faculty of
Mississippi State University
in Partial Fulfillment of the Requirements
for the Degree of Doctor of Philosophy
in Chemical Engineering
in the Dave C. Swalm School of Chemical Engineering

Mississippi State, Mississippi

May 2008

ELUCIDATION OF REACTION PATHWAYS FOR CATALYTICALLY CRACKED UNSATURATED LIPIDS

By

Tracy John Benson

Approved:

_____	_____
Rafael Hernandez Assistant Professor of Chemical Engineering (Director of Dissertation and Advisor)	Mark G. White Professor of Chemical Engineering (Committee Member)
_____	_____
Mark E. Zappi Dean of Engineering University of Louisiana at Lafayette (Committee Member)	W. Todd French Assistant Professor of Chemical Engineering (Committee Member)
_____	_____
Clifford E. George Professor of Chemical Engineering (Committee Member)	W. Glenn Steele Interim Dean of Engineering of Bagley College of Engineering
_____	
Rudy Rogers Professor of Chemical Engineering (Graduate Coordinator)	

Name: Tracy John Benson

Date of Degree: May 2, 2008

Institution: Mississippi State University

Major Field: Chemical Engineering

Major Professor: Dr. Rafael Hernandez

Title of Study: ELUCIDATION OF REACTION PATHWAYS FOR CATALYTICALLY CRACKED UNSATURATED LIPIDS

Pages in Study: 153

Candidate for Degree of Doctor of Philosophy

This study investigated the cracking chemistry as model lipids were reacted over a benchmark catalyst, H-ZSM-5, and two industrially used catalysts, faujasite and silica-alumina. Initial work began with a homogeneous system in which oleic acid, an unsaturated free fatty acid, and triflic acid, a Bronsted superacid, were reacted at low temperatures. Results indicated that protonation began at the double bond with cracking occurring in the direction away from the carboxylic end and producing a multiplicity of branched saturated fatty acids. Heterogeneous cracking on H-ZSM-5 at 400°C indicated that acylglycerides initially crack due to protonation occurring on the outside surface of the catalyst. Secondary cracking formed olefins (C_2 – C_4) which then oligomerize to form aromatic hydrocarbons that were within the range of components for gasoline. Catalysis using faujasite and silica-alumina indicated that acylglycerides require milder cracking conditions than typical crude petroleum, indicating that lower temperatures and lower catalyst to feed ratios will be required to achieve the same reactant conversions as seen in petroleum refineries.

DEDICATION

I would like to dedicate this research to my father, Carl E. Benson, whose never-ending support has been the motivation for this work. My first math lesson came from his demonstration of how sine and cosine are used to determine roof pitches. Also, as a mechanic and steel worker, some of his abilities to work with his hands were passed on to me. For this, I am very grateful.

ACKNOWLEDGEMENTS

I want to express my gratitude to my major professor, Dr. Rafael Hernandez, for providing me the chance to pursue my Doctor's degree in Chemical Engineering and for being so patient with me over the past years. Dr. Hernandez has been a great help and inspiration to me. He is readily available to answer my questions and to give direction to my research. Also, I want to say thank you to my committee members, Dr. Todd French, Dr. Mark White, and Dr. Mark Zappi, and Dr. Clifford George. They have been as helpful as Dr. Hernandez. I would also especially like to thank William E. Holmes for his help and direction with laboratory equipment. Because of Mr. Holmes, I am now proficient at using mass spectrometry as an analytical tool. I would also like to thank Dr. Earl Alley who has been very helpful with teaching me analytical techniques, proper organic analysis protocols, and reaction mechanisms. I am also thankful to the United States Department of Energy for the financial support of my project.

I am also extending my gratitude to the undergraduate students who have worked on this project with me: Tray Achorn, Jarrod Smith, Bethany Thompson, and Allison Forks. I would also like to thank Ms. Sherre Denson, Ms. Ellen Weeks, and Ms. Sandra Shumaker for their help with office needs and assistance.

TABLE OF CONTENTS

LIST OF TABLES

TABLE

LIST OF FIGURES

FIGURE

CHAPTER I

INTRODUCTION

Limited petroleum supplies and global warming concerns caused by the significant increase in fossil fuel utilization have prompted researchers to explore renewable raw materials for producing fuels and chemicals. This can be readily seen with the exponential growths of both the fuel-ethanol and biodiesel industries [1]. Also, as can be seen from Figure 1.1 [2], the consumption of fossil fuels is expected to increase at least through the year 2030. Utilization of renewable fuels will reduce CO_2 concentrations in the biosphere, eliminate U.S. dependence on foreign oil, and provide sustainable energy.

Lipids, such as vegetable oils and animal fats, are being used for producing diesel-like fuels. One example is biodiesel, a mixture of methyl esters usually produced from the reaction of methanol and vegetable oils, catalyzed by a strong base, such as sodium methoxide. Biodiesel is considered a "green fuel" since it does not introduce new carbon into the biosphere unlike petroleum diesel, and it blends well with petroleum diesel and enhances the lubricity of ultra low sulfur diesel. These positive aspects of biodiesel have contributed to a production increase from 500,000 gallons in 1999 to 75 million gallons in 2005 (see Figure 1.2) [1].

Several disadvantages of the biodiesel production process could limit its growth in the near future. While biodiesel is a strong candidate for displacement of large quantities of petroleum, it has several shortcomings that may prevent it from replacing petroleum. First, biodiesel production has been limited to row-crop plant oils that require intense land use and labor. Second, transesterification processes require refined vegetable oils to comply with biodiesel quality standards. The inventory of refined vegetable oils is limited and the prices are higher than non-food quality related lipids. Third is the production of glycerine. When biodiesel is produced from vegetable oils and animal fats, the primary reaction by-product is glycerine [3]. The growth of the biodiesel industry has caused glycerine prices to plummet, eliminating in the near future any potential profits from this by-product stream.

The use of raw materials with a high content of free fatty acids, such as brown grease and tall oil, require either a two-step process of acid-catalyzed esterification followed by base-catalyzed transesterification of triglycerides or a much slower one-step acid-catalyzed esterification. Both processes require higher capital cost compared to the basic transesterification, because of the additional unit operations and the expensive materials of construction needed to resist more corrosive raw materials [3].

From these weaknesses, it is clear that more robust conversion technologies are necessary to meet the market demands of renewable energies. One possible solution is the production of "green fuels" from the catalytic cracking of lipids into gasoline-like and diesel-like fuels. While this new process would use row-crop oils as raw materials, it would also utilize lipids from animal sources and microbial sources such as oleaginous yeasts, oil-rich algae, and municipal waste water sludges. Moreover, undesired

byproducts could be reduced, or eliminated, from the catalytic cracking process. The glycerol backbone of acylglycerides could be converted into propane during the cracking process. Another advantage to this approach would be employment of current petroleum refining practices for renewable fuel production. Also, production of biofuels *via* catalytic cracking of lipids similar to petroleum refining for producing gasoline and diesel may offer a commercially-attractive alternative to biodiesel technology.

This research demonstrates the ability to use lipids as a feedstock for the production of green gasoline and green diesel. Furthermore, a complete breakdown of the cracking products is shown along with possible reaction pathways for the production of these products. As this information has not been reported before in the available literature, it is the intent of this research to provide clear reaction schemes to facilitate commercialization of green fuels.

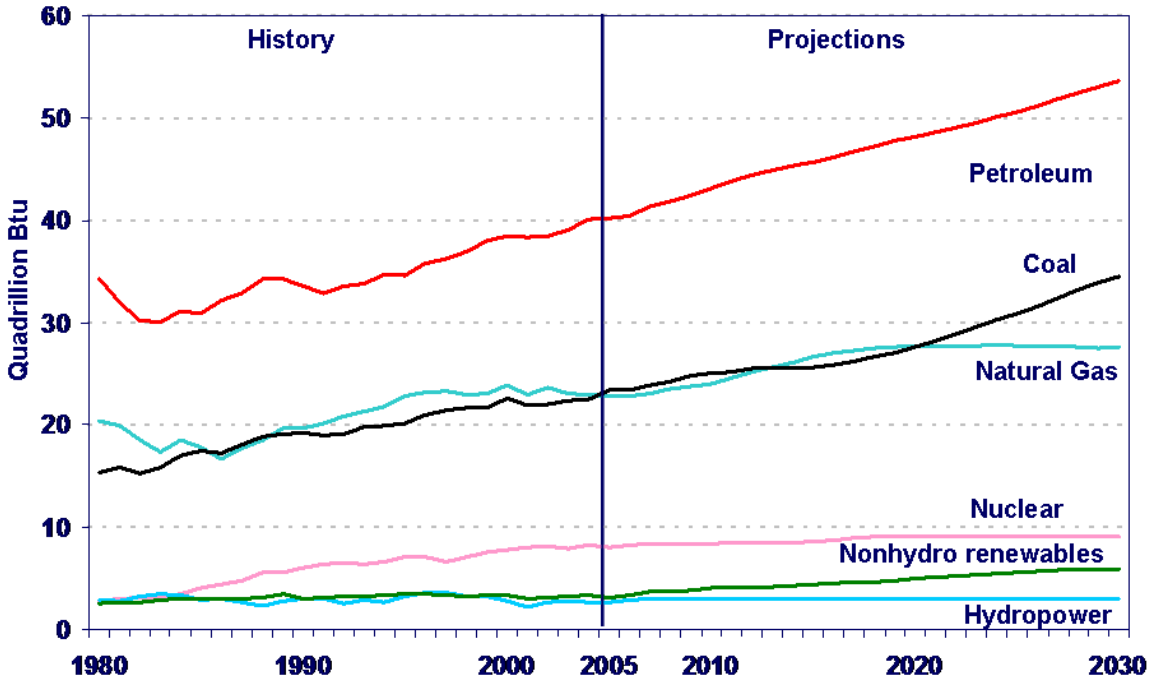

Figure 1.1. U.S. Energy Consumption by Fuel (1980 – 2030) [1].

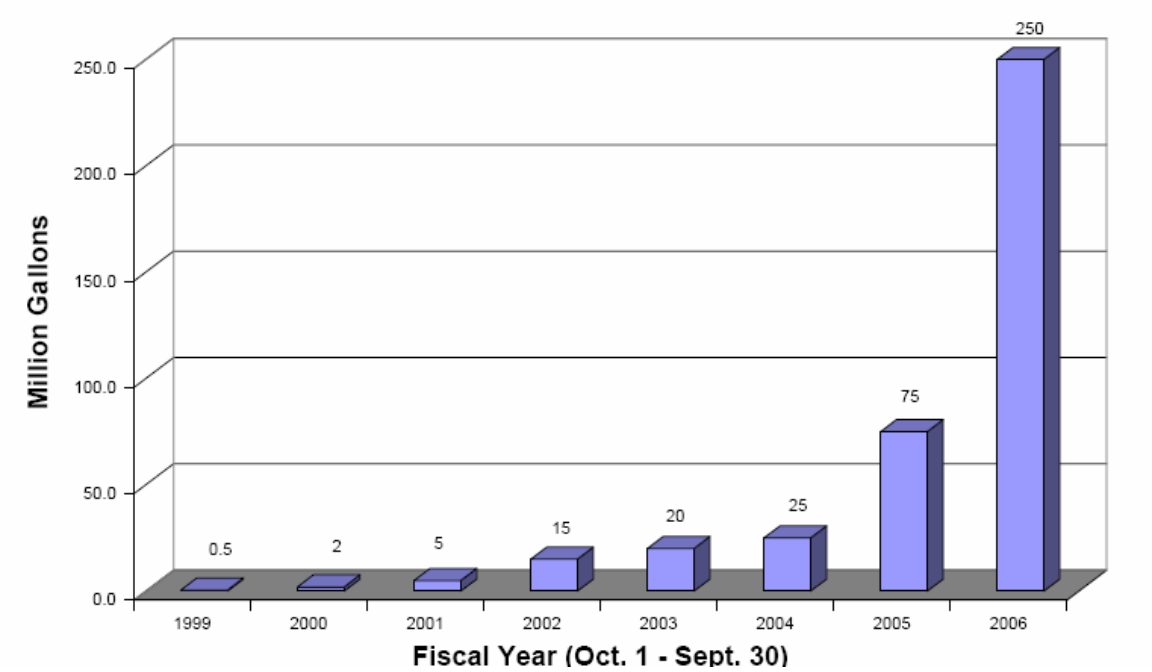

Figure 1.2. Estimated Biodiesel Sales in the United States [2].

CHAPTER II

LITERATURE REVIEW

Since the late 1990's, biodiesel, a mixture of fatty acid methyl esters formed from the reaction of triglycerides and methanol, has been commercially produced as a transportation fuel. Biodiesel is a renewable fuel that adheres to ASTM D-6751 list of regulatory compliance measures. As a consequence of the biodiesel reaction, glycerine is produced as an unwanted byproduct. Also, biodiesel production is limited to saponifiable lipids; therefore, lipids such as sphingolipids and steroids are not utilized [3]. With these shortcomings, another renewable fuel is sought that better utilizes available lipid sources, reduces unwanted byproducts, and is deliverable into the current petroleum refining infrastructure.

Background of Heterogeneous Lipid Cracking

A new approach to lipid utilization in transportation fuels has been considered by Bakhshi and co-workers (Canada) and Bhatia and co-workers (Malaysia) who have developed gasoline-like and diesel-like fuels from plant oils [4 – 12]. Both groups used heterogeneous cracking to decarboxylate and deoxygenate lipids. Bakhshi's group used canola oil, and Bhatia's group used palm oil as feedstocks.

The catalytic conversion of canola oil to fuels (Prasad and Bakhshi, 1986) indicated that 60 to 95 wt % conversion was achieved at 340 - 400°C, respectively. The products formed were an organic liquid product (OLP), C_3 – C_4 paraffinic gases, and water. The OLP was mainly gasoline range organics (GRO) that were 60 – 70 wt % aromatics [4]. Table 2.1 illustrates the yield of each product. Co-feeding of steam resulted in increased catalyst life and altered the gaseous product to mostly olefinic hydrocarbons [5].

A typical laboratory set-up for heterogeneous reactions of plant oils and product handling can be seen in Figure 2.1. The plant oil was pumped at a rate of 2 – 4 g/hr using a syringe pump onto a micro-reactor made of 316 stainless steel with ~1 g catalyst. Upon reaction, the liquid products were condensed into a liquid product collector, and the gaseous products were collected separately. The liquid product was analyzed for its aqueous content and for its hydrocarbon composition. Gas analysis was performed on the gaseous products to determine both inorganic and organic compositions. The spent catalyst was washed with hexane to remove residual, unreacted oil and then analyzed for coke [4].

Idem, *et al.* (1997) used canola oil as a model to determine the effect of different catalytic properties such as acidity, basicity, crystalline structure, and pore size on cracking reactions (Table 2.2 and Fig. 2.2). They determined that the important factors for producing a high yield from catalytic cracking of canola oil to liquid product were the catalyst crystalline structure and catalyst shape selectivity. Crystalline catalysts offer more surface area in which active acid sites initiate the cracking of the molecule. Shape

selective characteristics, such as that of ZSM-5, allow for minor cracking. Minor cracking results in large production of organic liquid products (OLP) and small productions of gaseous products. Also, catalysts with basic centers, such as calcium oxide and magnesium oxide, impede the decomposition of long chain oxygenated hydrocarbons. It was shown that reactions using basic catalysts yielded similar products as thermal cracking (i.e. long chain hydrocarbons and oxygenated hydrocarbons), but secondary cracking required for the formation of aromatic compounds could not be formed from the basic catalysts [6].

Adjaye, et al. (1996) studied canola oil cracking using mixtures of H-ZSM-5 and silica-alumina. Lipid cracking using only silica-alumina results in a high fraction of OLP of mainly aliphatic hydrocarbons. Adding H-ZSM-5 to the silica-alumina results in less coke formation but an increase in gaseous product formation. Increasing H-ZSM-5 amounts (0 – 40 wt %) gradually changes the OLP to predominately aromatic hydrocarbons. These findings were attributed to the amorphous nature of the silica-alumina catalyst versus the highly crystalline nature of the zeolite. Silica-alumina contains both Bronsted and Lewis acid sites, but both are largely inaccessible because of the amorphous character. Therefore, few acid sites are available to the canola oil for cracking, and thus, the silica-alumina has lower activity. The crystalline zeolite, on the other hand, has a higher activity due to acid sites that are accessible by the canola oil feed. Also, the ZSM-5's crystallinity offers shape selectivity towards the formation of products. Shape selectivity was identified as the key reasoning for the aromatization of the ZSM-5 products. The aromatization reactions involve hydride shifts, cyclization, and

isomerization reactions that occur from intermediate olefins. Amorphous catalysts can convert these intermediate olefins only to aliphatic hydrocarbons [7].

Additional studies for the conversion of canola oil to hydrocarbons included the influence of Pt/HZSM-5, a bifunctional catalyst, and the influence of steam catalysis. Pt/HZSM-5 was formed from exposure of H-ZSM-5 to platinum through chloroplatinic acid (H_2PtCl_6) in a slurry for 24 hrs. The slurry was then evaporated to dryness at 110°C and then calcined at 500°C for 6 hrs. Cracking results using Pt/HZSM-5 showed increased isomerization functionality of the catalyst with greater yields for isobutane (rather than n-butane) and isobutylene (rather than n-butene) [8]. Addition of steam to the catalytic process resulted in decreased coke formation, along with lower gas formations, and the extent of aromaticity. In addition, overall compound selectivity decreased with the addition of steam. It was suggested from this work that the steam reduces the rates of hydrogen transfer reactions [9].

Catalytic conversion of palm oil to hydrocarbons over H-ZSM-5 catalyst indicated similar results as shown by canola oil. In a temperature range of 340 - 420°C, 40 – 70 wt % conversion could be achieved. The resulting products were GRO, diesel range organics (DRO), kerosene range organics, light hydrocarbon gases, coke, and water. A maximum of 40 wt % GRO was observed at 400°C and a weight hourly space velocity of 2 h^{-1}. The hydrocarbon gases were chiefly propylene and propane (16 wt % of gas yield) and $C4^+$ hydrocarbons (11.6 wt% of gas yield) [9, 10]. Other catalysts studied were zeolites β and USY. These gave lower conversions, 24 and 30 wt %, respectively, but higher selectivity for DRO and lower productions of gaseous products

[10].

Cracking of palm oil over H-ZSM-5 using multiple Si/Al ratios showed significant differences in product selectivities. Reactions were carried out at 450°C and Si/Al ratios of 50, 240, and 400. Although overall conversion was ~96% for all Si/Al ratios, gas yields decreased from 17.5, 14.0, and 8.2 wt%, respectively, for each increase in Si/Al ratio. Also, higher ratios showed more selectivity towards gasoline and kerosene fractions and less selectivity towards the diesel fraction [11].

In other studies, palm oil and a mixture of fatty acids were converted into gasoline, kerosene, diesel, and gaseous products using microporous, mesoporous, or composite catalysts. The composite catalysts were prepared by coating ZSM-5 with a layer of mesoporous MCM-41 or with SBA-15. The rigorous coating procedure included the mixing of the two catalysts, in their respective unprotonated forms, are crystallizing them at 423K for 24 hrs. After water washing and filtration, the combined catalysts were calcined at 813K for 6hrs [12]. The SBA-15 was coupled with a tri-block copolymer for enhanced hydrothermal stability [13]. For composite catalysts, conversion of the fatty acid mixture increased as alumina was added to the mesoporous mixture. Relatively large pore mesoporous catalysts resulted in higher selectivity toward diesel. In contrast, the liquid product generated using relatively small pore catalysts showed higher selectivity toward gasoline [14, 15]. The mesoporous catalysts, MCM-41 and SBA-15, had pore sizes ranging from 18 - 22Å. Composite catalysts used a foundation catalyst, such as SBA-15, coupled with a supporting catalyst [13 – 16].

Table 2.1. Product Composition for the Conversion of Canola Oil over Various Catalysts

Product	Empty Reactor	ZSM-5	Silica-alumina	Calcium Oxide
Composition (wt %) in Gas Phase				
CO + CO2	4.6	3.7	5.6	5.1
Hydrogen	1.1	0	0.8	0.8
Methane	10.5	5.3	10.7	9.9
Ethylene	31.5	8.7	29.9	27.3
Ethane	9.1	6.9	8.4	10.7
Propylene	17.5	16.1	16.9	17.3
Propane	1.3	18.9	2.2	5.6
i-Butane	0	8.0	0.1	0
n-Butane	10.2	9.1	8.9	11.7
Iso-butylene	1.3	9.1	2.4	2.9
1-Butene	0.5	1.9	1.3	0.4
Dimethyl ether	0.1	0	0.1	0.1
C5+	12.2	11.0	12.4	7.8
Composition (wt %) in Liquid Phase				
Benzene	4.4	8.1	9.4	4.7
Toluene	2.9	18.7	7.7	3.2
Xylenes	0.9	15.0	4.2	0.6
Ethyl benzene	0.3	4.4	3.0	0
C9+ aromatics	3.6	8.8	11.7	3.2

Table 2.1. Continued

C6+ aliphatics	1.9	7.0	18.1	6.6
Oxy-CxHy	7.2	9.2	11.0	15.4
Unidentified	75.5	28.8	35.6	66.3

Notes:

a) Reaction temperature is 400°C for all reactions
b) Weight Hourly Space Velocity (h^{-1}) is 15.4 for empty reactor and 12.1 for all others

Background of Solid Cracking Catalysts

Heterogeneous, high temperature cracking catalysts have been used extensively in the petroleum refining and commodity chemicals industries. These catalysts can vary greatly in the reactions they perform depending upon their crystallinity, acidity, basicity, pore size, surface area, and shape selectivity. Characteristics for some of the more prominent catalysts are shown in Table 2.2.

Solid catalysts can first be divided into crystalline and non-crystalline. Crystalline catalysts, such as ZSM-5, USY, Mordenite, and Erionite, have highly ordered atomic arrangements. The crystalline structures for ZSM-5, USY, Mordenite, and Erionite are tetrahedral, cubic, orthorhombic, and hexagonal, respectively. Non-crystalline catalysts, such as silica, γ-alumina, and silica-alumina, have amorphous structures with large pore sizes up to 150 Å [17].

ZSM-5, in particular, is a shape-selective catalyst developed by Mobil Research and Development Corp. in the mid-1970's [18]. Its intrinsically high acidity is ideal for development of catalytic cracking mechanisms. ZSM-5, sold by Zeolyst International (Valley Forge, PA), is generated in a tetrapropylammonium form $|((C_3H_7)_4NOH)_4|$ $[Si_{95.7}$ $Al_{0.3}$ $O_{192}]$ and is calcined to produce the acidic form $|H_{0.32}|$ $[Si_{95.68}$ $Al_{0.32}$ $O_{192}]$. Calcination involves heating the solid to 500°C under a stream of nitrogen for 6 hrs. The chemical structure of ZSM-5 follows the Lowenstein's rule that no two aluminum atoms will be adjacent to each other [18,19]. ZSM-5 is a shape selective catalyst that has small pores that intersect to form large super cages. Therefore, compounds are spatially restricted when entering and exiting the catalyst structure.

The acidity of ZSM-5 can be altered by adjusting the ratio of silica to alumina atoms. Acid sites are formed when H (or other proton) binds with Al atoms. Hydrogen atoms become protonated during de-alkylation which occurs from calcination. By decreasing the number of tetrahedral Al atoms, i.e. increasing the Si/Al, fewer protons will be present. In turn, this decreases the number of acid sites but increases the acidic activity of the remaining sites [20 – 22].

Table 2.2. Characteristics of Commonly Used Cracking Catalysts

Catalyst	Crystallinity	Structure	Pore Size (Å)	Surface Area (m^2/g)	Si/Al	Cation	Acidity	Shape Selectivity
Silica	Amorphous	na	114	211	No Al	Neutral	None	None
γ-Silica	Amorphous	na	149	241	0	Neutral	None	None
Silica-Alumina	Amorphous	na	31.5	321	0.79	Neutral	Bronsted & Lewis	None
Ultra-stable Y	Highly Crystalline	Cubic	7.4		>3	H		
Mordenite	Highly Crystalline	Orthorhombic	6.7	112	10 – 20	H		
Erionite	Highly Crystalline	Hexagonal	3.8		4	"N"		Very High
ZSM-5	Highly Crystalline	Tetrahedral	5.5	425	>20	H	Mostly Bronsted	Very High

Deactivation of Zeolites

Deactivation of zeolites occurs from the formation of coke. Coke is a variety of large hydrocarbon molecules that are hydrogen deficient. These molecules are typically polynuclear aromatics. Coke forms from catalyzed reactions that occur parallel to, and in competition with, desired reactions. Formation of coke affects the activity and selectivity of the catalyst by either blocking of the catalyst pores or from poisoning of the acid sites [23].

Time-on-stream analysis of fixed-bed micro-reactors reveal that coke is usually acid catalyzed [24]. Time-on-stream concept assumes that catalysts age from simply being used. As zeolites are acid catalysts, managing coke formation is problematic. When paraffins, oxygenates, and other organics are cracked, olefins form as intermediate compounds. The olefins form oligomers, then mono-aromatics, and then finally poly-aromatics [23]. Shape selective catalysts offer an order of magnitude less coking than large pore catalysts. However, a difference worth noting is small pore zeolites such as Erionite and Ferrierite (3.8Å) do not form cyclic molecules, while intermediate pore zeolites such as ZSM-5 (5.4Å) permit formation and diffusion of simple aromatic molecules. This anomaly indicates that coking is a spatially demanding reaction [25].

Fundamental Chemistry of Catalytic Hydrocarbon Cracking

Well established chemistry for the catalytic cracking of hydrocarbons has evolved through the petroleum industry. Crude petroleum consists of a vast assortment of large, long-chain, bulky hydrocarbons that are not easily consumed by internal combustion

engines. As such, these compounds have been catalytically cracked since the 1930's through carbocation and free radical mechanisms. Thermal cracking, i.e. pyrolysis, proceeds by free radical chain mechanisms. Catalytic cracking, however, proceeds via ionic chain mechanisms [26, 27].

Kissin (2001) summarized the carbenium ion formation for the protonation of alkenes. Carbenium ions are tri-coordinated carbocations that can develop when Bronsted acids complex with the double bond of an alkene. Primary products from acid-catalyzed alkene cracking include H-atom shifts (Eqn. 2.1), double bond shifts, alkyl group shifts (Eqn. 2.2), and the formation of alkanes with the same number of skeleton carbons. Secondary products of alkene cracking are alkene oligomers and C – C β-bond scission products. Tertiary cracking occurs when the formation of hydrocarbons requires more than one step of the C – C bond scission or C – C bond formation. For example, the reaction of propylene in the presence of a zeolite catalyst initially undergoes β-bond scission and then charged intermediates oligomerize to form molecules that have up to 45 carbons. The oligomerization, along with additional methyl and hydride shifts, constitute tertiary cracking [28].

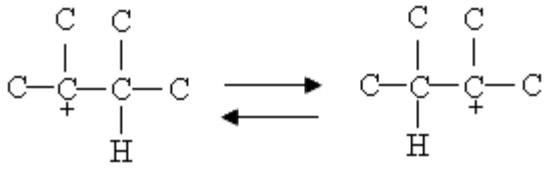

(Eqn. 2.1)

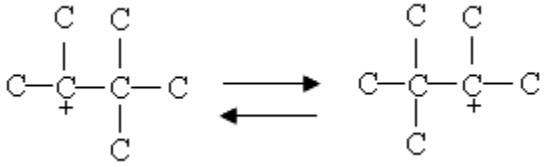

(Eqn. 2.2)

Alkane cracking is analogous to alkene cracking but significantly slower reaction rates. Although alkane cracking mechanisms do not include oligomerization, they do include the formation of carbenium ions that can undergo β-bond scissions. Figure 2.3 demonstrates the reaction chemistry from the catalytic cracking of an alkane. In this example, n-octane is protonated which results in a series of hydride and methyl shifts to form secondary and tertiary carbocations. β-scission, which is slow for primary and secondary carbocations but fast for tertiary carbocations, results in the breaking of the second bond away from the tertiary carbocation. This scission results in the formation of an olefin and an additional tertiary carbocation [20].

Another mechanism proposed by Olah and Prakash (1985) is the formation of a non-classical carbocation called a carbonium ion [27]. This type of carbocation uses a tetra- or penta-coordinated protonated carbon. Carbonium ions in superacids readily release H_2 (or small alkanes such as methane or ethane) and form carbenium ions. For this reason, cracking chemistry for alkanes follows a similar path as alkenes [28].

Typically, alkanes and alkenes experience skeletal rearrangements, also known as methyl shifts, to form secondary and tertiary carbocations before cracking. Secondary carbocations are ~17 kcal/mol more stable than primary carbocations, and tertiary carbocations are ~13 kcal/mol more stable than secondary carbocations. Hence, there exists a thermodynamic favorability to form branched hydrocarbons before cracking [20, 27, 28]. Compounds cracked through carbenium ions form a free olefin and a smaller carbenium ion, which develops into a chain mechanism requiring initiation, propagation, and termination steps [29, 30].

Aromatic compounds are produced due to olefin ions that oligomerize and cyclize. Cyclized olefin ions are formed from the saturation of the olefin molecule. This intermediate will then eliminate a hydrogen through pyrolysis. This, in turn, establishes a hydrogen-deficient cyclic molecule (i.e. aromatic) [27]. Once an aromatic compound forms, alkyl substitutions from disproportionation reactions increase the size and complexity of the aromatic. These complex compounds are polynuclear aromatics, highly hydrogen deficient, and can eventually develop into coke. The hydrogen deficiency of aromatic compounds provides the much needed hydrogen atoms required for the saturation of olefins [26 – 28].

In his review on catalytic cracking, Wojciechowski (1998) discusses several dichotomies of hydrocarbon cracking. One of which is the differences (and similarities) between pyrolytic and catalytic cracking. Both seem to proceed via chain mechanisms, but their differences contribute to different products and product yields. A dichotomy exists because many researchers have largely ignored the thermal component when defining catalytic cracking chemistry. Therefore, quantification of the catalytic mechanism becomes complicated and must be deconvoluted from thermal cracking mechanisms [26].

Production of Aromatics from Methanol

Vedrine, et al. (1980) have developed the chemistry for the conversion of methanol into hydrocarbons that are consistent with the makeup of gasoline. Using ZSM-5 catalyst at Si/Al ratios from 28 to 54.5, experiments reveal that methanol is first dehydrated into dimethylether and then into higher carbon molecules, such as

saturated aliphatics, olefins, and aromatics. The reactions occur due to Bronsted acid sites within the catalyst. A simplified schematic for this process can be seen in Figure 2.4 [31]. Similar results were found by Benito, et al. (1996) using a 2mm i.d. microreactor designed for ultra-low conversions. H-ZSM-5 (Si/Al 24 to 154 and 110 to 175°C) produced dimethylether, ethylene, propylene, and butylene as primary products. Reaction temperatures were kept low to discourage olefin formation from heavier product cracking. The concentration of heavier alkenes increased as acidity decreased (i.e. higher Si/Al ratios) and at higher temperatures. FTIR results of the adsorbed phase suggested the formation of methoxy groups from which oxonium ions are formed. The proposed solid/gas chemistry can be found in Figure 2.5 [32].

Cracking of Oxygenated Compounds

Investigations into the cracking of oxygenated compounds have been limited and the chemistry is not known nearly as well as that for alkanes and alkenes. Most work has been concentrated to compounds found within bio-oil and plant oils.

Adjaye and Bakhshi (1995) investigated cracking chemistry for model compounds found within bio-oil. Bio-oil is the liquid product of pyrolyzed wood. The model compounds included propanoic acid, 4-methylcyclohexanol, cyclopentanone, and acetic acid methyl ester. Reactions using H-ZSM-5 at 330 - 410°C indicated that combinations of cracking, deoxygenation, aromatization, and polymerization occur. The acid and the ester both seem to undergo two reaction routes. The first route entails decarboxylation (Eqn. 2.3 and Eqn. 2.4) to form CO_2 and hydrocarbon gases. The second route involves the formation of H_2O, aromatic hydrocarbons, and coke. This

second route deoxygenates the acids and esters which then form long-chain aldehydes and ketones [33]. Aldol condensation reactions are responsible for the formation of water when producing aldehydes and ketones [34, 35]. In aldehydes and ketone cracking, it appears that deoxygenation and decarbonylation are the starting steps, which leads to dehydration and alkene production [33].

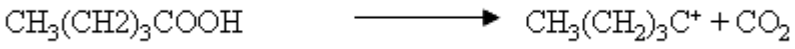

(Eqn. 2.3)

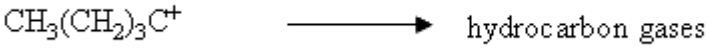

(Eqn. 2.4)

Similar results were obtained from reactions of fatty acids and their ester derivatives when reacted with Pd/carbon catalysts at 300°C. Mali-Arvela, et al. (2007) found that linear hydrocarbons were produced from decarboxylation of fatty acids (i.e. n-heptadecane from stearic acid). The cracking of ethyl stearate, however, proved to behave differently when reacted with different catalysts. When reacted over alkaline catalysts, decarbonylation was the initial cracking step. Acid catalysts used decarboxylation as the initial step. The main products, then, were n-heptadecane for alkaline catalyst and stearic acid for acidic catalyst. When the ester reaction was diluted with hydrogen gas (instead of inert gas), ethyl stearate reaction pathway was more decarbonylation and produced mostly n-heptadecane [36]. Reaction of tristearine under similar conditions formed primarily n-heptadecane with positional isomers of heptadecane and constitutional isomers of undecylbenzene [37].

Unsaturated fatty acids have been found to produce branched-chain fatty acids when reacted with large-pore zeolites such as faujasite at 240 - 260°C. Oleic acid reactions produced compounds with methyl and ethyl branching that were distributed along the alkyl chain of the fatty acid (Fig. 2.6). This was attributed to the C – C double bond migration on the acidic zeolite catalyst. The suggested mechanism included the intermediate formation of a three-membered ring carbocation for the formation of methyl branching and a four-membered ring carbocation for the formation of ethyl branching. As the ring opens, the formation of the branched-chain fatty acid occurs and a proton is released [38].

Use of Fluidized Catalytic Cracking for the Manufacturing of Hydrocarbons

Fluidized Catalytic Cracking (FCC) has become the industry standard for the production of transportation fuels since World War II. Catalytic cracking of crude petroleum began in the 1930's with the use of clays as catalysts and progressed towards synthetic silica-alumina catalysts. With the Arab oil embargo of 1973, crude oils contaminated with metals became the more abundant feedstock. Therefore, metals-resistant FCC became necessary and research was begun to fully understand the interactions between metals and catalysts. Also, heavier crude oils, which contain components with boiling points above 525°C, pose problems for refiners. These crudes have lower hydrogen to carbon ratios causing the addition of hydrogen within the reaction process necessary [39].

The Environmental Protection Agency banned lead as a fuel additive in 1984, and it became necessary to find catalysts that promoted the production of octane as a performance enhancer. Octane production for gasoline is rather sensitive towards FCC operating conditions. For example, increase in riser temperatures and reductions in catalyst/oil contact times will decrease hydrogen transfer reactions, which minimize secondary cracking, and will therefore produce olefin-rich gasoline with increased octane numbers. High octane gasoline can also be more easily produced from feedstocks rich in naphthenes and aromatics. The drawback of octane-promoting catalysts is less H-transfer reactions, promoting secondary cracking, which decreases the yields of gasoline in favor of low molecular weight gases [40, 41]

With the constraints as stated above, the use of shape-selective zeolites, such as ZSM-5, has become more prominent within FCC processes. These catalysts selectively crack low-octane n-paraffins into higher octane components. This, in turn, increases the octane number of the gasoline by a few points. Light olefins, such as propylene and butylene, become alkylated to high octane products, partially offsetting the loss of gasoline yields. Reactions using ZSM-5 inhibit coke formation and optimize downstream operations from increased production of high-octane gasoline [42].

A major disadvantage of the zeolite catalysts is poor thermal stability. To increase catalyst activity, methods have been developed to decrease the aluminum content of the catalyst in its framework, channels, or surfaces. Replacing the framework aluminums with the hydrogen-form greatly decreases the catalyst's thermal stability. For this reason, ZSM-5 has seen limited use within the petroleum refining industry. However, faujasites, such as US-Y, have shown promising results with high cracking

efficiencies and high thermal stabilities. Therefore, to obtain high octane numbers with high thermal efficiencies, ZSM-5 has been used as an additive to other catalysts. Addition of ZSM-5 (0.5 – 3 wt %) increases the iso to normal ratio of the aliphatic fraction of the gasoline. As ZSM-5 has a smaller pore opening than US-Y, complex oil molecules are restricted from entering the ZSM-5. This results in little effect of the primary cracking of petroleum but increases the overall octane of the fuel [33, 44].

Fundamentals of Mass Spectrometry

As mass spectrometry (MS) was utilized throughout each phase of this research, a review of the principle aspects of MS seems pertinent. MS is a tool through which compound analysis, both qualitative and quantitative, is performed as compounds are subjected to gas-phase ionization. The three basic elements of MS are 1) Ion Source, 2) Mass Analyzer, and 3) Ion Detector [45].

Ionization

The two modes of ionization are electron impact (EI) and chemical ionization (CI). In either case, a compound, or analyte, is fragmented to produce a multitude of charged ions, each with a specific mass/charge ratio, that are assembled into a collection called a mass spectrum. EI spectra are produced by bombarding analytes with a barrage of electrons (Fig. 2.7) to produce a series of M^+ ions. Production of electrons comes from passing a current through a thin metal filament. The filament, usually made of ruthenium, is a cathode, and the electrons are propelled across the ion source from their

attraction to an anode. The electrons' energy is dependent upon the difference in the potentials applied to the cathode and anode [45].

CI is a "softer" ionization technique that produces a less fragmented spectrum than EI. This smaller fragmentation allows for the determination of the analyte's molecular weight when the $(M+1)^+$ ion is formed as the dominant ion. These two ionization techniques compliment another when one compares the EI mass spectra with that of known compounds with the molecular weight obtained from CI analysis. Compound identification using EI begins with a library search using the MS software [46].

Chemical Ionization Reactions

The foundation of CI involves gas-phase chemistry in which a reaction gas is introduced into the ion source. A primary step uses EI to form ions from the reaction gas (Equation 3.3). A secondary step uses the reactant ion formed from the primary step to produce the $(M+1)^+$ ion. Typical reaction CI gases used in ion-molecule reactions include methane, isobutane, ammonia, and acetonitrile. These reaction gases are positive ion reagents yielding Bronsted acidic reactions through proton transfers. The desired reaction gas is chosen based upon proton affinity and energy transfer of the exothermic reaction. A reaction can only occur if the proton affinity for the analyte compound is greater than the one for the gas molecule. Analyte compounds that are sensitive to a particular CI gas can also form adduct ions. For example, methane can form $(M+17)^+$, $(M+29)^+$, and $(M+41)^+$ (Equations 3.4 – 3.6) and acetonitrile can exhibit $(M+40)^+$ ion along with the $(M+1)^+$ ion [46].

$(M+1)^+$ $CH_4 + e \rightarrow CH_4^{+*} \rightarrow CH_3^+ + H^*$ (Eqn. 3.3)

$(M+17)^+$ $CH_4^{+*} + CH_4 \rightarrow CH_5^+ + CH_3^*$ (Eqn. 3.4)

$(M+29)^+$ $CH_4^{+*} + CH_4 \rightarrow C_2H_5^+ + H_2 + H^*$ (Eqn. 3.5)

$(M+41)^+$ $CH_4^{+*} + CH_4 \rightarrow C_3H_5^+ + H_2$ (Eqn. 3.6)

Another ionizing gas, acetonitrile, is relatively new. Acetonitrile (MW=41) yields either $(M+1)^+$ or $(M+40)^+$ ion depending on formation of $(M+H)^+$ or $(M+CH_2CN)^+$, respectively. Long-chain hydrocarbons typically favor the $(M+40)^+$ ion formation due to the more thermally stable $(M+CH_2CN)^+$ cation [47, 48].

Quadrupole Ion Trap

The quadrupole ion trap (QIT) operates as an ion storage device and as a mass spectrometer (Fig. 2.8). As an ion storage device, the QIT employs an electric field to manipulate which ions to keep and which to discard. At a pressure of ~1 mTorr, the QIT operates as a mass spectrometer by measuring the mass/charge (m/z) ratios of confined ions. This measurement is accomplished by adjusting the potential well of the ion trap such that ions leave the potential well, and the trap, by ascending m/z order. The QIT consists of two conical lens and a ring lens that is shaped like a donut. Ions are stored, or trapped, in the finite interior volume between the conical lenses that form the endcaps and the center ring electrode. Ions pass through the trap, stored, and then released to the detector. Ions are expelled from the potential well be ramping the amplitude of the radiofrequency (RF) (Fig. 2.9). Each ion species has a unique RF by which it is ejected from the QIT. The M/Z of an ejected ion can be determined from the ramping rate and from the initial and final RF amplitudes. Figure 2.10 demonstrates the (a) trapping

and storage of ions and (b) the selective ejection of ions from RF ramping [49 – 51].

To control the population of trapped ions, either the RF voltage can be adjusted or waveforms can be applied to the quadrupole endcaps. In both cases, unwanted ions can be eliminated from the trap to avoid space charge affects. There exists within the QIT a finite volume in which ions can be stored, and elimination of unwanted ions allows for increased sensitivity due to longer ionization times and noise reduction. The RF can be segmented to allow for storage of one set of ions (i.e. m/z 10 – 50) and then for another set of ions (i.e. m/z 50 – 300). In the first segment, only ions with m/z 10 – 50 are stored and detected, and likewise for the m/z 50 – 300 [50].

Waveforms can be applied to the QIT to perform selected ion storage (SIS). Ion motions occur in oscillatory fashion and can be excited by absorption of energy at an appropriate RF frequency. When the amplitude of the ion's oscillation exceeds the dimensions of the trap, the ion collides with the trap and is no longer stored. The ion is then ejected from the MS system before it can enter the detector. SIS can be used to eliminate column bleed peaks, such as siloxanes (m/z 207, 281, and 355), associated with operating GC columns at higher temperatures [52 – 55].

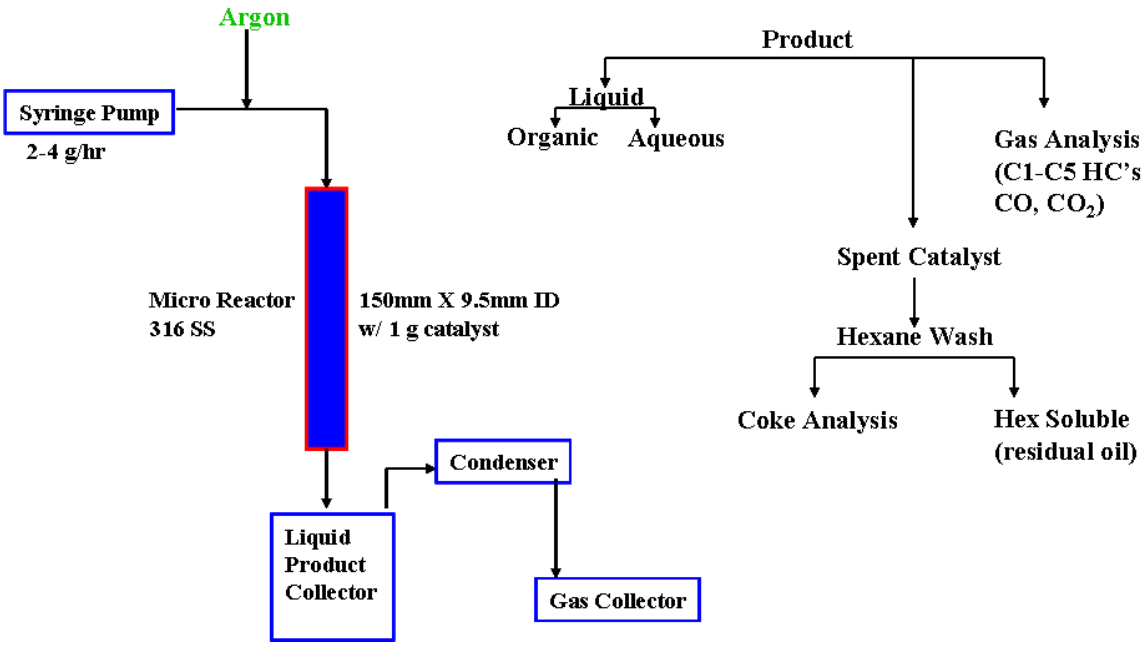

Figure 2.1. Typical Laboratory Set-up for the Reaction and Product Handling of Triglycerides

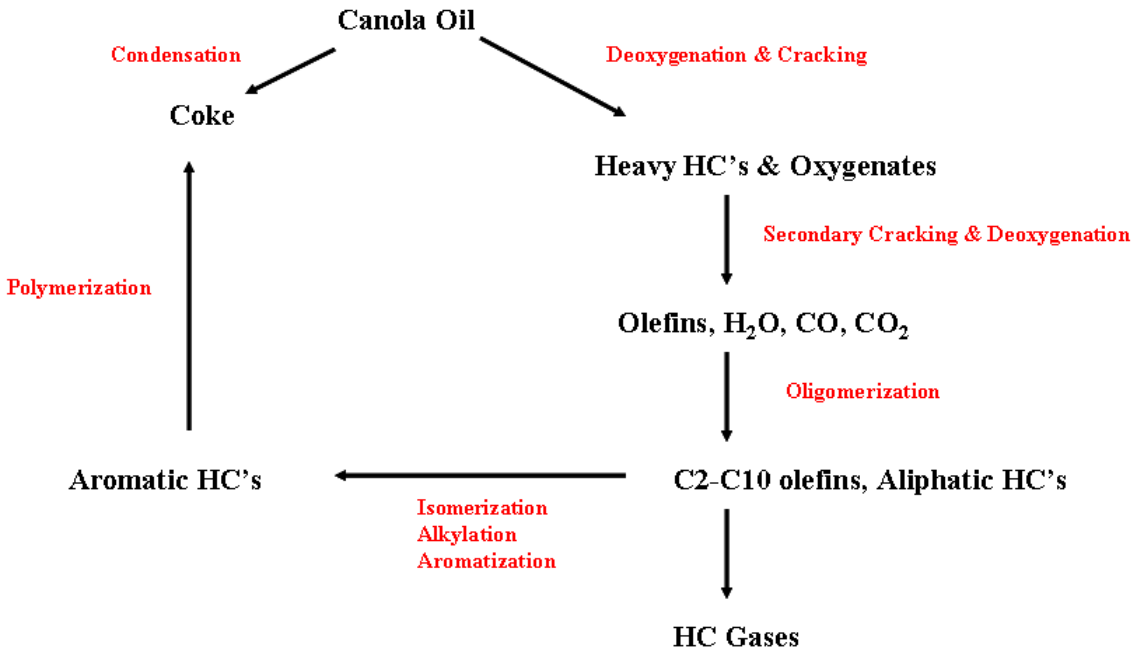

Figure 2.2. Reaction Pathway Proposed for the Cracking of Canola Oil

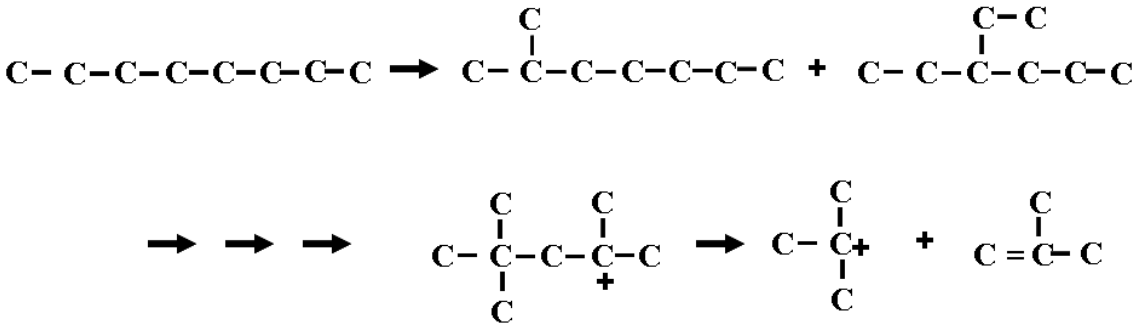

Figure 2.3. Reaction Chemistry for the Cracking of n-Octane to form an alkene and another carbocation.

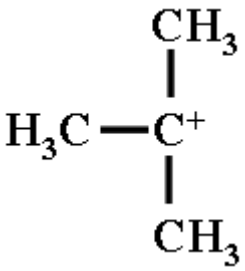

Figure 2.4. Example of a Tertiary Carbenium Ion.

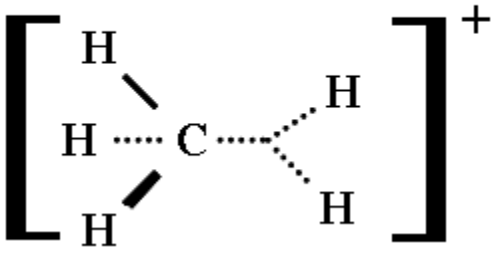

Figure 2.5. Example of a Carbonium Ion.

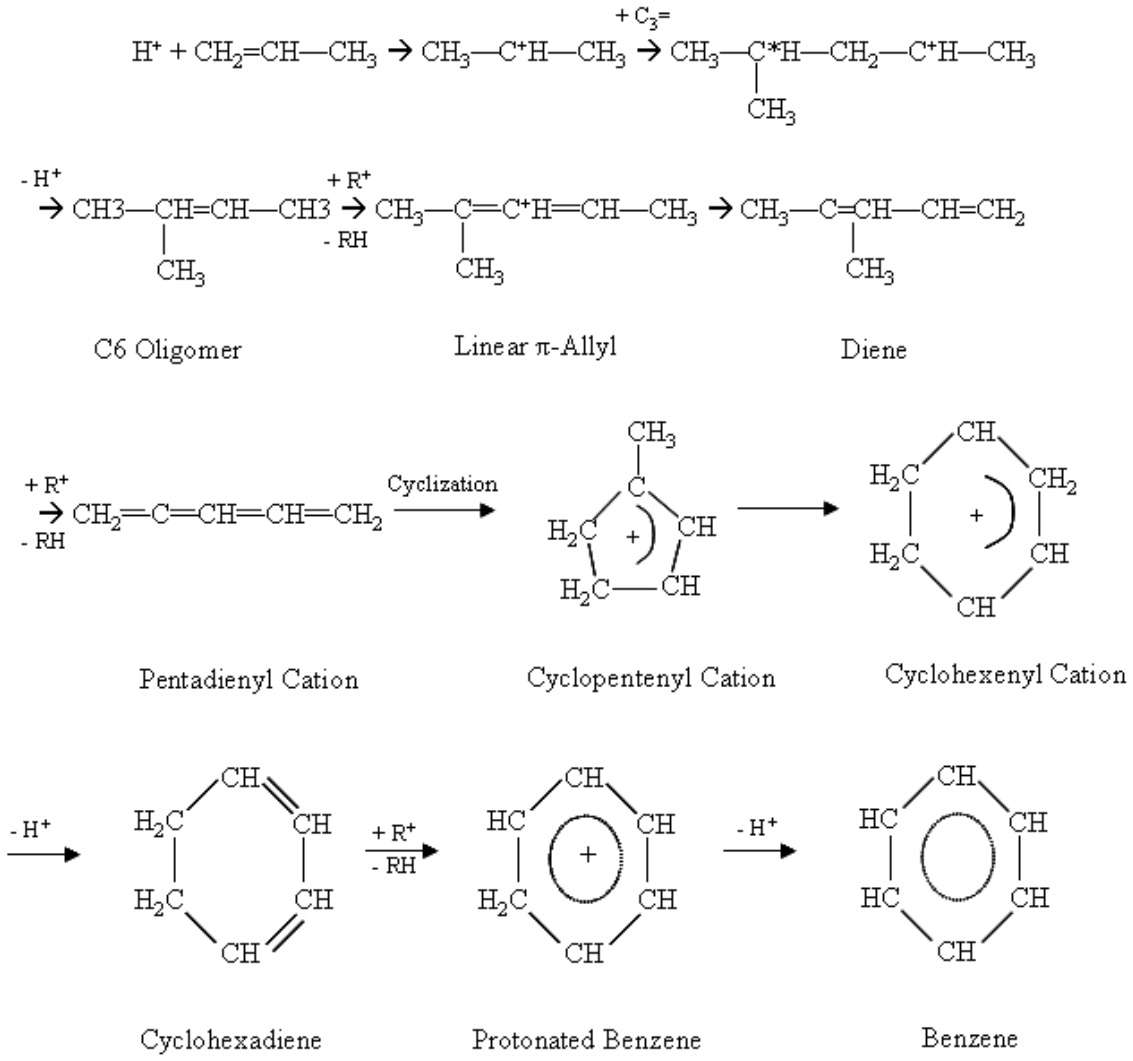

Figure 2.6. Proposed Mechanism for the formation of Aromatic Compounds from Alkane and Alkene Hydrocarbons.

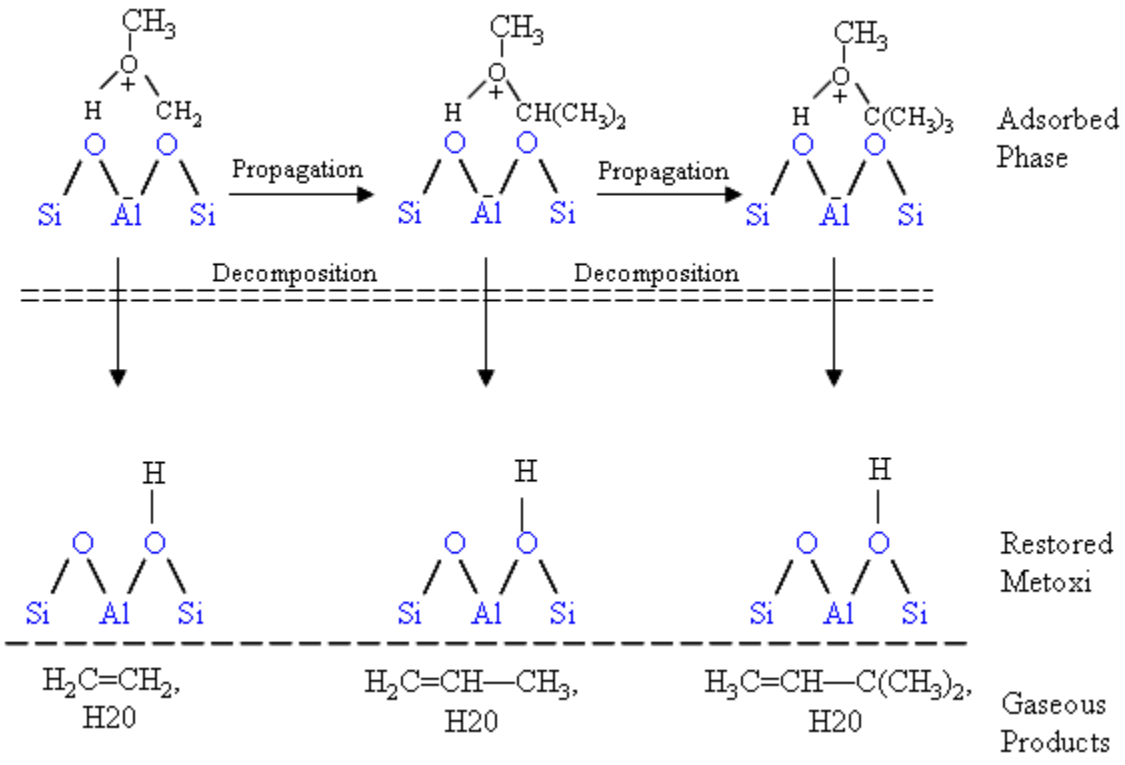

Figure 2.7. Proposed Mechanism for the Formation of Primary Products from the Cracking of Methanol.

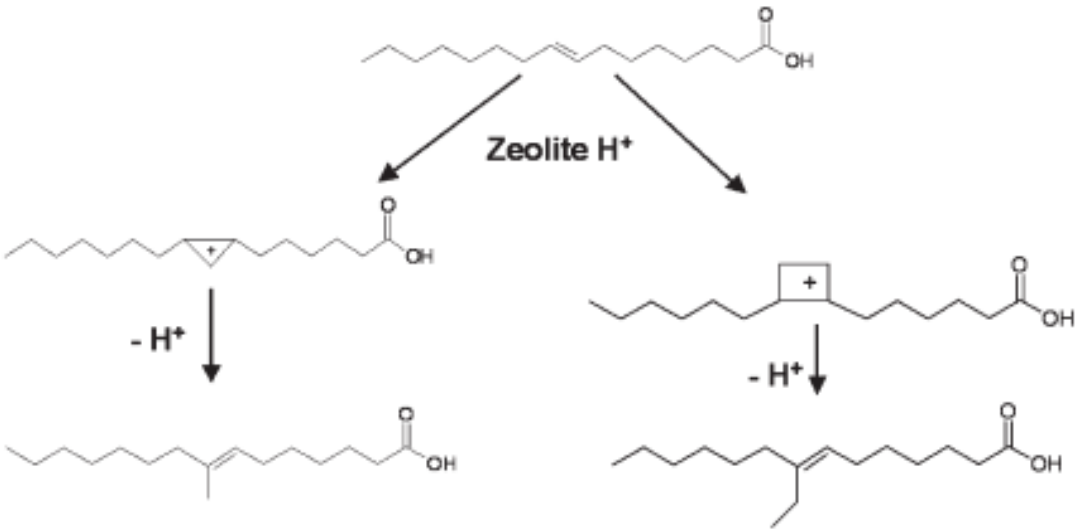

Figure 2.8. Mechanism for Saturation of Unsaturated Fatty Acid.

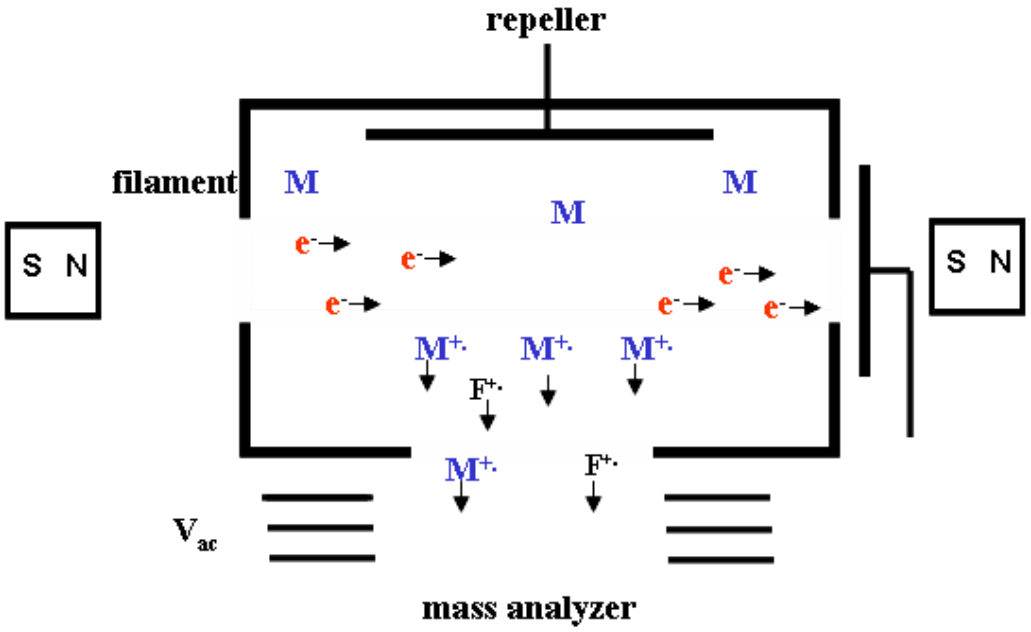

Figure 2.9. Bombardment of Analyte, M, with Electrons in Electron Impact Mass Spectrometry.

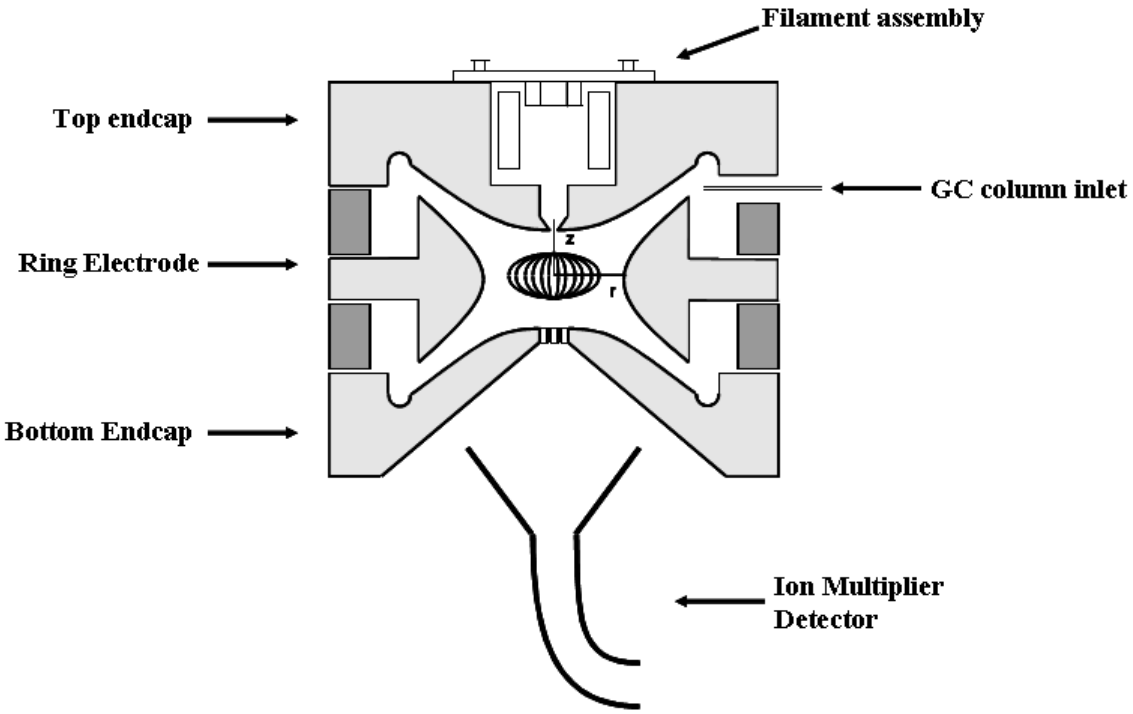

Figure 2.10. Diagram of Quadrupole Ion Trap.

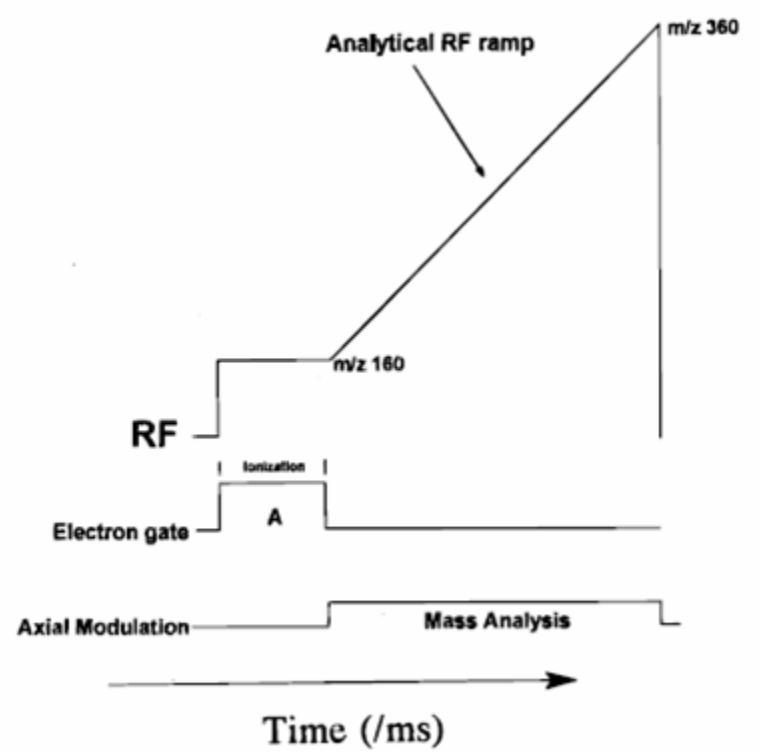

Figure 2.11. Typical Scan Function for Electron Ionization Mode.

NOTE: The ionization period (shown at position A) is immediately followed by ramping of the RF used for ion ejection.

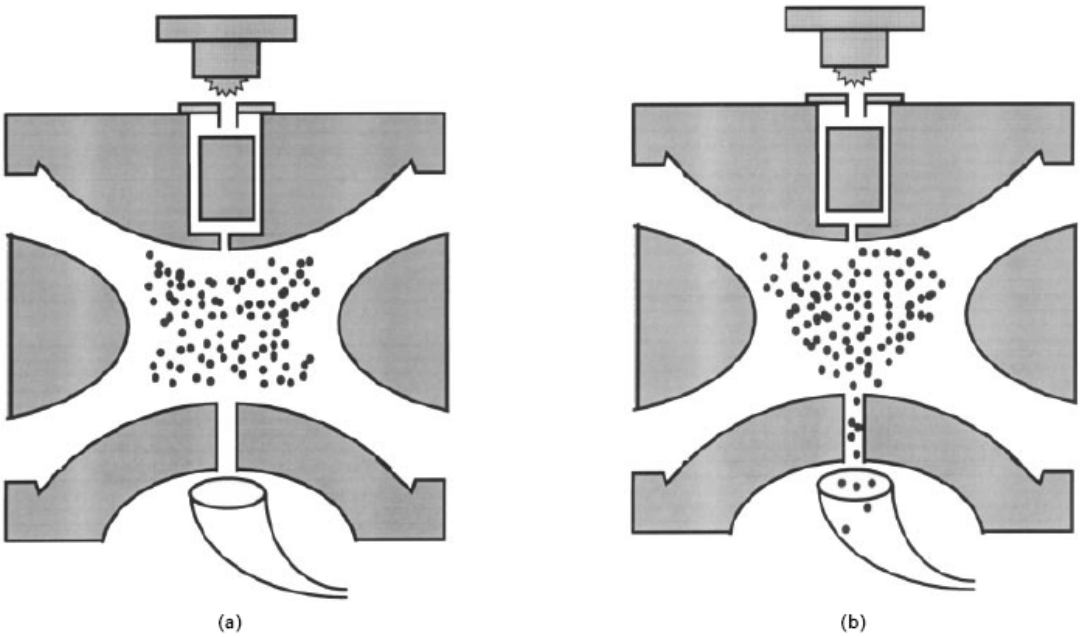

Figure 2.12. Diagram for Quadrupole Ion Trap

NOTE: (a) Stored Ions and (b) Ejection of Ions with RF Ramping. (Typical formation and storage of ions is 0 – 30 ms, and typical ejection timing is 30 – 85 ms.)

CHAPTER III

RESEARCH HYPOTHESIS AND OBJECTIVES

Research Hypothesis

The aim of this research was to further the development of renewable fuels. In doing so, it is conceivable to reduce the use of fossil fuels as the major source of transportation energy. In 2006, the United States imported 3.7 billion barrels of petroleum and domestically produced 1.9 billion barrels of crude petroleum. Of the total 5.6 billion barrels of oil, 92.6% were used for transportation fuels. As a consequence, 1.75 billion U.S. tons of exogenous CO_2 were produced from the combustion of transportation fuels. U.S. Department of Energy projects a 1.3% annual increase in motor fuel usage over the next 25 years. Therefore, as supplies of crude petroleum decrease, either from decreased production or from political reasons, and as demand increases, energies from renewable resources will be required to maintain current standards of living.

In recent years, ethanol and biodiesel have emerged as renewable alternatives to petroleum fuels. The newly developed biodiesel industry has had, and continues to have, many hurdles to overcome. Some of which include the development of an independent

infrastructure for marketability, new ASTM standards, test markets for manufacturers' warranties, and production of the unwanted byproduct glycerine. With these caveats in mind, this research hypothesizes the formation of a petroleum alternative that utilizes production strategies already in place within the petroleum industry, namely heterogeneous catalysis, uses the existing petroleum pipeline infrastructure (service stations, fuel delivery, etc.), and also reduces the production of unwanted byproducts. These "green" fuels (aptly named for their environmental friendliness) can be produced from the same lipid sources as biodiesel, but also, from phospholipids, sphingolipids, and even steroid lipids that are not amenable towards the transesterification processes used for biodiesel production.

Research Objectives

The main objective of this research was to develop the chemistry associated with the cracking of lipids. Model compounds were identified and catalytically reacted to determine the pathways for generating products. Since all previous research efforts have concentrated on overall cracking products (i.e. conversion up to 95%), this research looks at the initially cracked products to determine the primary products that are formed from initial contact with the catalyst.

Phase I

Develop reaction mechanism for the cracking of palmitic acid (a saturated fatty acid) and oleic acid (an unsaturated fatty acid). These two organic acids were chosen as models of the major components in plant and animal oils. For example, oleic acid, or *cis*-

9-octadecenoic acid, is an 18 carbon fatty acid with a symmetrically placed double bond. Palmitic acid, or hexadecanoic acid, is a 16 carbon saturated fatty acid. The free fatty acid content of olive oil is 83% and 8% [56], canola oil is 60% and 5% [57], oleaginous yeasts 52% and 24% [58], soybean oil 23% and 8% [59], and sewage sludge oils 30% and 36% [60], of oleic acid and palmitic acid, respectively. These model compounds were reacted using triflic acid, a liquid superacid, at low temperatures to investigate the extent of Bronsted acidity on the cracking of fatty acids, without thermal affects.

Phase II

Develop reaction mechanisms for acylglycerides (mono-, di-, and triolein) using heterogeneous catalytic methods. The effects of catalyst surface acidity and temperature of initial cracking products were investigated using ZSM-5 (SiO_2/AlO_3 = 23). Once the cracking mechanisms were developed using ZSM-5, a well-defined benchmark catalyst, two industrially used catalysts, faujasite and silica-alumina, were tested to determine product compositions.

CHAPTER IV

METHODS AND MATERIALS

Phase I: Homogeneous Cracking of Model Fatty Acids

Phase one of this research sought to establish fundamental information on the cracking of plant, animal, and microbial oils by reacting model compounds with a model Bronsted acid catalyst. Inasmuch, the homogeneous catalytic cracking of oleic and palmitic acids, major components of plant and animal oils, using the superacid trifluoromethanesulfonic acid (triflic acid). These two organic acids were chosen as models of the major components in plant and animal oils. For example, oleic acid, or *cis*-9-octadecenoic acid, is an 18 carbon fatty acid with a symmetrically placed double bond. Palmitic acid, or hexadecanoic acid, is a 16 carbon saturated fatty acid. The free fatty acid content of olive oil is 83% and 8% [56], canola oil is 60% and 5% [57], oleaginous yeasts 52% and 24% [58], soybean oil 23% and 8% [59], and sewage sludge oils 30% and 36% [60], of oleic acid and palmitic acid, respectively.

The choice of model catalyst was dictated by the need to examine the effect of Bronsted acidity, alone, on the cracking of the organic acids in the absence of thermal cracking. Thus, we chose an acid that could be used at sufficiently low temperatures so as to suppress thermal cracking. Triflic acid is 100 times more acidic than fuming

sulfuric acid with a Hammett acidity of -14.1 [61].

Chemicals

All chemicals (oleic acid, palmitic acid, triflic acid, and solvents) were obtained from Sigma-Aldrich at their highest available purity and were used without further purification. All gasses (argon, hydrogen, air, and helium) were of ultra high purity grade.

Reactions

Extreme care was taken to avoid skin contact or inhalation of triflic acid. All reactions were completed in a VAC glove box under an atmosphere of argon to reduce hazardous exposure and to exclude oxygen and water as unwanted reactants. Triflic acid hydrolyzes in the presence and water, and oxidation of reactants, either by water or oxygen, was undesirable for these cracking reactions. The reaction vessels were 60 ml vials that could be capped with a mini-inert valve for gas sampling. Reactions for this study were conducted at 25°C and 100°C for palmitic acid and 0°C for oleic acid. The reaction temperature for palmitic acid was first studied at 25°C. Upon the determination of no reaction at 25°C, reaction at 100°C was performed. For oleic acid, reactions at 25°C were too fast to obtain initial cracking information; therefore, 0°C was chosen to slow the reaction for the determination of initial cracking products. Screening experiments indicated that the reactions could be completed in 6 hours.

Triflic acid was first added to a stirred vial followed by oleic acid or palmitic acid. A 10:1 molar ratio of triflic acid to fatty acid was needed to obtain a homogenous

mixture between the two components. The reactions were quenched with sodium bicarbonate water (5% m/v) that was added until bubbling stopped, indicating neutralization of protonated species.

After quenching of the reactions, the vials were removed from the glove box and prepared for analysis. Sample preparation included extraction of the products with methylene chloride or chloroform and removal of solvent using a rotary evaporator. Methylation, required for gas chromatography analysis, was conducted by reacting a 6:1 molar ratio of methanol to initial oleic acid content using 375 mM sulfuric acid in methanol at 60°C for a minimum of 6 hours. All other analytical procedures were conducted using non-methylated samples.

Analytical

NMR Spectroscopy

Proton and carbon NMR spectroscopy were conducted on the chloroform extract (organic phase) of reaction mixtures and the aqueous material collected from the aqueous quenching step. The NMR instruments used in this study are located in the NMR Facility at Mississippi State University. The proton NMR samples were analyzed on an AMX 600 (MHz) Bruker system. The carbon NMR samples were analyzed on an AMX 300 (MHz) Bruker system. Chloroform was removed from the organic phase using a rotary evaporator. The solvent-free sample was then diluted using deuterated chloroform, 50 mg/mL, with 0.05 % v/v TMS (tetramethylsilane) as internal standard. Deuterium oxide with 1.0% v/v DSS (2,2-Dimethyl-2-silapentane-5-sulfonate) internal standard was added

to the aqueous samples for NMR testing. All NMR spectra were collected at room temperature and ambient pressure. Spectral analysis was made using MestRec software.

Infrared Spectroscopy

Attenuated Total Reflectance – Fourier Transform Infrared Spectroscopy (ATR – FTIR) was used for infrared spectral analysis. The instrument used was a Perkin Elmer Spectrum 100 spectrophotometer that used a deuterated triglycine sulphate detector and a Helium Neon laser. The optical system scans from 7,800 to 370 cm^{-1}, and the ATR was a combined diamond and zinc-selenide crystal. Spectral resolution was 4 cm^{-1}.

Liquid aliquots of both the organic extract and aqueous samples were scanned from 4,000 to 650 cm^{-1}. A background scan was carried out before running the analysis, and the FTIR software corrected for the background noise. The organic extract was first concentrated to dryness using a rotary evaporator before droplet-sized aliquots were placed onto the diamond window of the spectrometer. The aqueous samples were tested with litmus paper and brought to a pH ~7, if need be, using sodium bicarbonate. A pH 7 was chosen to prevent damage to the spectrometer from acidic samples.

Gas Chromatography/Mass Spectrometry

Extracts were analyzed by GC/MS using a Varian 3600 GC equipped with a Varian 2000 ion trap mass spectrometer. Both electron impact ionization (EI) and chemical ionization (CI)) were used for product characterization. The splitless injector operated at 280°C. The separations were obtained using a Rtx-5ms column (30m x 0.25 mm, with a 0.25 μm film) manufactured by Restek. The oven was programmed with

an initial temperature of 50°C, held for 3 minutes and was then ramped to 150°C at 10°C/min, then ramped to 190°C at 1°/min, and finally ramped to 280°C at 10°/min and held for 2 min. The carrier gas was helium utilizing the Built in Purifier, BIP® (AirGas, Radnor, PA), and the chromatographic system utilized the NIST library to aid in compound identification. The extracts were derivatized with H_2SO_4 in methanol, as described above, to produce methyl esters for chromatographic analysis. The multiple peaks from the total ion chromatograms were identified using CI spectra to determine molecular weight. Quantitation of fatty acid isomers was performed while in EI mode using calibration curves for straight-chain saturated fatty acids obtained from standard compounds. The Supelco FAME-37 mix, containing saturated and unsaturated straight-chain compounds, was used as quantitation compounds. It was assumed that the peak observed in the product at the retention time of each saturated straight-chain standard was the straight-chain fatty acid. Estimation of branched-chain fatty acid isomers was made by assuming the response of the branched isomers was the same as the corresponding straight-chain fatty acids.

Phase II: Heterogeneous Cracking of Model Lipid Compounds

Heterogeneous reactions and analyses were performed using an in-house built reactor/analyzer termed the Quatra C (Cryogenic Capillary Catalytic Cracker). Details of this device are found in Chapter VI.

The second phase of this work seeks to establish fundamental cracking chemistry of animal, plant, and microbial lipids by reacting model compounds over a model solid catalyst.

This work focuses on the heterogeneous reaction of oleic acid and 1-monoolein, 1,3-diolein, and triolein. The 1-monoolein, 1,3-dioelein, and triolein are mono, di-, and triglycerides, respectively, with oleic acid as the fatty acid moiety. While it is the triglycerides that are the most common lipids found in nature, the mono- and diglycerides were used to help understand the reaction chemistry with each additional fatty acid group along the glycerine backbone.

The model catalyst used in this study was H-ZSM-5, a benchmark catalyst widely used for determining the cracking chemistry of hydrocarbons. Discovered in the mid-1970's, ZSM-5 is a highly acidic, highly crystalline shape-selective catalyst with bidirectional, intersecting channels [13, 14]. The ZSM-5 used in this work had an average pore size of 5.5 Å, 1 μm particle diameter, and a surface area of 425 m^2/g.

Chemicals

1-Monoolein, 1,3-diolein, and triolein were obtained from Larodan Fine Chemicals (Malmo, Sweden). Oleic acid, palmitic acid, and compound standards were obtained from Sigma-Aldrich. All chemicals were purchased at their highest available purity and were used without further purification. Carrier gas for the reaction/analysis system was helium utilizing the Built in Purifier, BIP® (AirGas, Radnor, PA). The ZSM-5, Si/Al = 23 and 280, catalyst was purchased from Zeolyst International (Valley Forge, PA). The catalyst was received in the ammonium form and then calcined at 550°C for 12 hours in air using a muffle furnace to produce the acidic form.

Reactions/Analyses

Reactions and analyses were performed using the Quatra C which utilized online chromatographic analysis and mass spectrometry. Glass catalyst tubes were used for reaction temperatures up to 400°C. Quartz tubes were used for higher temperature reactions to reduce any possible interactions with silaceous glass at high temperatures.

Chromatography of reactants and products was possible using a Restek Rxi-1ms (30m X 0.53mm, with a 1.50 μm film). This is an ultra-low bleed column with a temperature range of -60°C to 350°C. The thick film and sizeable temperature span allows for separation of a wide range of molecular weight compounds. The GC oven was programmed with an initial temperature of -20°C, held for 3 minutes and was then ramped to 10°C at 5°C/min, then ramped to 250°C at 10°C/min, and finally ramped to 320°C at 15°C/min and held for 3 min. Liquid carbon dioxide was used for cool-on-column analysis and was of refrigerant grade. Quantitation was performed using calibration curves from standard compounds.

The detector for this system was a Saturn 4D MS equipped with a quadrupole ion trap and waveboard technology allowing selected ion storage and selected ejection chemical ionization. The mass spectrometer was configured to operate in either EI (electron impact) or CI (chemical ionization) mode. Reaction runs operated in EI mode were segmented to analyze for different mass-charge ranges. Lower molecular weight compounds eluting during the first 10 minutes were scanned from 10 to 80 m/z, and then for the remainder of the chromatographic run the mass range was from 50 to 200 m/z to analyze higher molecular weight compounds. The difference between the two segments lies in the use of selected ion storage (SIS). During EI mode, SIS RF waveforms were

used to remove siloxane masses m/z (207, 281, and 355) from the spectra. This produced lower detection limits and full scan data for compound identification. Also, during the latter segmentation, mass spectra tuning parameters were used that would result in less fragmentation of hydrocarbon molecules during ionization. This shifts the mass/charge intensities away from the low end towards the high end, resulting in easier identification of compounds.

Performing Cracking Reactions

Cracking reactions were performed by first adding H-ZSM-5 catalyst to the reaction tube. Mass amounts varied between 5 to 25 mg. Silanized glass wool was used to hold solid catalyst in place and to reduce channeling through the catalyst. After filling, the reaction tube was placed inside the reaction zone of the Quatra C. The desired temperature was set, and the catalyst was allowed time for off-gassing of water vapor. The air/H_2O indicator for the mass spectrometer was monitored, and once within acceptable levels, the reaction/analysis was initiated. Operating the mass spectrometer with too much air or H_2O can burn-out the detector filament; therefore, air levels below 0.5 amu and H_2O levels below 15% were used as indicators to ensure long-term use of detector filament.

The carrier gas, helium, was set to have 20 mL/min flow through the catalyst bed and through the chromatographic column. To measure this flow, a GC flow meter was used to measure 19 mL/min venting from the open-split interface. The open-split

interface is designed to always allow 1 mL/min to the mass spectrometer. The split flow for the reactant injector was held at 24 mL/min.

Reactions were performed by placing ~1 mg of reactant inside a glass crucible to be used with the Chromatoprobe. Each reaction condition was tested in duplicate, and quantitation of compound peaks was made while operating mass spectrometer in EI mode. Chemical ionization experiments were performed immediately following the EI experiment, and thus, used the same catalyst bed as the EI run. This proved to be acceptable as the number of peaks, along with their respective retention times, in CI mode corresponded well with those in the EI mode.

Thermal Gravimetric Adsorption

Thermal gravimetric adsorption (TGA) was used to determine the mass of coke deposited on the catalyst during the cracking reactions. The TGA instrument used was manufactured by Thermo Cahn.

CHAPTER V

REACTIONS OF FATTY ACIDS IN SUPERACID MEDIA: IDENTIFICATION OF EQUILIBRIUM PRODUCTS

The present work seeks to establish fundamental information on the cracking of plant, animal, and microbial oils by reacting model compounds with a model Bronsted acid catalyst. This phase of the project focuses on the homogeneous catalytic cracking of oleic and palmitic acids, major components of plant and animal oils, using the superacid trifluoromethanesulfonic acid (triflic acid). These two organic acids were chosen as models of the major components in plant and animal oils. For example, oleic acid, or *cis*-9-octadecenoic acid, is an 18 carbon fatty acid with a symmetrically placed double bond. Palmitic acid, or hexadecanoic acid, is a 16 carbon saturated fatty acid.

The choice of the model catalyst was dictated by the need to examine the effect of Bronsted acidity alone on the cracking of the organic acids in the absence of thermal cracking. Thus, we chose an acid that could be used at sufficiently low temperatures so as to suppress thermal cracking. Triflic acid is 100 times more acidic than fuming sulfuric acid with a Hammett acidity of -14.1 [61]. Superacids are capable of catalyzing a host of organic chemical reactions, such as isomerization, cracking, alkylation,

acylation, and carboxylation at temperatures near room temperature [21, 27]. The use of a liquid acid as a model catalyst eliminates the effects of pore sizes and solid crystallinity upon the reactivity results.

The objective of this phase of the project was to determine if the Bronsted acidity of triflic acid was capable of cracking and decarboxylating oleic and palmitic acid. In most experiments, evidence of fatty acid cracking was collected by determining equilibrium products. Positive results from triflic acid reactions do not assure cracking and decarboxylation of oleic acid via the Bronsted and Lewis acid sites present in zeolites. However, negative results with the super acid would suggest that the intrinsic acidity of zeolites may not be capable of achieving cracking and/or decarboxylation. To our knowledge, the effect of acidity on the product distribution of cracking oxygenated feedstocks using zeolites has not been isolated from thermal cracking, crystalline structure, and pore size.

Results and Discussion

In the case of palmitic acid, there appears to be no change upon reaction with triflic acid at either 25 or 100°C reaction temperatures. None of the analytical techniques employed indicated otherwise. The saturated fatty acid offered no place for which the triflic acid could protonate. Higher temperatures could perhaps allow protonation to occur at the carboxylic acid. This, however, would require vapor phase reactions and would induce thermal affects, neither of which were within the scope of this work.

Reactions for NMR and FTIR analysis were allowed to run to completion. Proton NMR analysis of oleic acid indicated vinyl protons (5.34 ppm chemical shift) and

allylic protons (2.01 ppm). Analysis of the extract of the organic-phase, post-reaction (Fig. 5.1) indicated a loss of both vinyl and allylic protons; thereby, indicating saturation of the double bond. The absence of vinyl carbons was confirmed with ^{13}C-NMR analysis. The peak at 180 ppm indicates the presence of the carbonyl group of the carboxylic acid in both the starting material and the products. GC/MS results (Fig. 5.4 and 5.5) show that a multitude of fatty acids of varying molecular weights were produced. This is also supported by ^{1}H-NMR (Fig. 5.1) data where the relative ratio of the CH_3 band at 0.87 ppm of the proton spectra is about 2:1 for reacted versus unreacted oleic acid, which suggests an increase in the number of methyl groups, probably due to branching along the carbon chain. In the FTIR spectrum (organic phase), the band at 1,710 cm^{-1} (Fig. 5.2) is consistent with the carbonyl bond of a carboxylic acid. The well-defined bands between 2,800 and 3,100 cm^{-1} are due to C-H stretching within the aliphatic molecule with weak O-H absorption from the carboxylic acid, which is consistent to the spectra for hexadecanoic acid. An interesting feature of the NMR spectra is the lack of aromatic resonances between 6 – 8.5 ppm in the ^{1}H-NMR spectra and between 120 – 160 ppm in the ^{13}C spectra.

These results suggest that the Bronsted acid reacts with long chain unsaturated fatty acids at the double bonds (Fig. 5.3). Aqueous samples from the aqueous, quenching step showed no evidence for compounds other than inorganics, as confirmed by NMR and FTIR analysis of these samples.

Results obtained from GC/MS (Fig. 5.4 & 5.5) are consistent with those from NMR and FTIR indicating the presence of a multiplicity of saturated fatty acids. CI mass

spectral data (Fig. 5.6) yielded molecular weight information. Reaction products were characterized using mass spectrometry according to molecular weight and structural type using standards from Sigma Aldrich and with the aid of the MS software. Samples were prepared for mass spectral analysis by quenching the reaction after only 10 minutes so as to minimize secondary reactions. The only qualitative difference between the shorter term reaction and longer runs was the absence of the unreacted oleic acid at longer reaction times. The peak distributions for the remaining peaks were very similar (Fig 5.4 & 5.5).

The cracking products from oleic acid (Fig. 5.4 & 5.5) yielded a complex mixture, mostly fatty acids, that have been identified within the liquid organic product. The compounds identified were C9, C10, C11, C12, C13, C14, C16, and C18 fatty acids. As indicated from the NMR and FTIR data, the fatty acids present in the product were saturated, and according to the NMR and GC/MS, many branched-chain isomers were present in the products (Fig. 5.6).

It appears that in all cases that the carboxylic acid group was unchanged by the reaction, and the logical first step in the reaction is protonation of the oleic acid by the triflic acid at the carbon-carbon double bond. Then, the position of the charge on this protonated intermediate probably migrates away from the carboxylic acid end of the molecule. This migration trend is supported by the lack of fatty acid compounds less than 9 carbons length indicating that the smallest fatty acid (i.e. C9:0) results from cracking while the double bond is in its initial position. Longer chain fatty acids result as the intermediate charge migrates away from the carboxylic acidic end before cracking.

Table 5.1 shows the fatty acids quantified using standards and the total fatty acids for each molecular weight group that have been identified using mass spectral analysis. To quantitate the branched compounds, peak areas were compared to that of the corresponding fatty acid straight chain compound. The mass of organic liquid product accounts for 83% of the original mass of the oleic acid, and the total identified products were 87% of the methylene chloride extractable mass.

Figure 5.7 shows one possible reaction scheme for the cracking of oleic acid. Step 1 is the protonation of the double bond. Step 2 is the migration of the charge by hydrogen transfer. Step 3 is the cracking of the molecule into shorter chain carboxylic acids and hydrocarbon gases. The reaction shown is the production of hexadecanoic acid (C16:0) and ethylene.

Table 5.1. Product Distribution for Oleic Acid Reacted to Completion

Compound Name (Scientific)	Compound Shorthand	Straight-Chain Concentration (mg/ml)	Total Isomeric Concentration (mg/ml)
Nonanoic Acid	C9:0	3.073	3.073
Decanoic Acid	C10:0	0.361	1.115
Undecanoic Acid	C11:0	0.238	1.991
Dodecanoic Acid	C12:0	0.480	3.354
Tridecanoic Acid	C13:0	0.307	1.572
Tetradecanoic Acid	C14:0	0.452	0.412
Hexadecanoic Acid	C16:0	0.876	0.876
Octadecanoic Acid	C18:0	0.193	0.713
		Total	13.106

The chemical reaction that appears to be occurring is the loss of two carbons from the oleic acid molecule. This is seen from the formation of fatty acid carbon chain

with an even number of carbon atoms. Odd numbered fatty acid chain lengths are probably formed from methyl shifts occurring before the β-scission. It is speculated that the formation of stearic acid (C18:0) comes from hydride abstractions.

The results presented for the cracking of oleic acid are consistent with the cracking of olefins in which the formation of saturated products proceeds *via* hydrogen transfer [20]. Likewise, olefins undergo series of hydrogen and methyl shifts due to the formation of carbenium ions producing secondary and tertiary carbocations. These carbocations experience double bond migrations, controlled by thermodynamic stabilities, producing olefinic cations before undergoing β-scission. Similarly to our work, the source of hydrogen in olefinic cracking reactions is not fully understood. It is suggested that H^- is abstracted from aromatic compounds that are produced during the cracking reaction [20, 26 – 28].

Conclusions

Strong Bronsted acids are capable of cracking unsaturated fatty acids into smaller carbon chain fatty acid molecules that can contain branched isomers. However, these strong acids did not crack saturated fatty acids. This suggests that acids with Bronsted activities attack the fatty acid molecule at the carbon-carbon double bond site. Protonation of the molecule results in a series of hydride shifts and methyl shifts along with β-scissions producing a series of branched chain fatty acid molecules. Neither fatty acid, saturated or unsaturated, could be decarboxylated using triflic acid in the liquid phase.

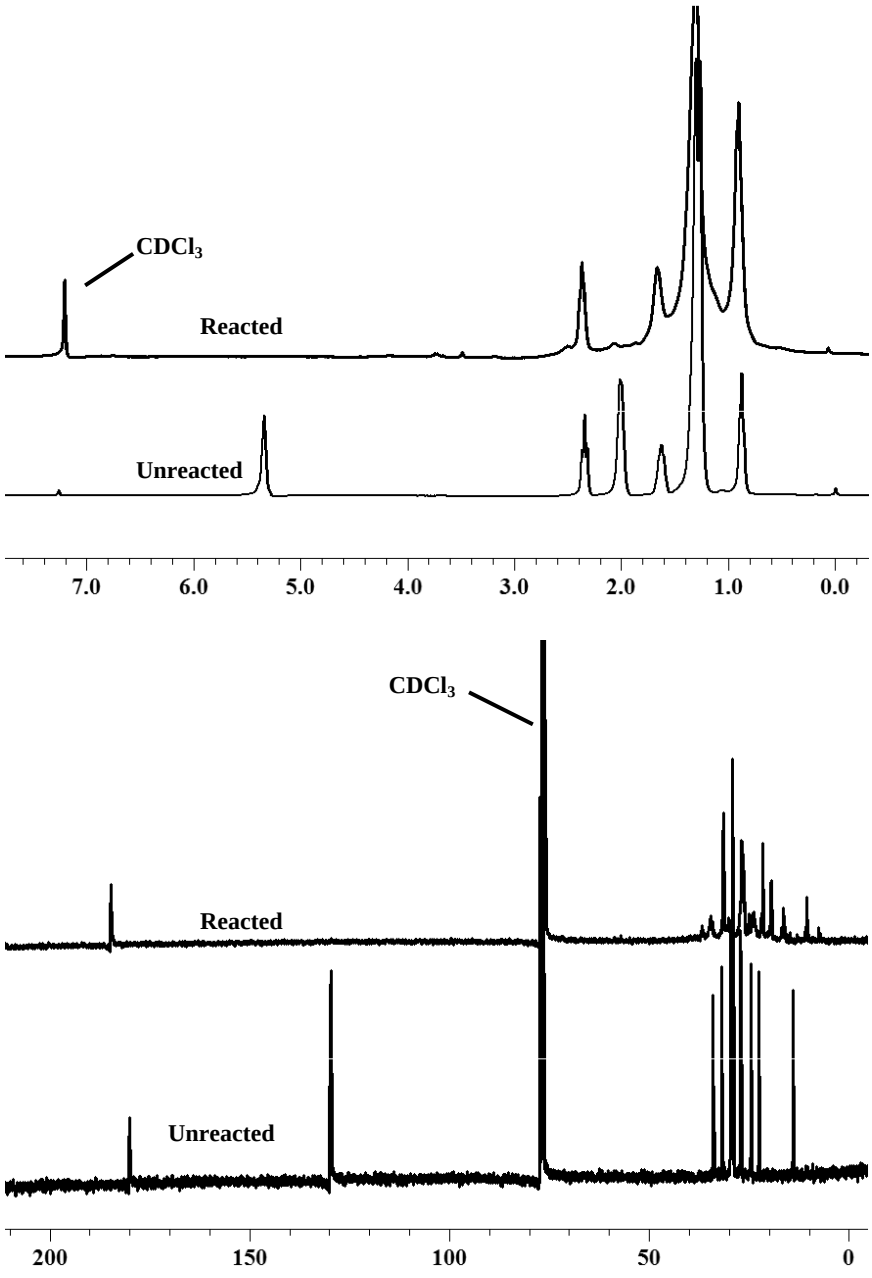

Figure 5.1. NMR Spectra for Oleic Acid/Triflic Acid Cracking

NOTE: (top) ^{1}H-NMR of oleic acid; (bottom) ^{13}C NMR of oleic acid. Reactions for NMR analysis were allowed to run to completion.

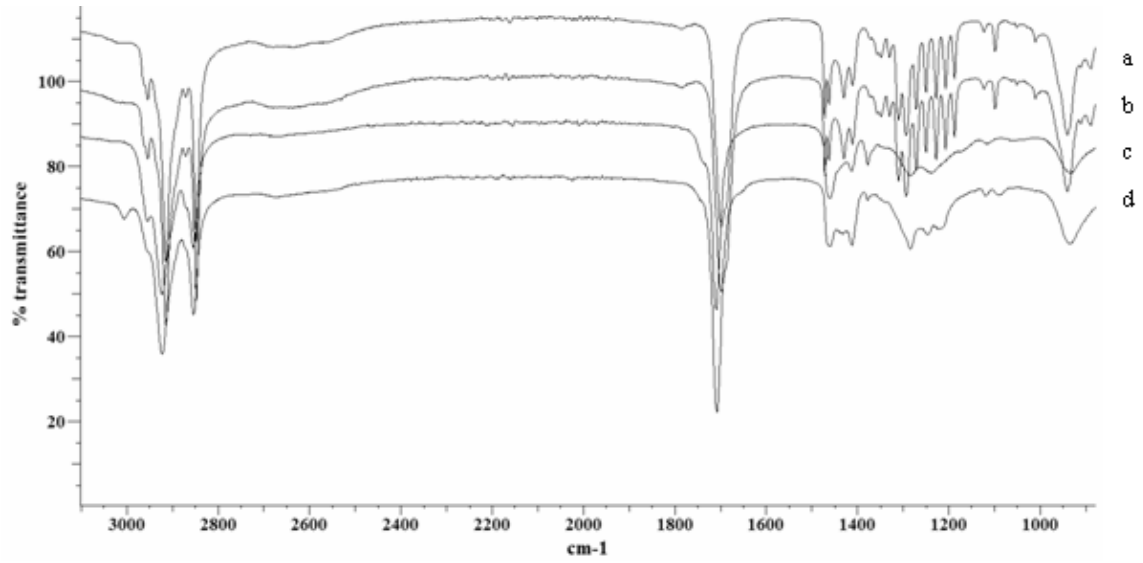

Figure 5.2. FTIR analysis of unreacted/reacted fatty acids.

NOTE: (a) palmitic acid reacted to completion at 25°C; (b) unreacted palmitic acid; (c) oleic acid reacted to completion at 0°C; (d) unreacted oleic acid.

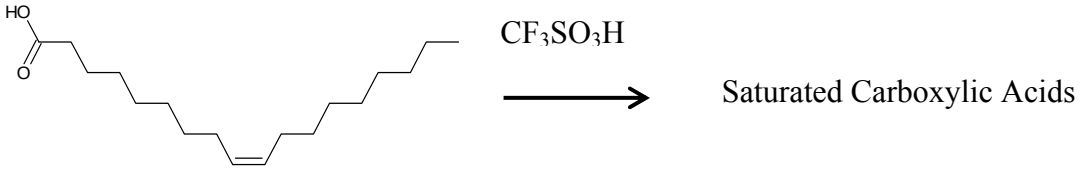

Figure 5.3. Reaction of oleic acid with triflic acid as suggested from the NMR and FTIR analysis

NOTE: Reaction temperature 0°C.

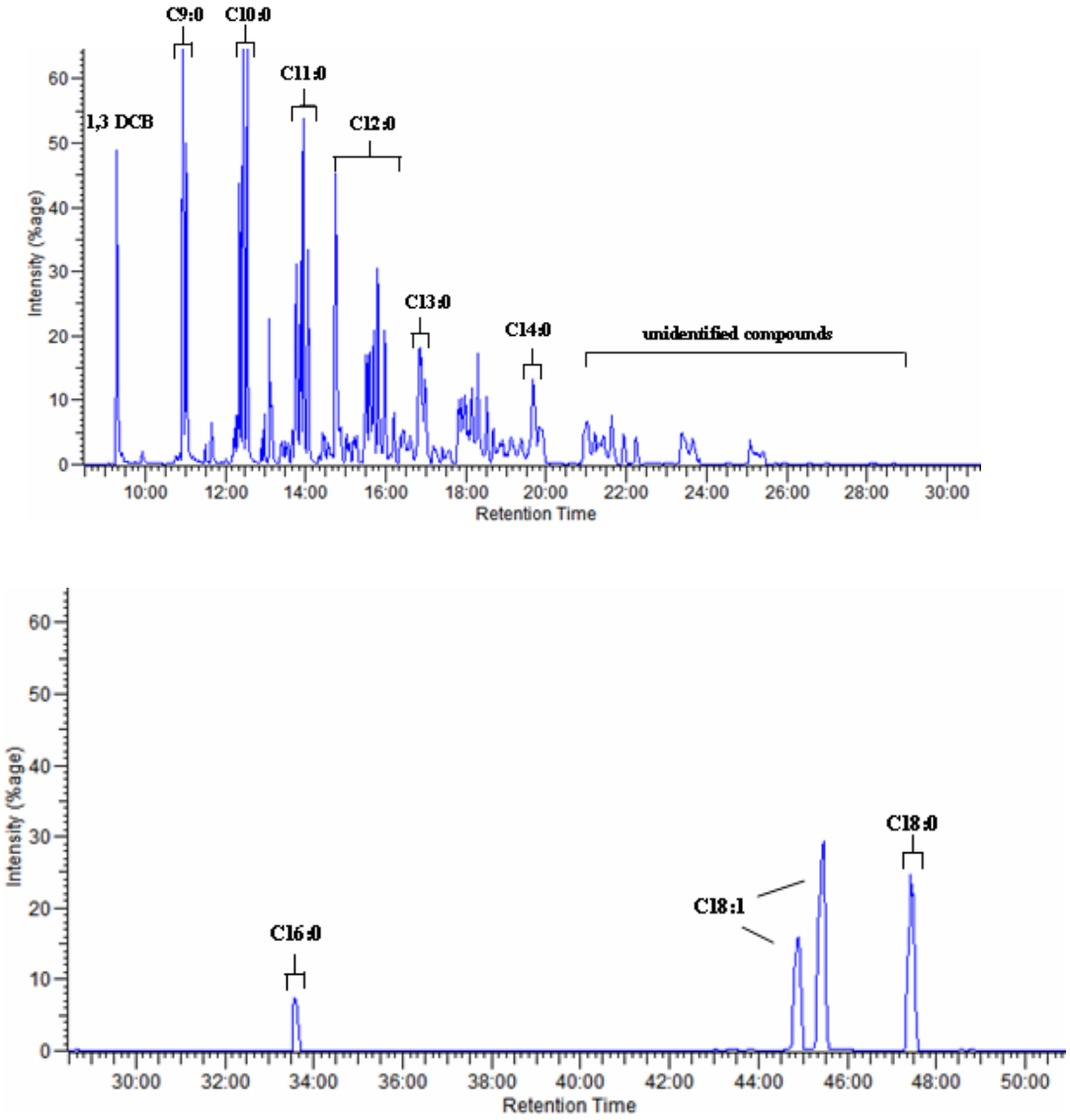

Figure 5.4. GC/MS total ion chromatogram (Chemical Ionization) for oleic acid

NOTE: Oleic acid was subjected to 10 min triflic acid reaction. Chromatograms are shown for retention times 8 to 30 minutes (top) and out to 48 minutes (bottom).

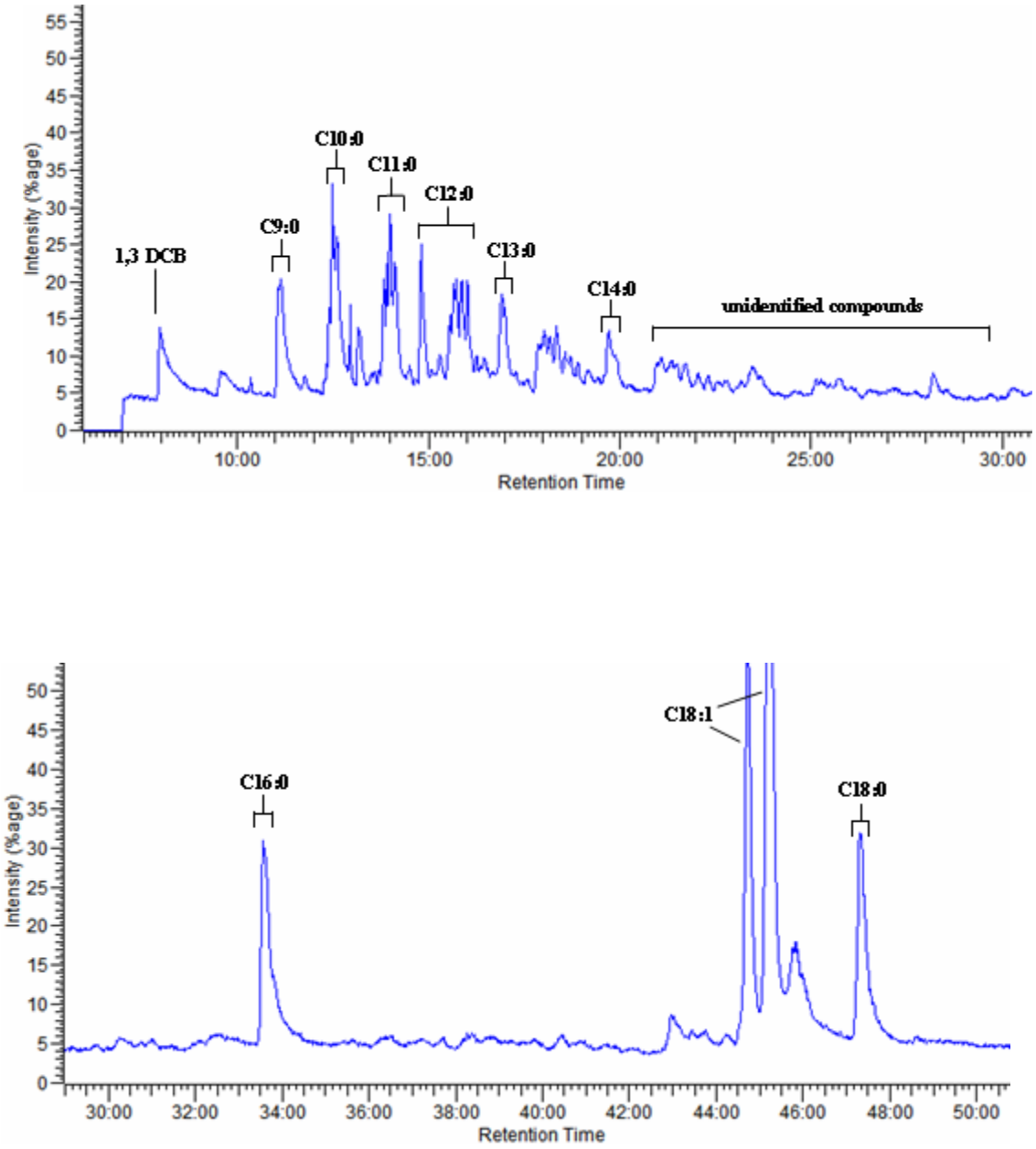

Figure 5.5. GC/MS total ion chromatogram (Electron Impact Ionization) for oleic acid

NOTE: Oleic acid was subjected to 10 min triflic acid reaction. Chromatograms are shown for retention times 8 to 30 minutes (top) and out to 48 minutes (bottom).

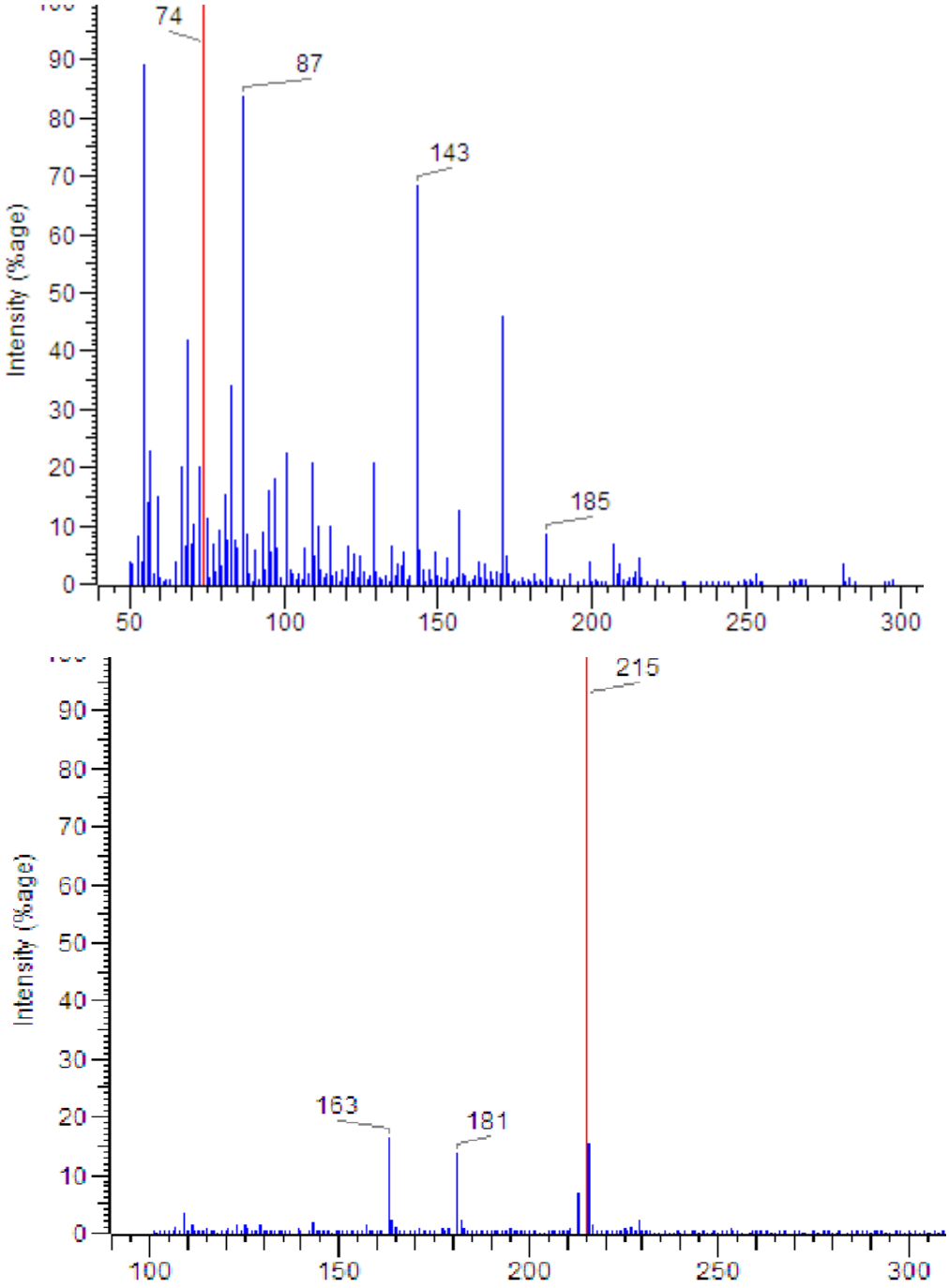

Figure 5.6. Example of mass spectral data: Electron Impact Ionization (top) and Chemical Ionization (bottom) for C12:0.

NOTE: The (m+1) ion from CI is 215, corresponding with that of dodecanoic acid methyl ester.

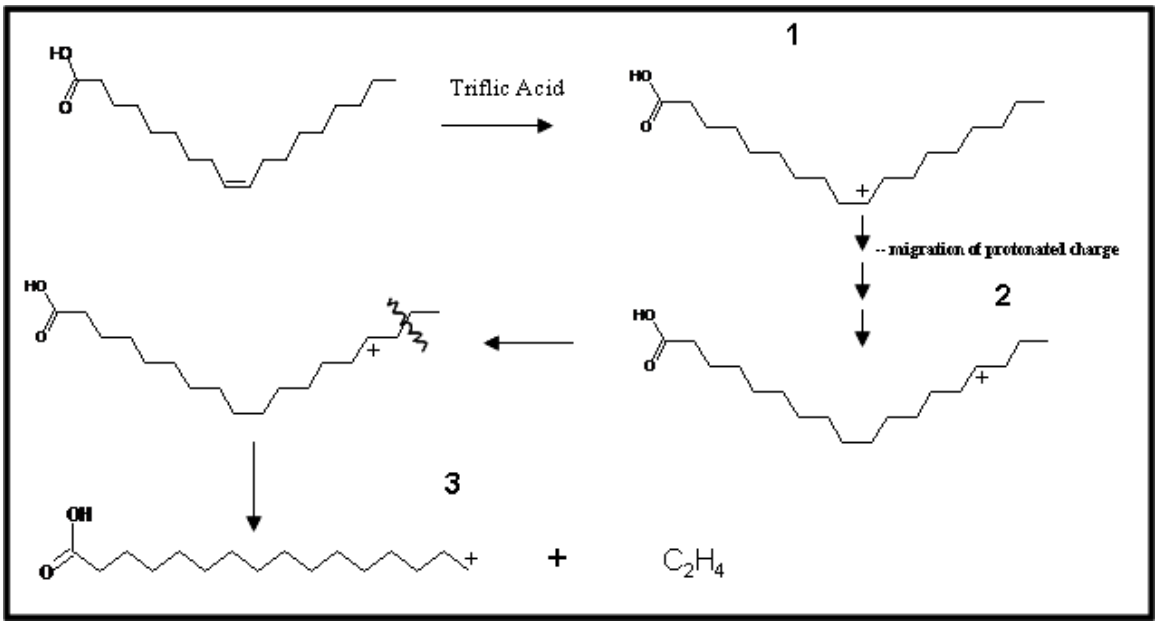

Figure 5.7. Proposed reaction chemistry for the cracking of oleic acid into saturated, shorter chain carboxylic acids.

NOTE: This particular example shows the production of hexadecanoic acid and ethylene.

CHAPTER VI

DEVELOPMENT OF A HETEROGENEOUS CATALYTIC CRACKING REACTOR UITLIZING ONLINE MASS SPECTROMETRY ANALYSIS

Introduction

In most chemical laboratory experiments, analysis of the reaction products can be a complex task, especially in the gas phase. Most experiments require a series of post reaction steps prior to analysis that may include separation of small molecular weight gases from heavier compounds. Condensation of the gaseous product stream may be required before analysis. These sample preparation steps increase the complexity, time required, and data variability. In this work, we have developed a catalytic cracking unit that is coupled directly to online GC/MS for analysis of products and unreacted material.

One valuable application of this device is the investigation of reaction chemistry of the catalytic cracking of oxygenated compounds such as fatty acids and other lipids. The products of these reactions may be useful as transportation fuels. Bakhshi and co-workers have investigated the cracking of canola oil and bio-oils on various catalysts [4 – 9]. The products from these catalytic reactions were CO and CO_2, and organic compounds including aliphatics, aromatics, alcohols, and ketones. Though these findings

are significant in the development of renewable fuels, little is known about the cracking chemistry of oxygenated compounds. This information will be necessary as ideal catalysts and reaction conditions are sought for industrial applications. Therefore, a tool that is capable of analyzing the initial reaction products as these compounds are decarboxylated and cracked is required.

The basis for this device, termed Quatra C (Cryogenic Capillary Catalytic Cracker), is an extension of Py-GC/MS (pyrolysis – gas chromatography/mass spectrometry) [62] and RGA/MS (residual gas analyzer/mass spectrometry) [63] and allows one to quickly test the performance of a reaction on a specific catalyst. Py-GC/MS is a pyrolysis reactor capable of performing high temperature reactions with online GC/MS analysis. RGA/MS is a mass spectrometer that operates in series with a reaction device to perform continuous analysis of reaction products. The uniqueness of the Quatra C is that it has a heterogeneous catalytic reactor that is an integrated component of the gas chromatograph, making it user friendly and far less expensive than conventional laboratory catalytic reactors. The catalyst tube, which can be glass or quartz, is easily serviceable allowing quick changes from one catalyst loading to another. The objective of this work was to devise a system that would be capable of performing heterogeneous chemical reactions with direct, rapid qualitative and quantitative analysis for the development of catalytic reaction mechanisms and optimization of these reactions.

One problem associated with this internal reactor is that the GC column inlet is subjected to temperatures above its normal operating limits. This leads to increased column degradation and column bleed, allowing higher levels of siloxanes to enter the

mass spectrometer. This reduces the sensitivity that can be achieved. To help solve this problem, selected ion storage RF waveforms were used to eject unwanted siloxane ions (mass to charge ratios 207, 281, and 355), from the quadrupole ion trap [52 – 55]. Elimination of these ions from the MS results in reduced chemical noise producing chromatograms with lower detection limits and enhanced National Institute of Standards and Technology (NIST) (Gaithersburg, MD, USA) library searches.

Materials and Methods

Reaction/Analytical Equipment

A Varian (Walnut Creek, CA, USA) 3600 gas chromatograph with front and rear injectors was used both as a reactor and for GC separations. The chromatographic column selected was a Restek (Bellefonte, PA, USA) Rxi-1ms (30m X 0.53mm, with a 1.50 μm film). This is an ultra-low bleed column with a temperature range of -60°C to 350°C. The thick film and sizeable temperature span allows for separation of a wide range of molecular weight compounds. A Varian Chromatoprobe was utilized for direct injection of solid samples using a temperature programmed injector. An open-split interface, manufactured by SGE Analytical Science (Victoria, Australia), was utilized on the column outlet to split the flow of analytes entering the mass spectrometer and to maintain constant flow on the detector. The detectors for this system were a Saturn 4D MS equipped with a quadrupole ion trap and waveboard technology allowing selected ion storage and selected ejection chemical ionization and a thermal conductivity detector for accurate analysis of fixed gases.

Chemicals

To validate the instrument, H-ZSM-5, a heterogeneous catalyst obtained from Zeolyst International (Valley Forge, PA, USA), was used. The catalyst was received in the ammonium form and then calcined at 550°C for 12 hours in air using a muffle furnace to produce the acidic form. The H-ZSM-5 catalyst used in this study had a particle diameter of ~1μm, surface area of 425 m^2/g, and pore diameter of 5.5Å. The validation experiments were carried out using 0 to 25 mg catalyst at 400°C and 11.0 mL/min helium flow. All chemicals (hexane and analytical standards) were obtained from Sigma-Aldrich at their highest available purity and were used without further purification. Liquid CO_2 was used for cool-on-column analysis and was of refrigerant grade. To reduce contamination and moisture concentration in both the chromatographic system and mass spectrometer, the BIP (Built in Purifier) helium technology from AirGas (Radnor, PA), was used to purify carrier gas. The BIP delivers ultra-high purity gas and is more reliable by replacing external, in-line purifiers that require maintenance. BIP helium has specifications of <10 ppb O_2, <20 ppb H_2O, <100 ppb total hydrocarbons, and <5 ppm N_2. This resulted in a cleaner analysis reducing stationary phase bleed and poor resolution due to GC column degradation. This is critical in identification of complex chromatograms with multitudes of overlapping unknowns.

Reactor/Analyzer Development

A device was desired that could accept solid, liquid, or gaseous reactants, which could then react on a catalyst bed, and the reaction products determined, both qualitatively and quantitatively. To do this, several features of the GC needed to be

redesigned and augmented for analysis of the reactions. The concept was to inject a reactant into the front injector of the GC and allow the reactant to flow via a heated transfer line to the rear injector which houses the catalyst bed, where the reaction occurs. The helium carrier gas then transfers the products onto the GC column for chromatographic analysis (Fig 6.1). The temperature for each section, reactant injector, catalytic reactor, and GC oven, can be independently controlled and monitored throughout the reaction sequence.

The front programmable injector was raised approximately 1.5 inches to allow for addition of a transfer line from the front injector to the reaction tube (rear injector). An aluminum platform was constructed on which to position the front injector. The transfer line from the injector to the catalyst tube was 1/8 inch stainless steel tubing heated isothermally by heating tape that was controlled with a rheostat placed externally to the machine.

A brass endcap was used to replace the septum and septum nut on top of the reaction zone. Catalyst bed operating temperatures were greater than which high temperature septa could be obtained. Otherwise, only flow combination modifications were necessary to convert the rear injector to a catalyst reactor.

An open-split interface was installed to control the volume of gas entering the mass spectrometer so that the gas velocity through the catalyst bed could be varied without affecting the performance of the mass spectrometer. This interface was heated in a typical GC ionization detector block so that temperature could be controlled through the GC control system. The operating temperature of the splitter, 325°C, was the same as for

the transfer line going into the MS. Split ratio was controlled by adjusting the flow of helium through the restrictor orifice of the interface.

The reaction zone was fabricated from ¼ inch OD glass tubing (7.2 cm long X 3.9mm ID) that had been thoroughly cleaned using sonication with acetone and methanol (30 min each) and then heat treated in a 500°C furnace. The cooled glass catalyst tubes were packed with catalyst using silanized glass wool above and below the catalyst matrix to hold catalyst in place and minimize channeling. To maintain constant hydrodynamics inside the reactor, silica gel (200/400 mesh) was mixed with the H-ZSM-5 in an appropriate amount to keep a constant total amount of solids.

The mass spectrometer was configured to operate in either EI (electron impact) or CI (chemical ionization) mode. During EI mode (Fig 6.2), selected ion storage RF waveforms were used to remove siloxane masses m/z (207, 281, and 355) from the spectra. This produced lower detection limits and full scan data for compound identification. Reaction runs operated in EI mode were segmented to analyze for different mass-charge ranges. Lower molecular weight compounds eluting during the first 15 minutes were scanned from m/z 10 to 50, and then for the remainder of the chromatographic run the mass range was from 50 to 425 m/z to analyze higher molecular weight compounds.

Screening experiments using calibration standards were performed to determine the optimum timing for mass/charge segmentation of the mass spectrometer based on retention times between lower and higher molecular weight compounds. The GC oven was programmed with an initial temperature of -40°C, held for 3 minutes and was then

ramped to 10°C at 5°C/min, then ramped to 50°C at 25°C/min, and finally ramped to 130°C at 10°C/min and held for 2 min. Using this oven program, a segmentation split for the mass spectrometer was chosen at a retention time between the elution of hexane and benzene. Benzene is the lowest molecular weight aromatic compound that was expected from the catalytic cracking of hexane. Segmentation allows for greater sensitivity due to inherent limitations to the maximum number of ions that can be stored within the ion trap. Selected ejection chemical ionization was used to confirm the molecular weight of the reaction products. Acetonitrile was used as CI gas. It has a more thermally stable ion adduct than most other commonly used chemical ionizing reagents [43, 44].

Instrument Validation

To validate this instrument, a series of reaction/analysis experiments were conducted using the solid catalyst H-ZSM-5. Due to the abundance of available literature, hexane was chosen as the test reactant. The cracking of hexane results in compounds with molecular weights not amenable for acetonitrile CI analysis, so EI was used for product identification. The NIST library was used to aid in compound identification. Quantitation of compounds was performed from calibration curves using C_1-C_6 paraffin and C_2-C_6 olefin gas standards manufactured by Scotty Specialty Gases, Inc. and Gasoline Range Organic standard obtained from Supelco.

Figure 6.3 shows a typical chromatogram with the elution of low molecular weight products near the front end and aromatic compounds after the elution of unreacted hexane. The application of different mass range segments during different elution times gave lower detection limits for low molecular weight compounds which allowed

for easier interpretation of chromatograms and mass spectra.

An important goal in the design of the Quatra C was the ability to provide reproducible results with an acceptable amount of error. To assess this aspect, a series of replicate experiments were performed to determine reproducibility. Using 5 mg H-ZSM-5 catalyst, 1.0 mL hexane headspace (i.e. liquid hexane in helium atmosphere), and catalyst tube linear velocity of 1.0 cm/s, six reaction/analysis runs were performed. These reactions had an average percent conversion of 13.0 ± 0.5 and an average unreacted hexane concentration of 522 ± 3.09 μg. These results verify that this instrument system can deliver reproducible data with low variability for heterogeneous cracking reactions.

For statistical validation, duplicate reactions/analyses were performed and error bars have been included in Figures 6.4 and 6.5. All statistical error was calculated from plus and minus one standard deviation. Six reactions/analyses (plus duplicates) were performed (0 to 25 mg catalyst) to determine the extent of hexane cracking with increasing reaction residence times (Table 6.1). Experiments were conducted by injecting 0.5 mL headspace volume into the reactant injector. Reactions with no catalyst, but with silica gel and glass wool, were performed to determine what thermal affects, if any, occur in the cracking of hexane.

Table 6.1. Experimental results for statistical validation of the Quatra C.

Runs	Mass Catalyst, mg	Linear Velocity, cm/s	Headspace Inject Vol., mL	Avg. Conv, %	Std. Dev.	Unreacted Hexane, µg	Std. Dev.
1 – 2	0	1.5	0.5	<1	-	300	-
3 – 4	20	1.5	0.5	70	1.2	88.8	0.36
5 – 6	5	1.5	0.5	6.1	0.24	279	0.72
7 – 8	15	1.5	0.5	32	3.47	201	10.30
9 – 10	10	1.5	0.5	20	1.33	238	3.94
11 – 16	5	1.0	1.0	13	0.52	522	3.09
17 – 18	25	1.5	0.5	79	1.16	62	3.49
19 - 20	17	1.5	0.5	59	1.37	121	4.12

These results have demonstrated the effectiveness of catalytic cracking on the laboratory scale with small amounts of catalyst, thereby reducing costs of experiments while maintaining integrity of results. Validation tests of the Quatra C correlated well with literature values for the cracking of hexane on H-ZSM-5 catalyst for all products except for ethene/propene and for butane (Fig 6.5). These exceptions can be attributed to conversion differences, 70 vs. 81, and catalyst Si/Al ratios, 23 vs. 36, for the Quatra C and the literature [64] values, respectively. It should also be noted here that direct comparison of results is difficult considering that fixed bed catalytic reactors found in most laboratories use continuous reactant flow methods for reactions rather than as a single pulse. These reactors use ~1g catalyst, compared to 25 mg for the Quatra C, and samples are taken at timed intervals. We feel that these differences are small when one compares the Quatra C and literature data sets. Furthermore, control experiments yielded no reaction from thermal effects and do not appear to have any effect on the catalytic cracking of hexane.

Figure 6.4 shows the percent conversion of hexane with different catalyst amounts. The initial reaction of hexane to cracked products is first order in hexane concentration and thus at low reactant conversion these kinetics should be observed [64 – 67]. However, at higher hexane conversions, the secondary reactions become apparent, such as coke formation, which are not first order. Thus, we expect that data of hexane conversion at large values of space-time will

not observe linear kinetics. These expectations apparently are confirmed when one plots ln(1-hexane conversion) versus mass of catalyst at constant carrier gas flow rate and at constant temperature (Fig. 6.4). The low conversion data (< 30%) appear to fit to a straight line; whereas the high conversion data falls much above an extension of this line. Notice also, that the extrapolation of the low conversion data to zero conversion does not intersect the origin thus reflecting that the space-time is not the same as the residence time in the reactor [20]. If the conversion is positive at zero space-time, *ergo* mass, then one might explain this result due to the strong adsorption of the reactants on the catalyst surface. On the other hand, if the conversion is negative at zero space-time, then bypassing of the "reactive" catalyst could explain the data as might be the case of a small amount of reactive catalyst that is diluted with inert solids in a short bed (L/D < 10).

These results have demonstrated the effectiveness of catalytic cracking on the laboratory scale with small amounts of catalyst, thereby reducing costs of experiments while maintaining integrity of results. Validation tests of the Quatra C correlated well with literature values for the cracking of hexane on H-ZSM-5 catalyst (Fig 6.5).

Conclusions

These results show that this instrument can be used to rapidly evaluate catalyst performance for different combinations of catalyst and reactants. Figures 6.6. and 6.7 demonstrate the usefulness of ion segmentation to evaluate the molecular ions of a desired product. By eliminating unwanted, high end ions

(i.e. those with m/z > 50), the quadrupole ion trap is capable of storing more of the lower m/z ions for greater sensitivity. Although CI was not used to identify the products formed from hexane cracking, in other experiments we have shown that the Quatra C is capable of performing CI analysis for compound identification.

The design of the Quatra C facilitates the quick removal and installation of catalyst beds. Catalyst beds can be packed with various amounts of catalyst and then stored in a desiccator until needed. One challenge with this system is optimization of chromatography while varying flow rates through the catalyst bed. Satisfactory chromatography was accomplished by lowering the amount of catalyst, thus reducing the amounts of reactant and products, preventing overloading of the GC column.

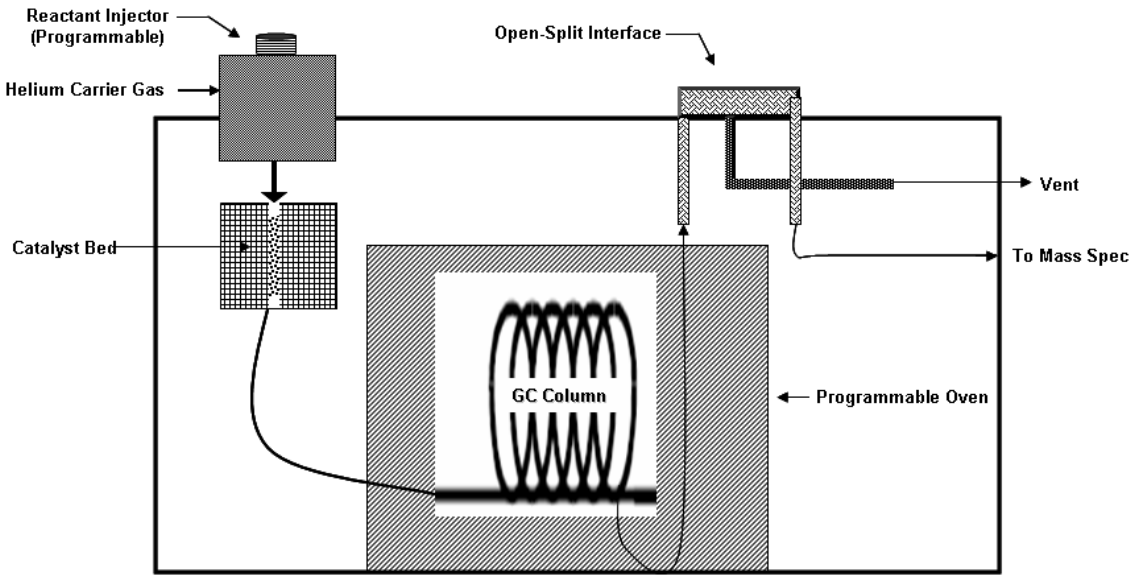

Figure 6.1. Diagram of Quatra C.

NOTE: This illustrates the rearrangement of the front injector and installment of the open-split interface.

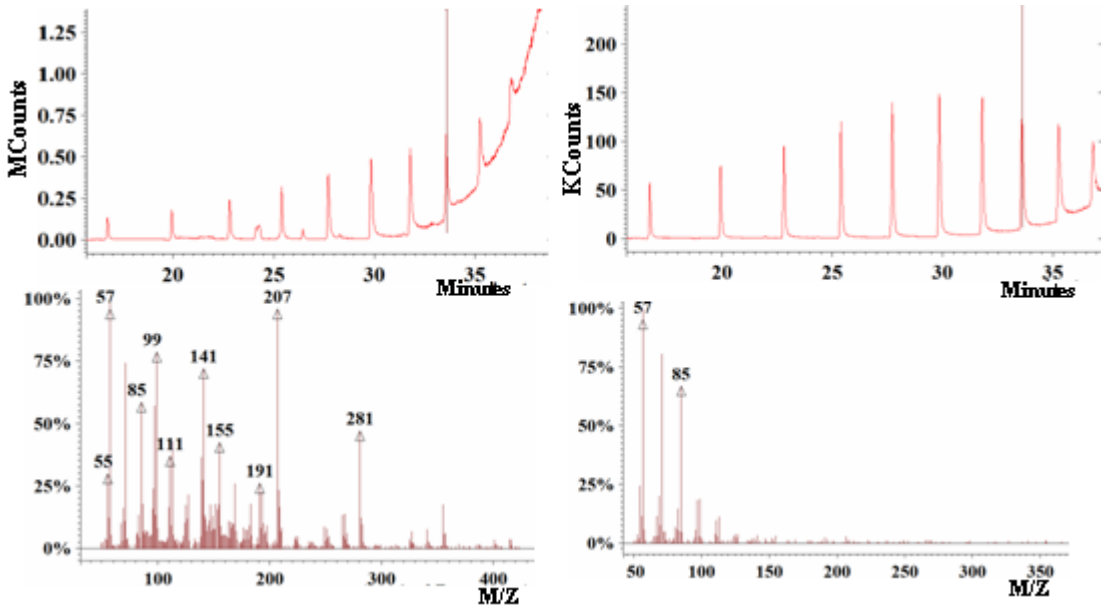

Figure 6.2. Comparison of total ion traces and electron impact ionization spectra.

NOTE: (left) without and (right) with selected ion storage for diesel range organics standards.

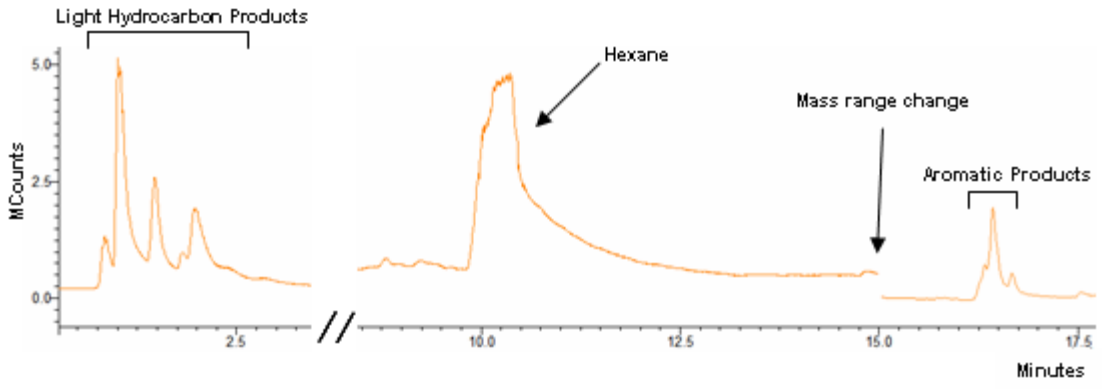

Figure 6.3. Typical EI total ion chromatogram for the cracking of hexane on H-ZSM-5.

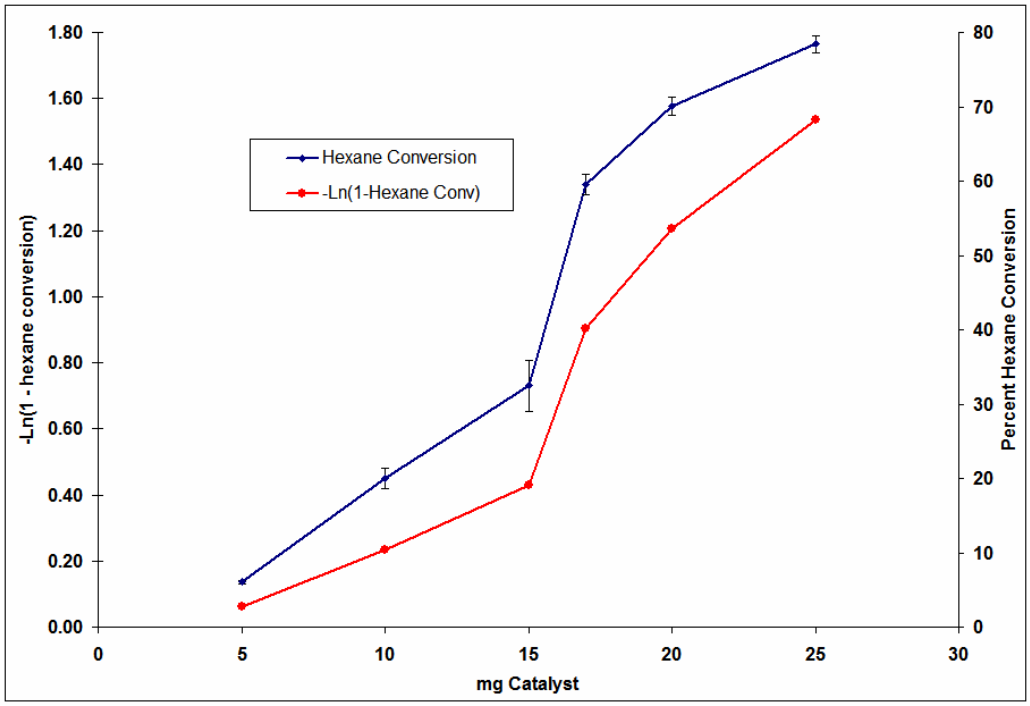

Figure 6.4. Correlation of amount of H-ZSM-5 catalyst (Si/Al=23) with conversion of hexane.

NOTE: T_{rxn}=400°C, Catalyst Tube Linear Velocity=1.535 cm/s.

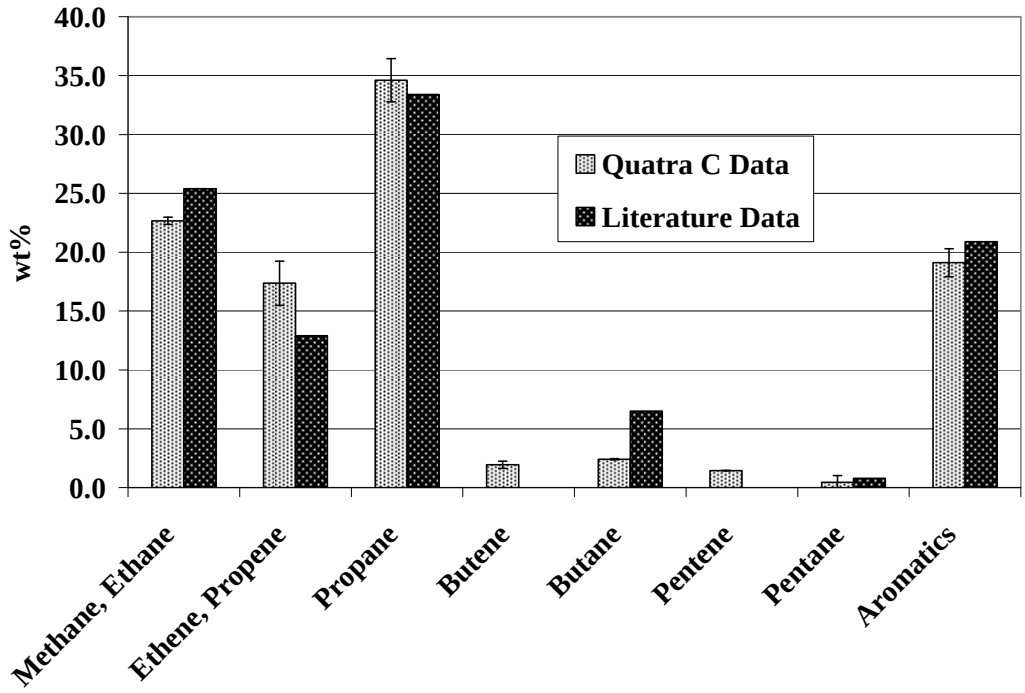

Figure 6.5. Comparison of hexane cracking products from the Quatra C to that found in literature.

NOTE: Quatra C data: T_{rxn}=400°C,70% conversion, Literature data: T_{rxn}=400°C , 81% conversion [60].

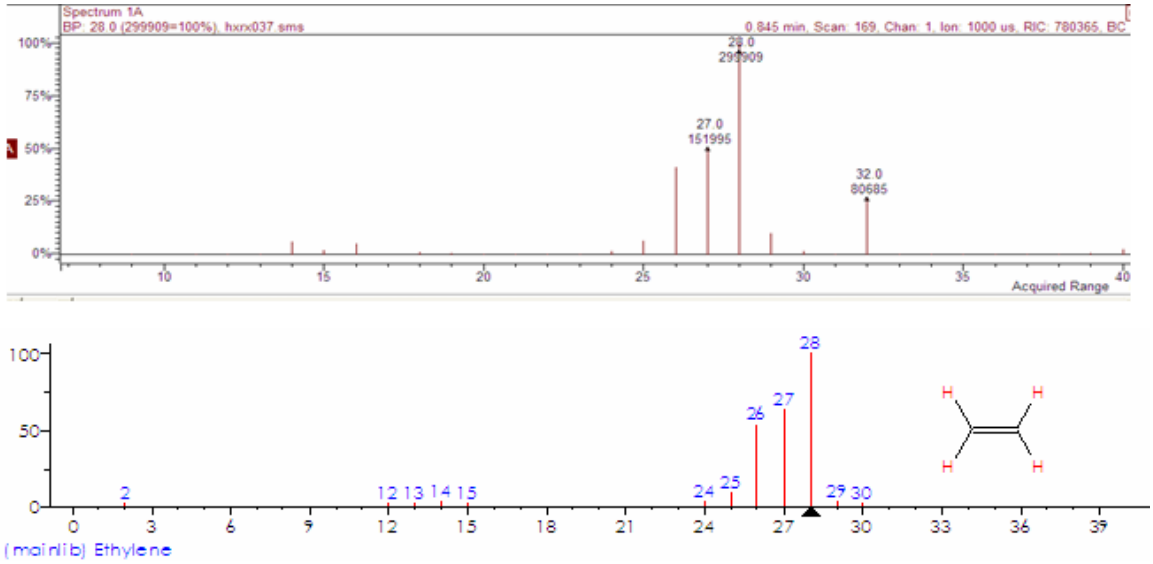

Figure 6.6. Comparison of Mass Spectra for Ethylene.

NOTE: (top) Obtained from the Varian software after hexane reaction on the Quatra C (data taken at 20% conversion), (bottom) Obtained from the NIST library.

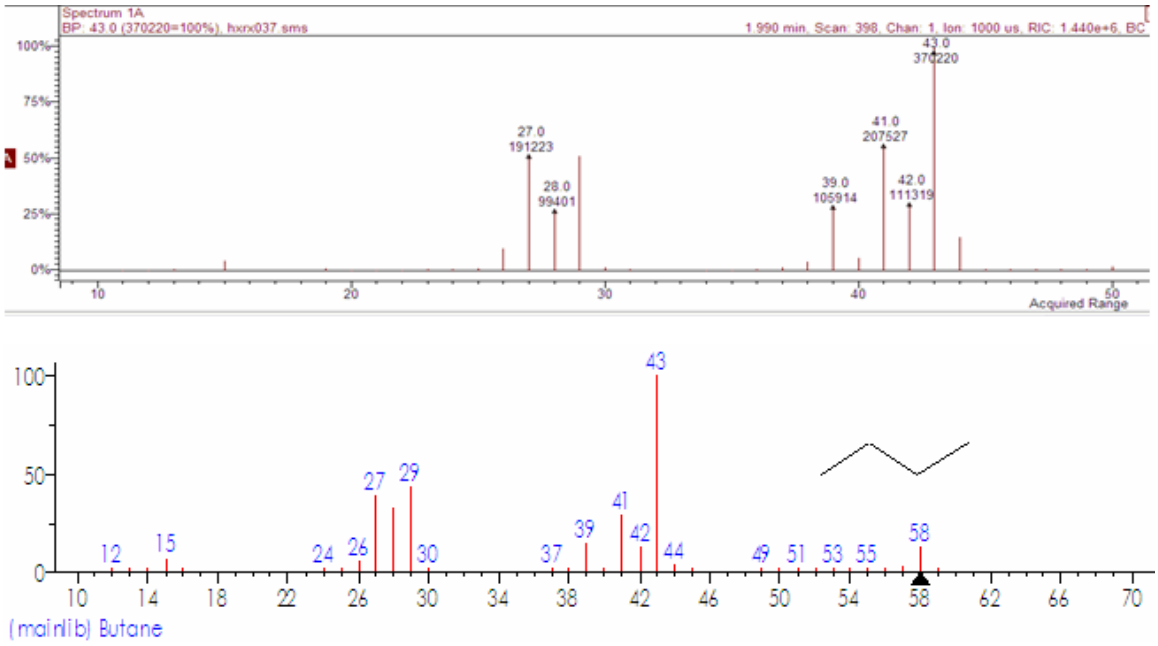

Figure 6.7. Comparison of Mass Spectra for Butane.

NOTE: (top) Obtained from the Varian software after hexane reaction on the Quatra C (data taken at 20% conversion, scanning M/Z 10 – 50), (bottom) Obtained from the NIST library.

CHAPTER VII

ELUICIDATION OF REACTION MECHANISM FOR THE CATALYTIC CRACKING OF ACYLGLYCERIDES ON H-ZSM-5

The present work seeks to establish the reaction mechanism for the heterogeneous catalytic cracking of acylglycerides. The acylglycerides studied were 1-monoolein, 1,3-diolein, and triolein. These lipids have a glycerol backbone with oleic acid as the fatty acid constituent. Oleic acid, which was also used in this study, is an 18-carbon unsaturated fatty acid with the double bond positioned between the 9 and 10 carbon position. The catalyst used was H-ZSM-5, which is a highly crystalline, highly acidic, and well studied zeolite [17, 18, 21]. Acylglycerides are found in many plant, animal, and microbial sources and have a potential use in the renewable fuels market. These glycerides were chosen as model reactants for the identification of reaction pathways of catalytically cracked lipids.

The catalyst, H-ZSM-5, used in this study has an intrinsically high acidity, mostly Bronsted, and was first synthesized by Mobil Research Laboratories (Princeton, NJ, USA) in the mid-1970's. It has a pore diameter of 5.4Å and a surface area of ~425 m^2/g. Although, H-ZSM-5 is not a commercially used catalyst, due to its instability at high temperatures, it works well for reaction mechanistic studies.

The objective of this phase of the project was to develop the specific reaction steps as glycerides are cracked into gasoline and diesel components. It was an important factor of this work to operate the reactions in a hydrogen free environment. Industrially operated hydrocrackers are fed hydrogen and operate at 2,000 psi and 1,400°F [68]. To our knowledge, the use of model glyceride compounds has not been studied to determine specific reaction steps during catalytic cracking.

Results and Discussion

For this study, the Quatra C was used for quick, online analysis of reaction products. As described in Chapter VI, the Quatra C uses small amounts of catalyst, usually 5 to 25 mg, and approximately 1 mg reactant for each experimental run. A typical reaction sequence begins with the loading of catalyst into a glass tube using glass wool to hold catalyst in place. The catalyst tube was then loaded into the reaction zone of the Quatra C and the temperature was raised to 400°C. Air and water were monitored using the mass spectrometer (MS), and reactions were not initialized until the air was within 5 amu and water less than 15% of H_2O^+/H_2O. Upon sufficiently low levels of air and water, reactions were run by injection of reactant (monoolein, diolein, or triolein) into the injection port.

Products were identified using MS and quantitated using TCD analysis. The chromatographic column used for the MS was an Rxi-1ms (30m X 0.52mm X 1.25µm) and the column used for the TCD was an RT-QPlot (30m X 0.53). The thick film, megabore column to the MS was selected for retention of compounds from C_1 to C_{30} hydrocarbons. The plot column to the TCD was selected for its ability to separate

fixed gases, as well as, gasoline range organics and naphthenic compounds that are precursors to coke. The temperature profile for the GC oven started at -40°C, hold for 5 min, ramp at 5°C/min to 60°C, then ramp at 8°C/min to 300°C, and finally hold for 12 min. The segmentation parameters on the MS were set to scan 10 – 80 for the first 10 min and then scan 50 – 200 for the remainder of the GC run.

Identification and Quantitation of Reaction Products

Figures 7.1 – 7.6 show the total ion chromatographs of reaction products for oleic acid and the mono-, di-, and triolein. Once a peak has been identified using MS methods, alignment of retention times using compound standards were used as further verification of a peak's identity. The overall product yields for the four reactants tested were (in mg/g) 453 for oleic acid, 68 for 1-monoolein, 323 for 1,3-diolein, and 216 for triolein. The largest difference between the compound identification of the oleic acid versus the glycerides occurs at the front-end of the chromatograms where C_1 – C_6 hydrocarbon gases elute. Due to the significantly higher yield, it appears from these results that oleic acid cracks more readily. Also, oleic acid cracking had a higher product yield in the light hydrocarbon gas range which may be the result of functional group differences between oleic acid and the esters of the acylglycerides.

Figures 7.7 – 7.10 show the product yields for all four reactants. Each of the reactants was reacted at 3 levels of catalyst loading (5, 10, and 20 mg). While this may not provide kinetic data, it demonstrates the change in products yields with increasing residence time. Figure 7.7 shows that as reactor residence times for oleic acid increased, so did the production of propylene and propane, in the light hydrocarbon region,

and benzene, toluene, naphthalene, and methylnaphthalene, in the aromatics region. Also, the yield of propenylbenzene decreased with increased residence times. For the glycerides (see Figures 7.8 – 1.10), the reaction yield for the remaining aromatics was low (less than 10 mg/ g reactant) and gave no specific trend in yield. Oleic acid, however, had relatively high yields for trimethylbenzene (up to 118 mg/g) and the naphthenic compounds (up to 72 mg/g).

Another comparison can be seen in Figure 7.11 which shows the weight percent composition for each product as fatty acid side chains are added to the glycerol backbone. These results were derived from the 20 mg H-ZSM-5 catalyst runs. As can be seen from these results, the addition of oleic acid side chains resulted in decreased production of CO, CO_2, ethane, and propenylbenzene and an increased production of propylene, C_4 olefins, C_4 alkanes, and C_5 olefins. The decrease in inorganic carbon is due to an increase in the ratio of carbons to oxygen in the reactant molecule. All other cracking products remained relatively unchanged. The differences in the yield trends between aliphatics and aromatics can be explained from slower diffusion of aromatics. Therefore, at a given residence time, aromatic compounds are in contact with the catalyst for longer periods of time. This allows for less time in which aliphatic compounds can oligomerize, cyclize, and aromatize. Table 7.1 shows the product compositions as divided between gas products and organic liquid products. A composition comparison is made between the glyceride reactants used in this study and canola oil [6] that had been reacted using H-ZSM-5 for a temperature of 400°C and a conversion of 83.6%. Conversions for this study are not available due to inherent limitations in determining reactant concentrations

using online analysis.

Table 7.1. Product Distribution of gas and organic liquid products.

Product	Canola Oil (Literature)	Triolein	Diolein	Monoolein
Composition (wt %) in Gas Phase				
CO + CO2	3.7	5.5	9.6	25.3
Methane	5.3			
Ethylene	8.7	7.5	10.9	0.0
Ethane	6.9	9.0	17.2	35.8
Propylene	16.1	32.2	30.9	19.6
Propane	18.9	9.9	20.1	11.2
C_4 Olefin	11	3.8	4.4	3.9
C_4 Paraffin	17.1	3.1	3.5	3.0
C_5 Olefin	--	3.1	3.4	1.1
C_5 +	11			
Composition (wt %) in Liquid Phase				
Benzene	8.1	39.3	35.0	30.6
Toluene	18.7	22.8	19.0	19.2
Ethyl benzene	4.4	5.5	1.0	3.1
Xylenes	15	1.1	1.5	1.3
C9+ aromatics	8.8	31.3	43.5	45.9

Development of Reaction Mechanism

Based on the acylglyceride cracking results, it was hypothesized that cracking of unsaturated lipids initiates at the double bond. Propenylbenzene and phenylbutene are formed through cyclization and aromatization steps. Further cracking results in alkyl-substituted aromatics, and coke precursors are formed from oligomerization of aromatic compounds.

To test this hypothesis, a series of experiments were conducted using some of the cracking products as reactants on the H-ZSM-5 catalyst. Toluene, m-xylene, propenylbenzene, and phenylbutene were reacted separately to evaluate the secondary product formation. Propenylbenzene was selected for further investigation due to its behavior, with respect to yield, as residence time increases. It was observed that the yield of propenylbenzene decreased with increased catalyst to oil ratios. Although, phenylbutene did not have similar responses to propenylbenzene, with respect to yield, it was chosen because of its structural similarity to propenylbenzene. Toluene and m-xylene were examined to determine whether or not ring-opening and subsequent cracking were occurring to produce paraffins and olefins.

As can be seen from Figures 7.12 and 7.13, toluene cracking on H-ZSM-5 produced chiefly benzene, and m-xylene produced mostly toluene. It is believed that methyl rearrangements and subsequent aromatic additions resulted in the formations of trimethylbenzene and methylnaphthalene, for toluene and m-xylene reactions, and also the formations of ethylbenzene and xylenes for toluene reactions. Table 7.2

illustrates the overall yield for each of the four components studied. (Note that at the time of these reaction runs no TCD was attached to the Quatra C; and therefore, only MS data was obtained for both identification and quantitation of compounds.)

Table 7.2. Reaction Conditions and Results for Intermediate Product Cracking

Compound	Mass H-ZSM-5 (mg)	Temperature (°C)	Conversion (%)	Predominant Product
Toluene	15	400	50	Benzene
Toluene	25	400	59	Benzene
Toluene	50	400	75	Benzene
m-Xylene	15	400	46	Benzene
m-Xylene	25	400	83	Benzene
m-Xylene	50	400	88	Benzene
Propenylbenzene	20	400	81	Benzene
Phenylbutene	20	400	95	Benzene

Figures 7.14 and 7.15 show the cracking results as obtained through GC/TCD for propenylbenzene and phenylbutene, respectively. While reacting on 20 mg H-ZSM-5, reaction conversions were 81% for propenylbenzene and 95% for phenylbutene. These results indicated significant breakdown of the parent compound to produce a variety of paraffinic, olefinic, mono-aromatic, and di-aromatic compounds. Interestingly, in terms of identified products, propenylbenzene had a mass balance of 58%, and only 34%

for phenylbutene. This perhaps might explain the anomaly seen in the lipid reactions (Figures 7.7 – 7.10) in which propenylbenzene production decreased with increased residence times but phenylbutene showed no specific trend. It is conceivable that phenylbutene is readily transformed to naphthalene, which also has 10 carbons. Once inside the catalyst pores of H-ZSM-5, phenylbutene can further cyclize and aromatize to form naphthalene.

Proposed Reaction Mechanism

The reaction mechanism believed to be occurring on H-ZSM-5 begins with the protonation of the double bond of the fatty acid constituent (Fig. 7.16). Figure 7.17 shows the molecular geometry of triolein with dimensions determined from equilibrium geometry calculations using Spartan software. Due to molecular size inhibitions, protonation occurs on the outside surface of the catalyst and not within the pores. The protonated charge migrates along the fatty acid moiety and β-scission results in cracking of the fatty acid moiety. The resulting charged species are small enough to readily enter the catalyst pores where additional reaction chemistry occurs. Cyclization steps result in the formation of aromatic compounds (chiefly propenylbenzene and phenylbutene). The propenylbenzene and phenylbutene are reaction intermediates that undergo series of methyl shifts, hydride shifts, and isomerizations to form additional mono-aromatic compounds. In conjunction with these intermediate reactionary steps, disproportionation reactions are occurring. Disproportionation reactions are also responsible for the formation of light olefins. The cyclization steps are believed to similarly to those

reported by Vedrine, et al. (1980) in which olefins are reacted with carbenium ion intermediates to form benzene, toluene, and xylenes (demonstrated below) and also by Fig. 2.4. [31].

$$C_2^{=} + C_4^{+} \text{ or } C_3^{=} + C_3^{+} \text{ or } C_4^{=} + C_2^{+} \longrightarrow \text{benzene}$$

$$C_4^{+} + C_3^{=} \text{ or } C_3^{+} + C_4^{=} \text{ or } C_5^{=} + C_2^{+} \text{ or } C_2^{=} + C_5^{+} \longrightarrow \text{toluene}$$

$$C_4^{=} + C_4^{+} \text{ or } C_3^{=} + C_5^{+} \longrightarrow \text{xylenes}$$

Decarboxylation and decarbonylation steps are believed to be responsible for the formation of CO_2 and CO, respectively. As can be seen from Figure 7.11, production of CO_2 is about 2.5 times (molar basis) greater than CO. For this reason, it is believed that decarboxylation is the dominant intermediate reaction for deoxygenation of the lipid molecule.

The formation of propenylbenzene is believed to be one possible path for which

Additions of mono-aromatic compounds result in the formation of naphthalene and methylnaphthalene, which are precursors to coke. Coke is a rather ill-defined, inherent byproduct of heterogeneous catalytic cracking reactions. Coke is a mixture of polynuclear aromatics that form inside the catalyst pores. When a coke molecule becomes too large to exit the pore, it poisons the catalyst by blinding off catalytic sites for future carbenium ion formations. In industrial applications, the coke is burned off in an air stream using higher temperatures than required for carbenium ion cracking reactions.

Reactions using ^{13}C labeled triolein (all 3 glycerol carbons were labeled) were conducted to determine the pathway of the glycerol carbons. Figures 7.18 and 7.19 show

the total ion chromatograms and corresponding spectra for ^{13}C Triolein and ^{12}C Triolein, respectively. When one compares the relative ratios of ions within each compound, there are negligible differences between the two reaction series. Therefore, it is unclear whether any of the carbons forming aromatics are derived from the glycerol backbone. From a statistical approach, there is a 1 in 18 (3 glycerol carbons compared to 45 fatty acid carbons) probability that an intermediate carbon atom stemming from the glycerol backbone will be seen as part of an aromatic compound. Therefore, no conclusive evidence in regards to the reaction mechanism can the obtained from this product analysis.

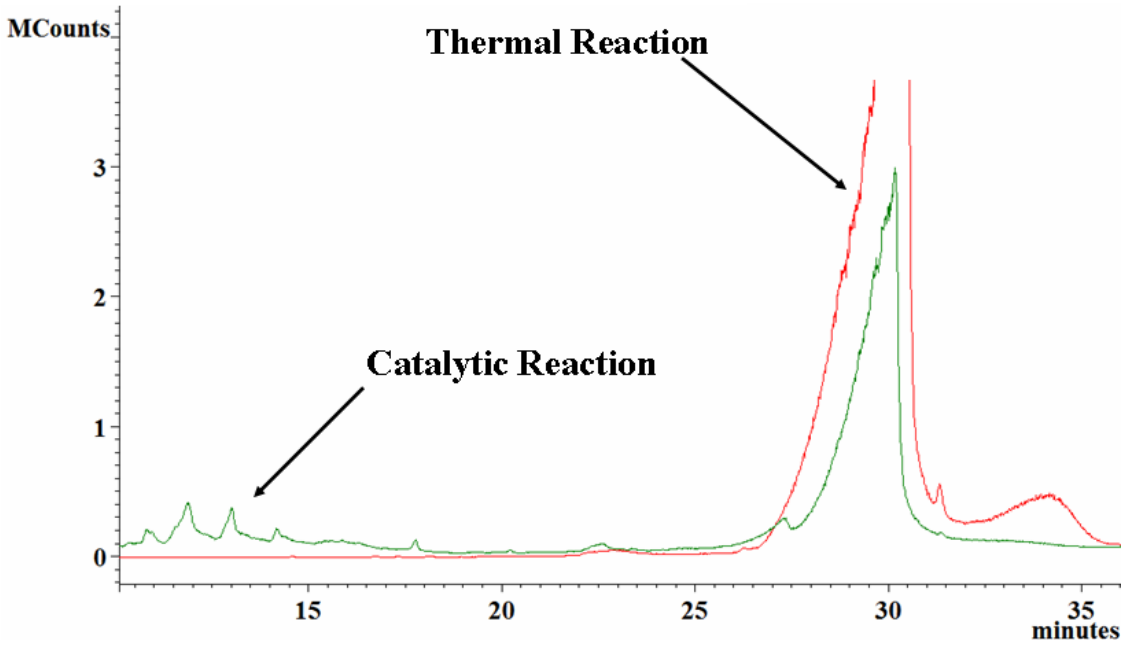

Figure. 7.1. Thermal vs Catalytic Comparison of Oleic Acid Reactions.

NOTE: (Reaction Conditions: T = 400°C for both, Thermal reaction has no catalyst, Catalytic reaction had 20 mg H-ZSM-5)

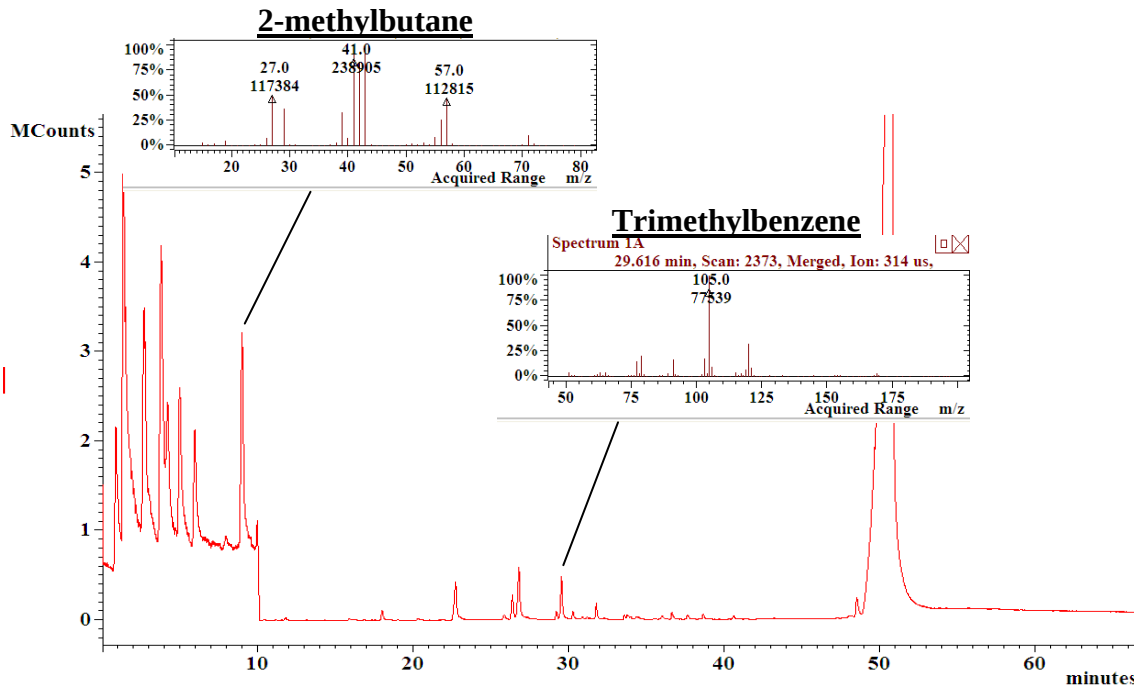

Figure. 7.2. GC/MS Total Ion Chromatogram for Oleic Acid Reaction.

NOTE: (Reaction conditions: T = 400°C, Catalyst/oil = 20)

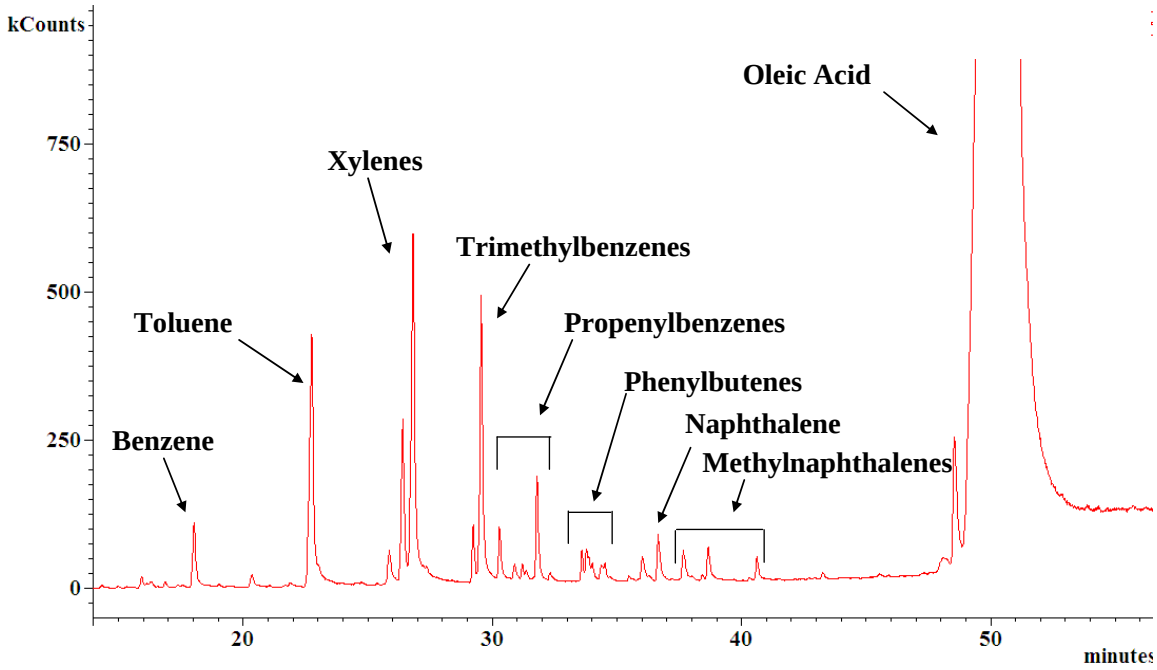

Figure 7.3. GC/MS Total Ion Chromatogram for Oleic Acid Reaction Emphasizing the Region of Aromatic Compounds.

NOTE: Reaction conditions: T = 400°C, Catalyst/oil = 20

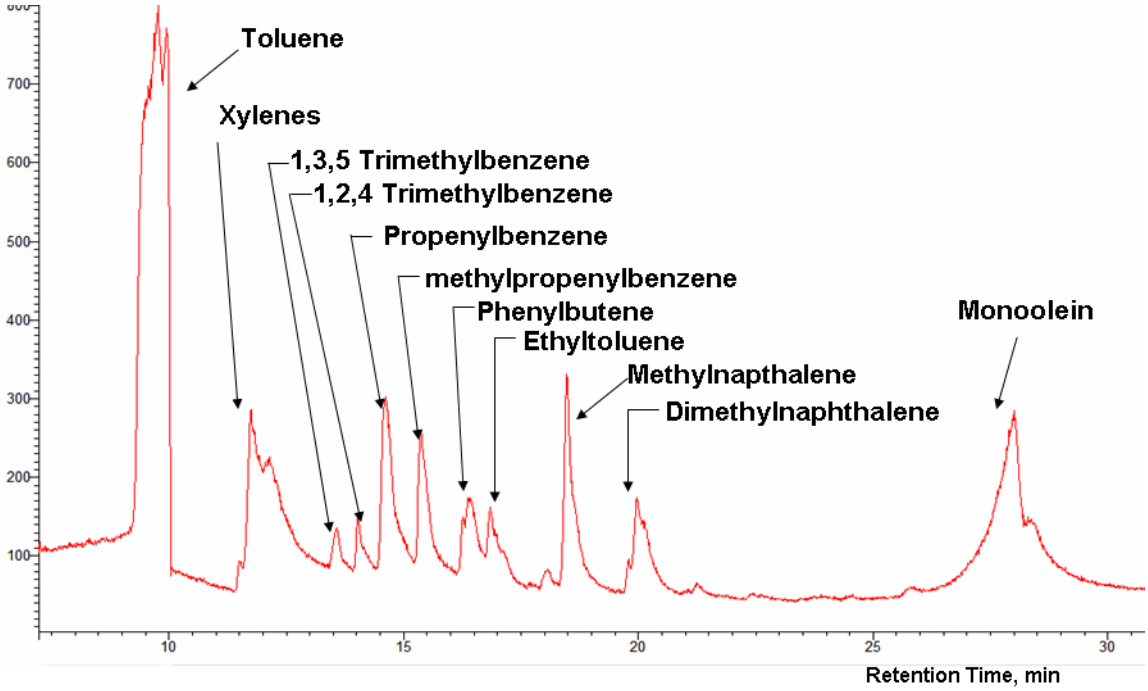

Figure 7.4. Total Ion Chromatogram for Monoolein Reaction.

NOTE: Reaction conditions: T = 400°C, Catalyst/oil = 5

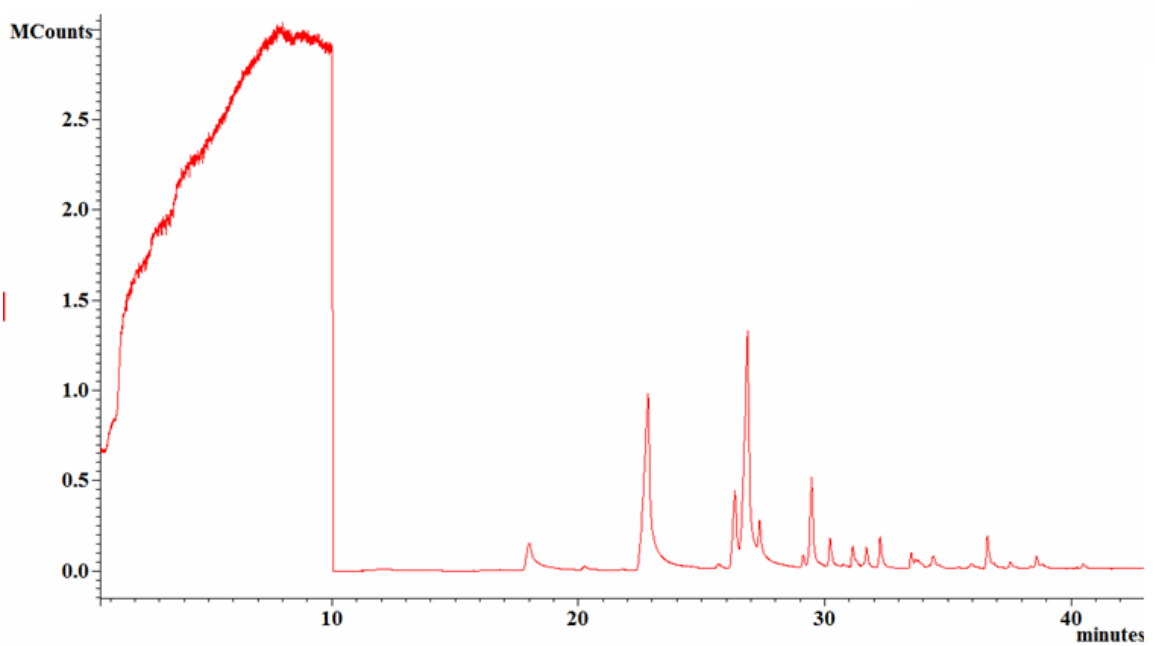

Figure 7.5. GC/MS Total Ion Chromatogram for Diolein Reaction.

NOTE: Reaction conditions: T = 400°C, Catalyst/oil = 20

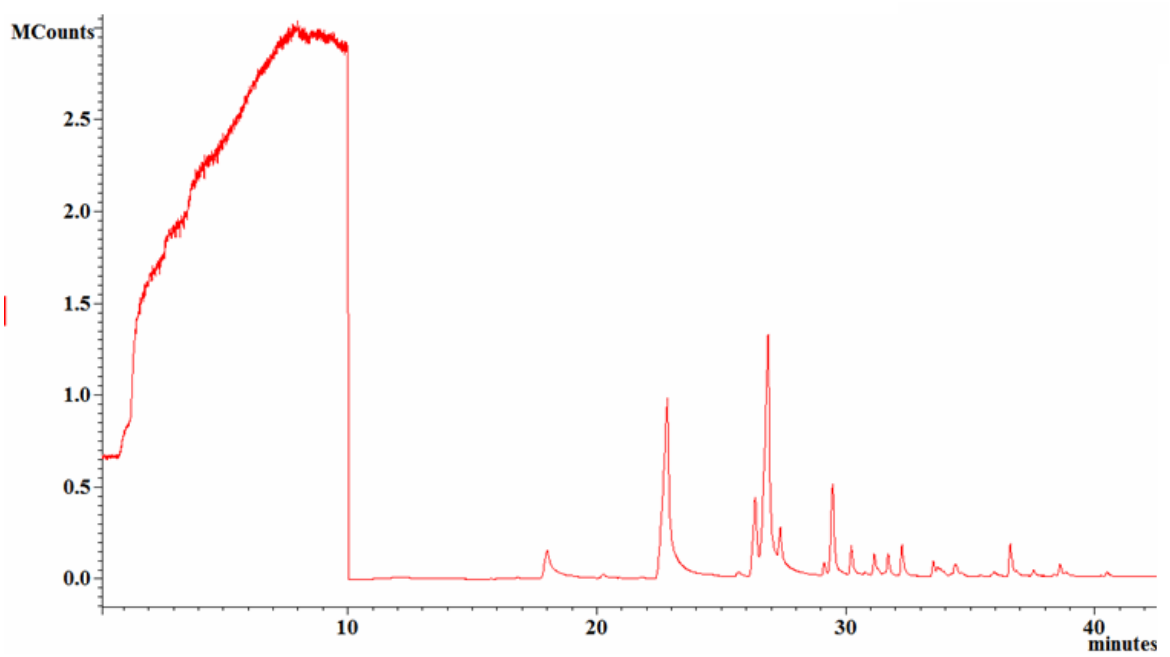

Figure 7.6. GC/MSTotal Ion Chromatogram for Triolein Reaction.

NOTE: Reaction conditions: T = 400°C, Catalyst/oil = 20

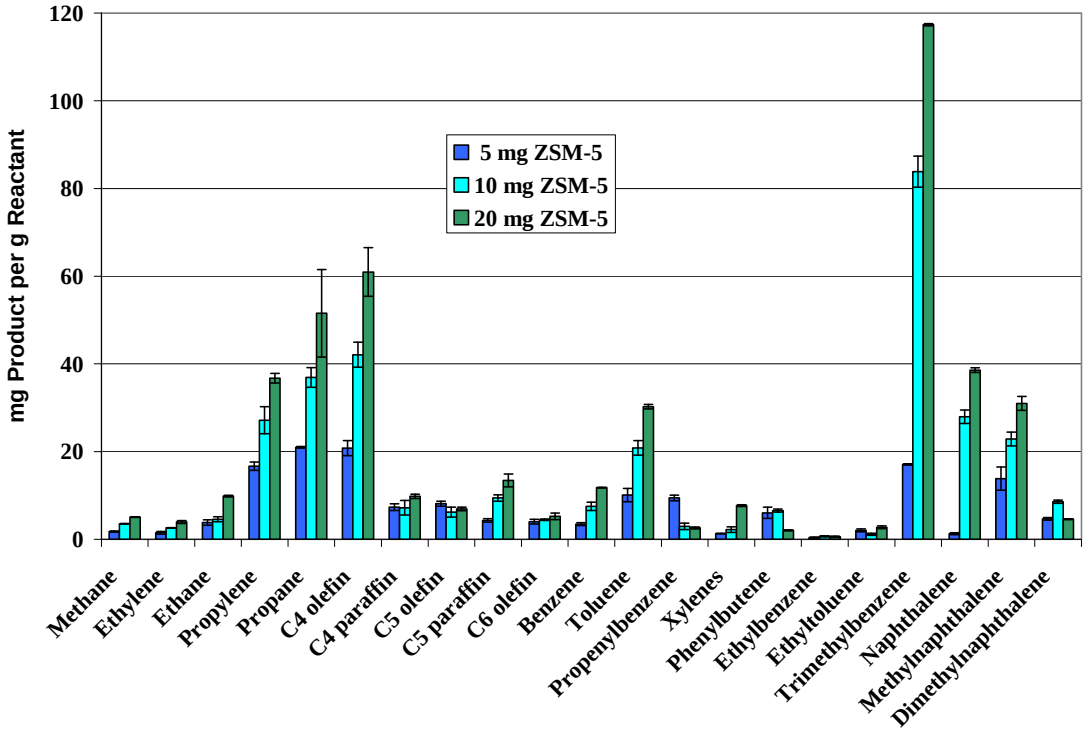

Figure 7.7. Product Yield for Oleic Acid Cracking.

NOTE: Reaction T = 400°C

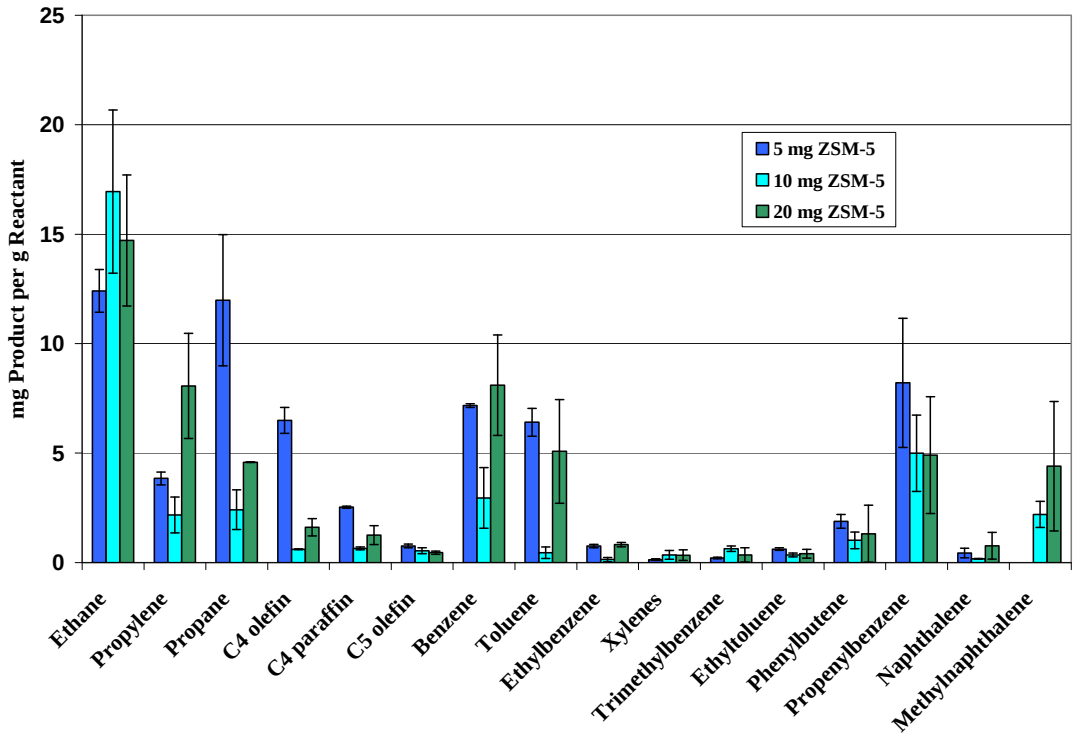

Figure 7.8. Product Yield for Monoolein Cracking.

NOTE: Reaction T = 400°C

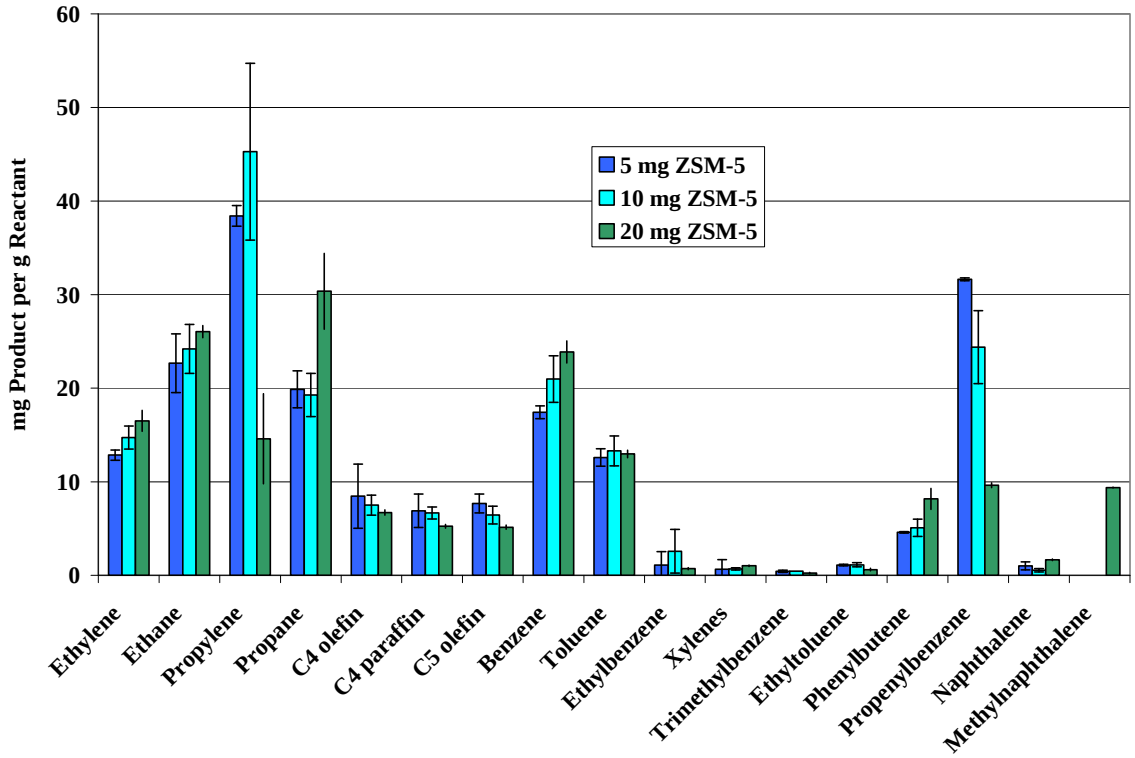

Figure 7.9. Product Yield for Diolein Cracking.

NOTE: Reaction T = 400°C

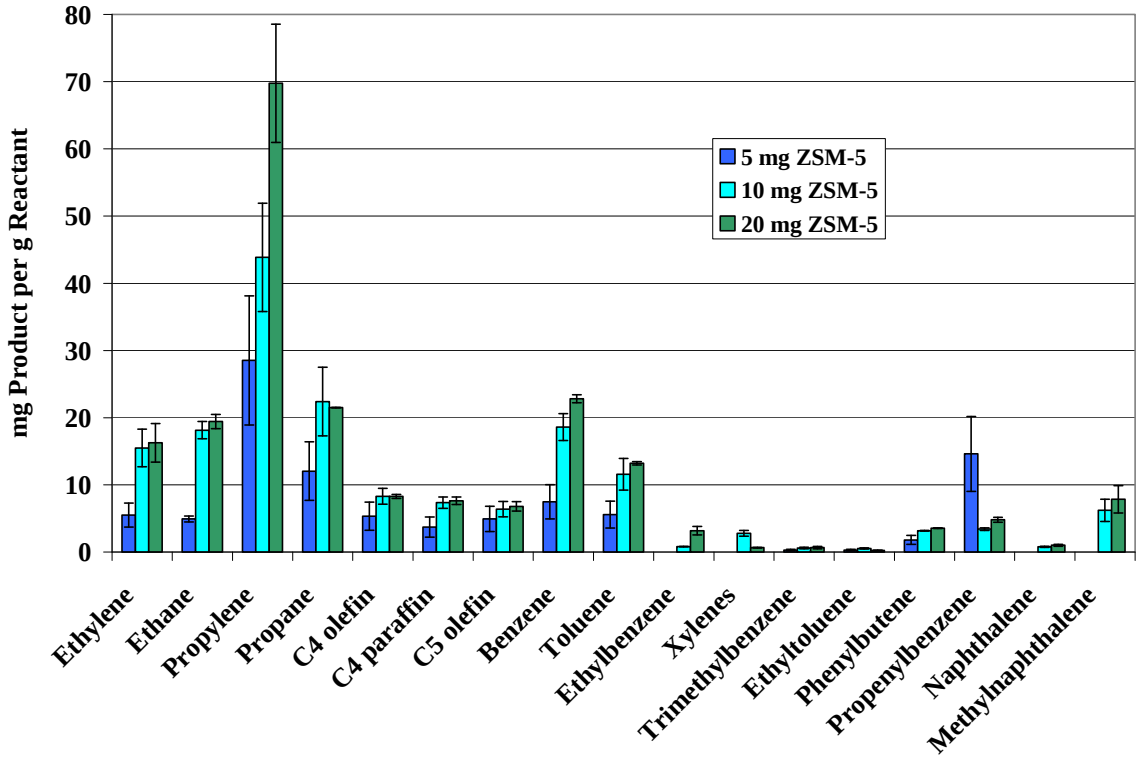

Figure 7.10. Product Yield for Triolein Cracking.

NOTE: Reaction T = 400°C

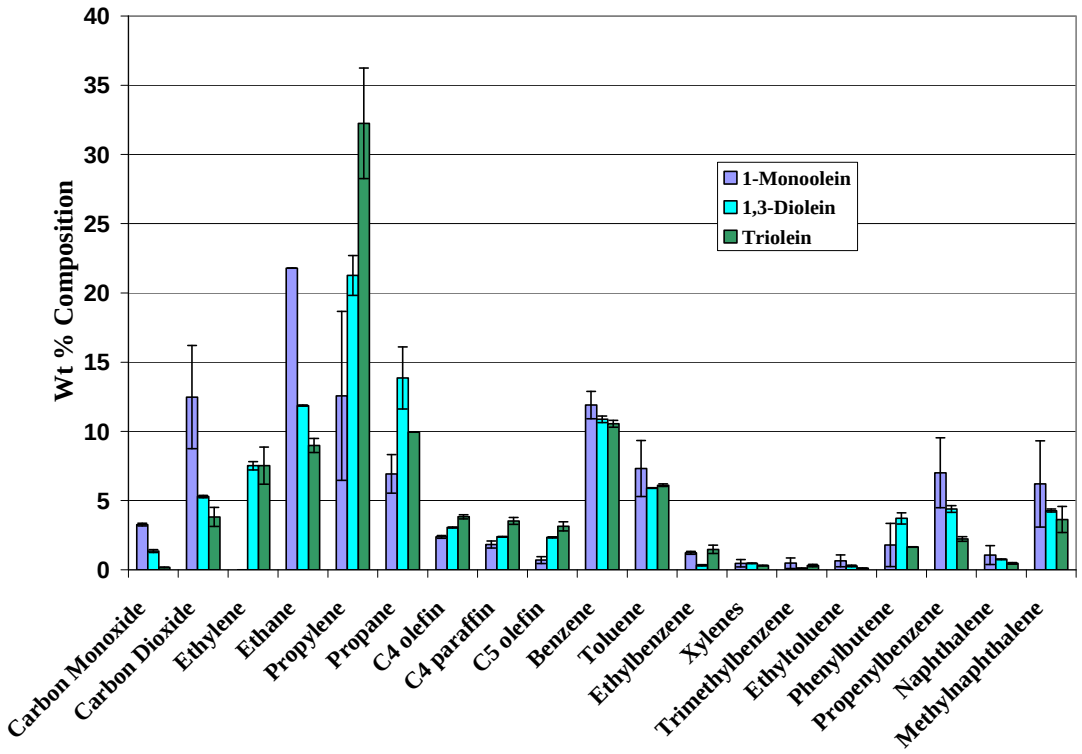

Figure 7.11. Comparison of Fatty Acid Additions to the Glycerol Backbone.

NOTE: 20 mg H-ZSM-5, 400°C

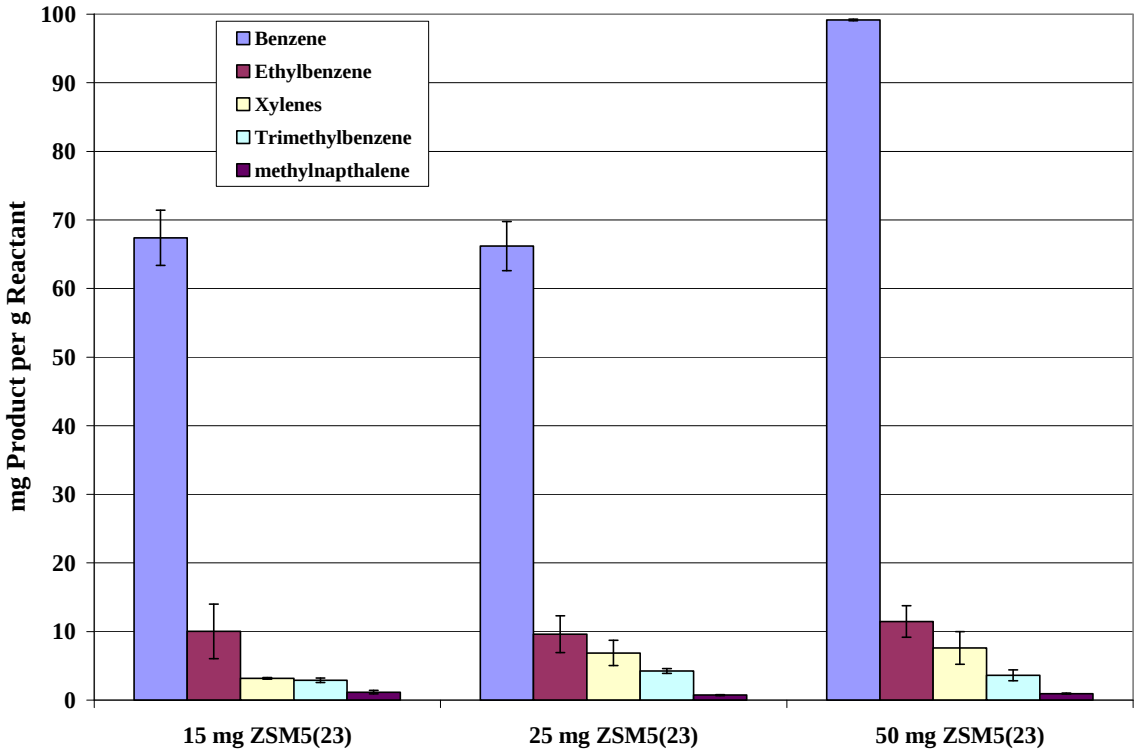

Figure 7.12. Product Yield for Toluene Cracking

NOTE: Quantification by GC/MS, Reaction T = 400°C

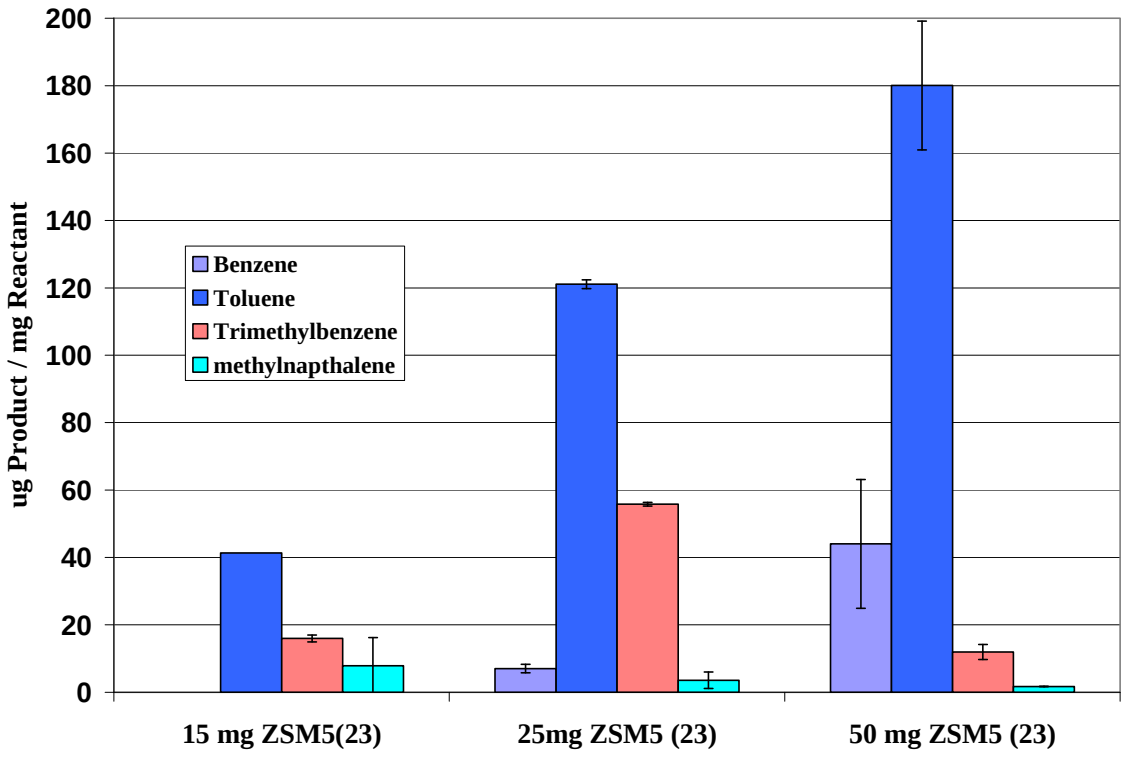

Figure 7.13. Product Yield for m-Xylene Cracking

NOTE: Quantification by GC/MS, Reaction T = 400°C

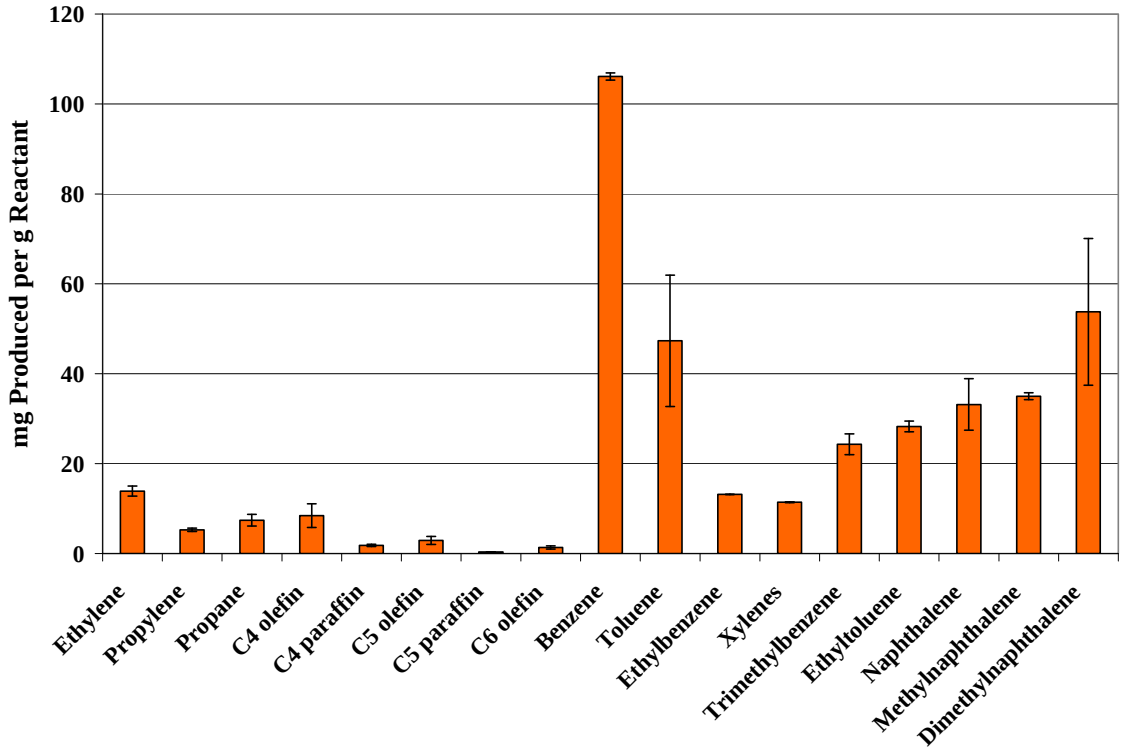

Figure 7.14. Product Yield for Propenylbenzene Cracking

NOTE: Quantification by GC/TC

D, Reaction T = 400°C

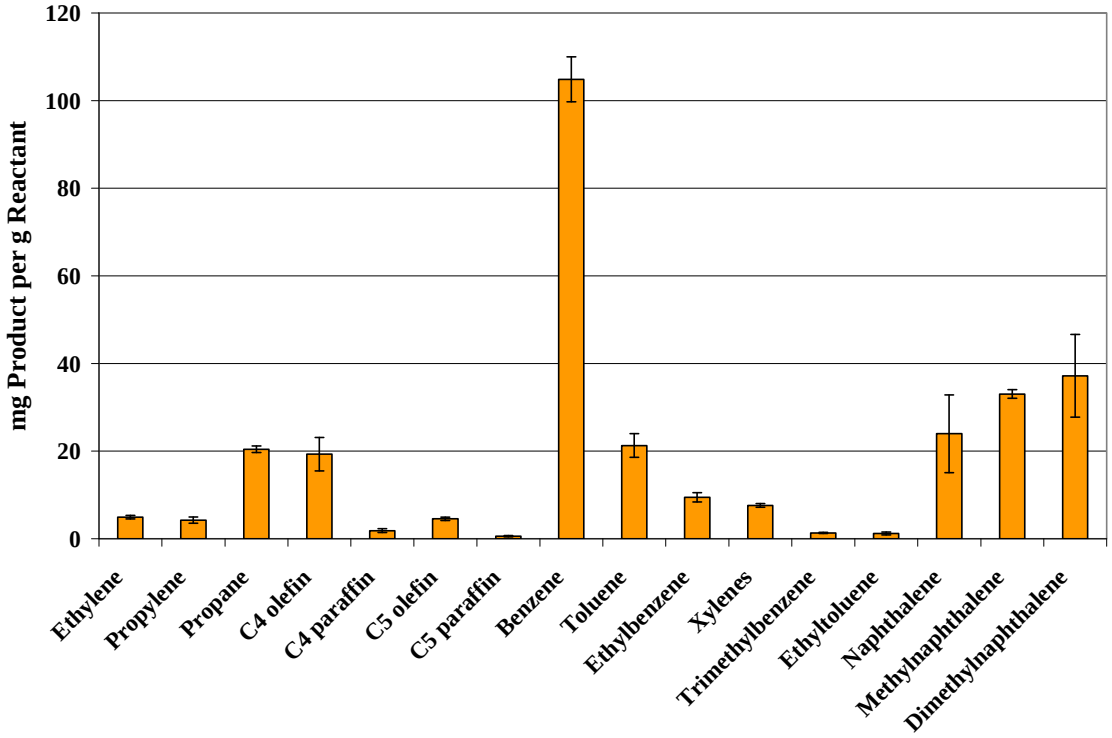

Figure 7.15. Product Yield for Phenylbutene Cracking

NOTE: Quantification by GC/TCD, Reaction T = 400°C

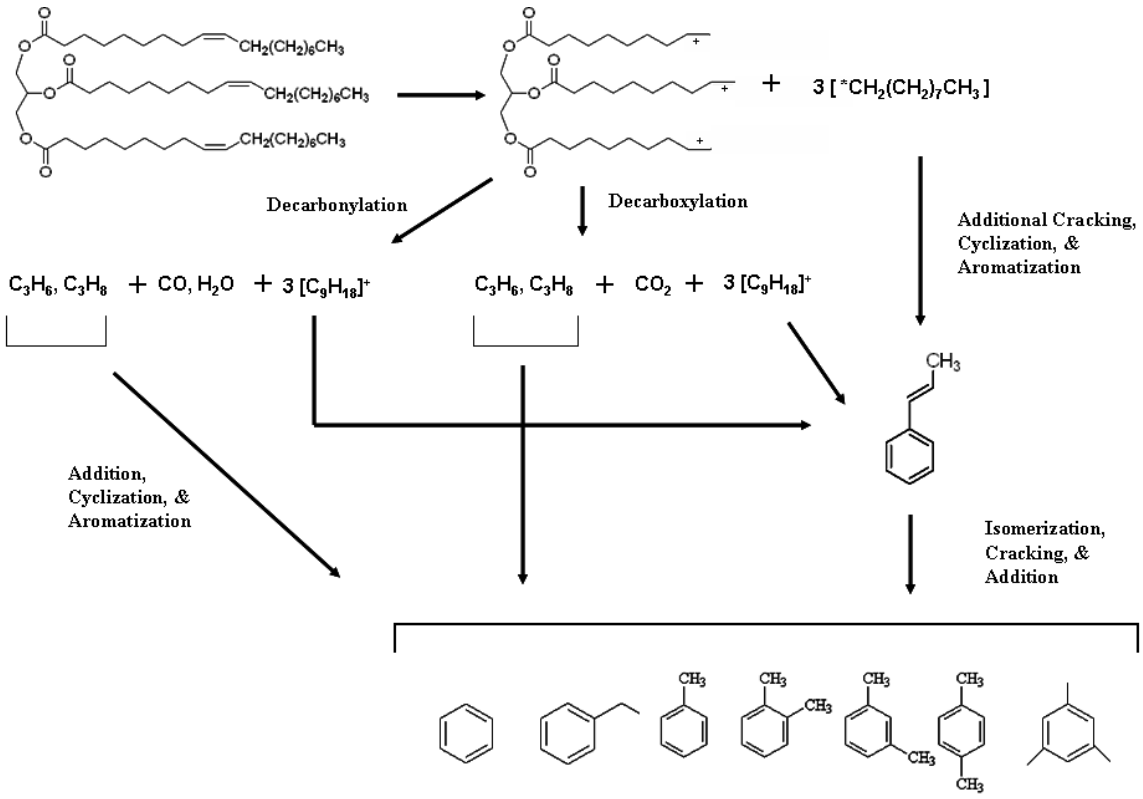

Figure 7.16. Proposed Cracking Mechanism for the Transformation of Acylglycerides to Green Gasoline

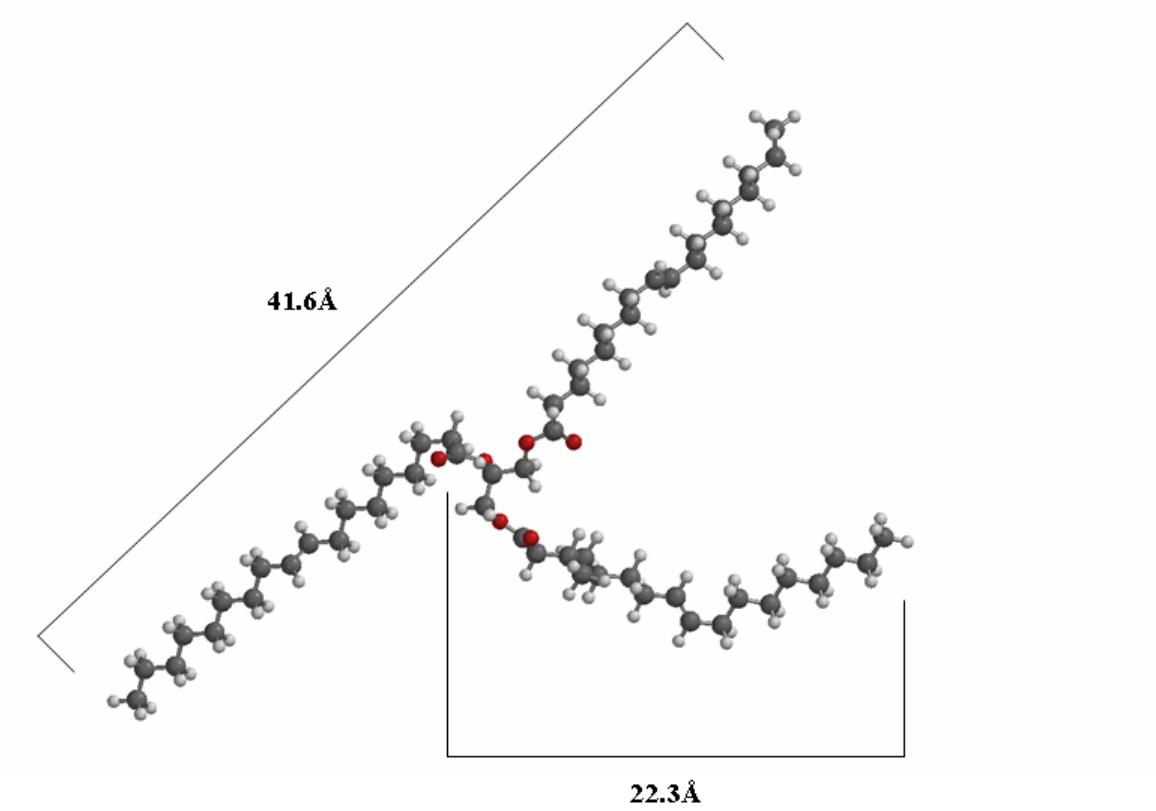

Figure 7.17. Molecular Geometry of Triolein

NOTE: Equilibrium Geometry from Semi-Empirical AM-1 Calculations

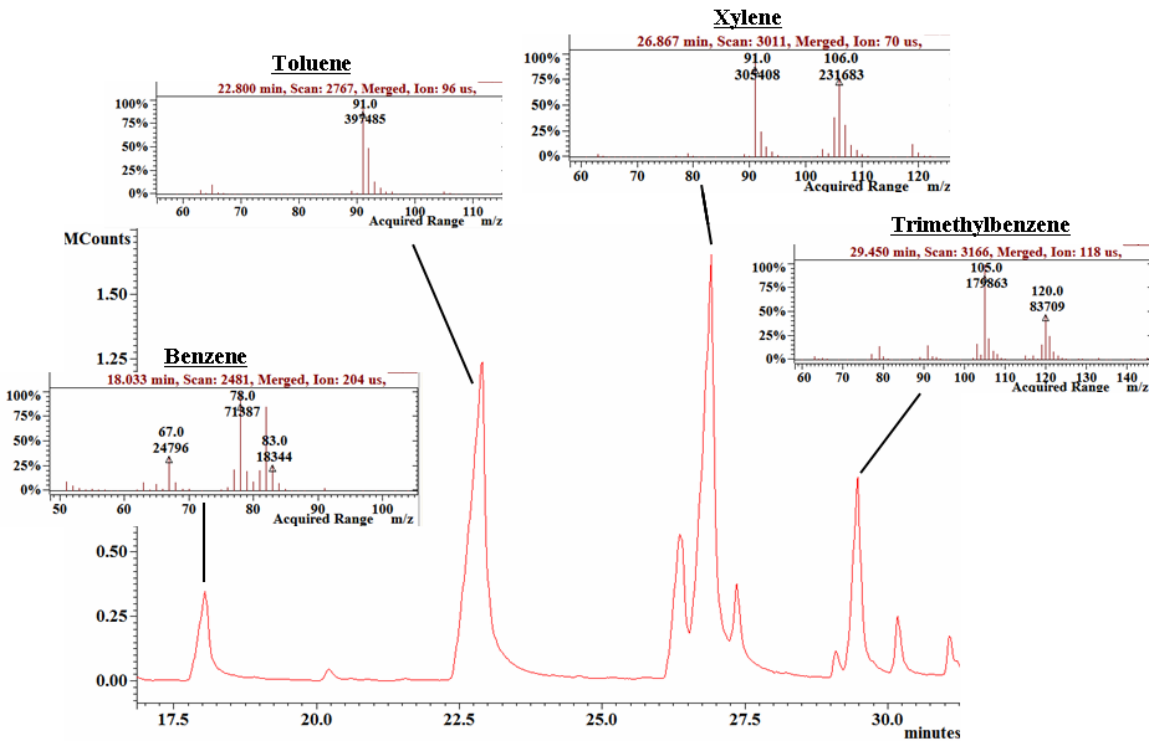

Figure 7.18. Aromatics Formation from ^{13}C Triolein Cracking on H-ZSM-5.

NOTE: Reaction conditions: T = 400°C, Catalyst/oil = 20

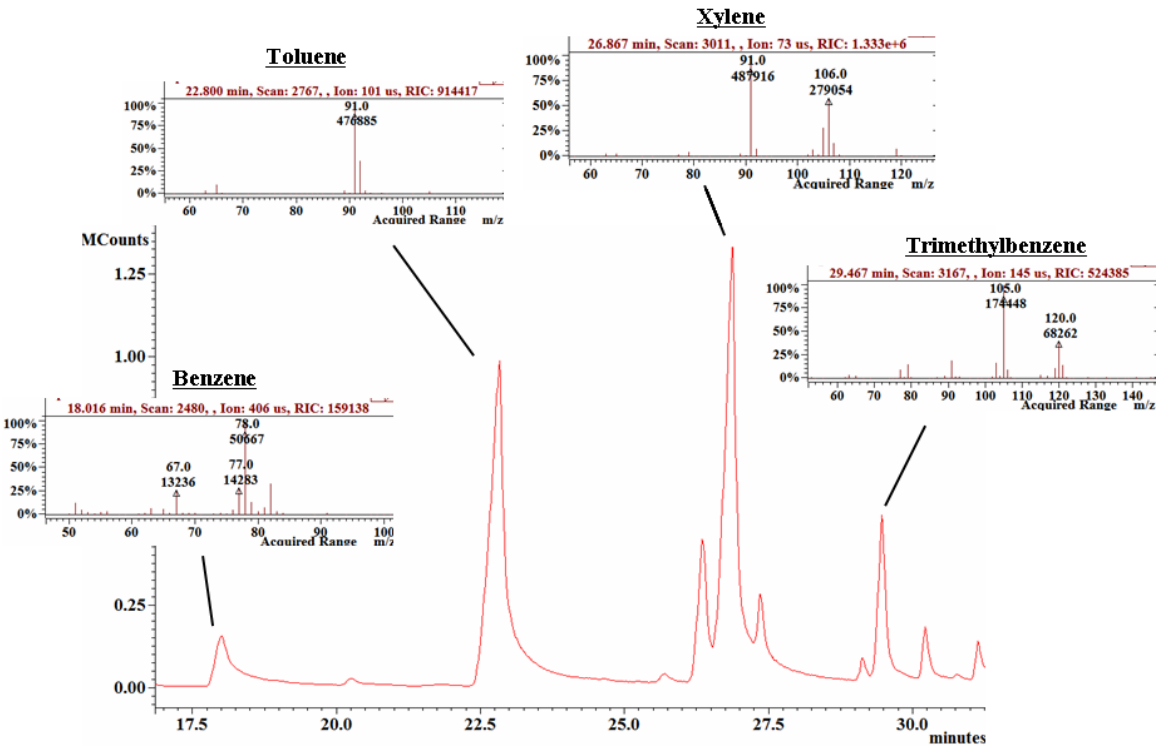

Figure 7.19. Aromatics Formation for ^{12}C Triolein Cracking on H-ZSM-5.

NOTE: Reaction conditions: T = 400°C, Catalyst/oil = 20

CHAPTER VIII

COMPARISON OF LIPID CRACKING USING COMMERCIAL CRACKING CATALYSTS

The present work seeks to establish the changes in product distribution as model unsaturated lipids are cracked using commercial catalysts that are typically used within the petroleum industry. One of the earliest heterogeneous catalysts used in the petroleum industry was the amorphous catalyst silica-alumina. As changes in fuel processing technology occurred and new environmental and governmental regulations were established, solid catalysts were modified to formulate different fuels. The new catalysts used were typically crystalline with shape-selective characteristics to produce fuels with specific molecular structures and explicit combustion capabilities [39 – 42]. While initial cracking mechanisms can be attained using H-ZSM-5, studies using more robust catalysts are necessary to predict the behavior of lipids cracked over commercially viable catalysts. It is the foresight of this work to show that oxygenated feedstocks, such as lipids, can be converted into transportation fuels while utilizing traditional cracking technologies. Doing so eases the transition from conventional crude petroleum to lipid based fuels.

Table 8.1. Physical Characteristics for Cracking Catalysts

Catalyst	Crystallinity	Pore Size	Surface Area
ZSM-5	Crystalline	5.4	425
Faujasite (Y)	Crystalline	7.4	780
Silica Alumina	Amorphous	65-130	300-600

Table 8.2. Physical Properties of Selected Cracking Products

Compound	Boiling Point (°C)	Specific Gravity	Molecular Weight
1,5-hexadiene	59.5	0.69	82.14
1,6-heptadiene	90.0	0.71	96.17
1,7-octadiene	115.5	0.73	110.20
1,8-nonadiene	142.5	0.86	124.22
Benzene	80.0	0.88	78.11
Toluene	110.6	0.86	92.14
Ethylbenzene	136.5	0.87	106.17
m-Xylene	137.5	0.86	106.17
1,3,5-trimethylbenzene	165.0	0.87	120.19
Phenylbutene	176.0	0.88	132.20
Propenylbenzene	179.0	0.91	118.18
Naphthalene	217.7	1.16	128.17
1-Methlnaphthalene	244.7	1.02	142.20
1,2-Dimethylnaphthalene	266.5	1.02	156.22
1,4,5-Trimethylnaphalene	145.0	1.00	170.25

The catalysts used in this work were silica-alumina and faujasite. Faujasite, also known as Y, is a zeolite used as a cracking catalyst and is renowned for its thermal stability as it can withstand temperatures as high as 793°C [17, 22]. The properties for silica-alumina, faujasite, and ZSM-5 can be found in Table 8.1. The selection of catalysts

allows for comparisons in adjustments to chemical and physical characteristics of catalysts. In particular, crystallinity, pore size, surface area, and acidity have been identified as key catalyst properties. The physical properties for selected products from cracking reactions can be seen in Table 8.2 [69, 70].

Results and Discussion

Identification and Quantitation of Reaction Products

Figures 8.1 and 8.2 show the total ion chromatograms for the products derived from cracking of triolein using faujasite and silica-alumina, respectively. Results indicate that lipid cracking on faujasite leads to similar products as H-ZSM-5. However, lipid cracking on silica-alumina leads to the formation of dienes instead of aromatic compounds. These data suggests that silica-alumina could be used as a cracking catalyst to deoxygenate acylglycerides but does not have the shape-selective characteristics of a zeolite to form aromatic compounds. Figures 8.3 and 8.4 demonstrate the individual product yields for mono, di-, and triolein cracking on faujasite and silica-alumina, respectively. As can be seen from Table 8.3, all three catalysts yield similar total product yields, but the breakdown within subgroups is quite different. For instance, H-ZSM-5 produced more low-molecular weight hydrocarbon gases, but faujasite yielded more products within the gasoline organics range. Also, as can be seen from Figure 8.4, cracking on silica-alumina produced more alkyl substituted naphthalenes than the other two catalysts.

Figure 8.3 allows one to compare the changes in individual product yields on acylglyceride cracking on faujasite as the addition of fatty acid moieties to the glycerol backbone increases. As a general trend, the individual products increased from monoolein, diolein, and triolein. Figure 8.4 shows similar results for the lipid cracking on silica-alumina. This trend, however, is not consistent for the naphthalene compounds.

Table 8.3. Total Product Yields for Triolein Cracking at 400°C

	ZSM-5	Y	Si-Al
C_2 - C_5 HC gases	150	89	86
C_6 - C_7 HC's	0	47	0
Total Aromatics	58	100	32
Total Dienes	0	0	124
Gasoline Range Organics	57	114	15
Total Products	208	236	243

Effect of Different Zeolite Catalysts on Lipid Cracking

A comparison of the results between H-ZSM-5 and faujasite catalysts can demonstrate the effects that pore size and catalyst acidity have on the product distribution from acylglyceride cracking (Figure 8.5). H-ZSM-5 produced more propylene (factor of 5.4) than faujasite. Also, H-ZSM-5 produced more benzene (factor of 6.6) and toluene (factor of 2.1). On the other hand, cracking on faujasite produced more phenylbutene (factor of 3.7), propenylbenzene (factor of 2.9), methylnaphthalene (factor of 5.9), higher molecular weight aliphatics, and other naphthalenes were produced when faujasite was used.

These results can be related to the physical and chemical properties of the catalysts. Smaller pore sizes generate molecules with smaller mean diameters. It is for this reason that C_6 and C_7 aliphatic molecules, phenylbutene, propenylbenzene, and naphthalenes were formed using faujasite catalyst and H-ZSM-5 produced more propylene, benzene, and toluene. These findings are supported by Olson and Haag (1984) in xylene isomerization. The H-ZSM-5 pores are large enough to allow 3 xylene molecules to enter and allow isomerization reactions to occur to an equilibrium point. Because of steric constraints, ZSM-5 selectively retards transalkylation of xylenes, which would form toluene and trimethylbenzene [71].

Effect of Crystallinity on Lipid Cracking

From Figure 8.5, the effect of catalyst crystallinity can be seen from the formation of dienes using silica-alumina and not from H-ZSM-5 or faujasite. The acidic nature of all three catalysts resulted in the scission of the unsaturated bond in the fatty acid moiety. The intermediates further cracked to form low molecular weight olefins (ethylene and propylene) which then oligomerize, forming C_4 to C_{10} olefins. The larger olefins dehydrogenate to form dienes. The olefins and dienes oligomerized together, cyclized, and formed aromatic compounds [6, 20, 29, 30].

The amorphous character of the silica-alumina permitted the formation of dienes within this sequence of events, but not the formation of aromatic compounds that were within the gasoline range organics. Previous research has shown that amorphous catalysts do not offer the shape-selective characteristics of crystalline catalysts [39].

Crystalline catalysts present the intermediate compounds with more acid sites on which additional reactions can occur.

Due to the lack of product formation using an empty bed (i.e. no catalyst), the formation of reaction intermediates appears to be strictly from catalyst activity. Also, the cracking results do not show the formation of methane, which derives from α-cracking during thermal conversion. Therefore, it is assumed that catalytic transformation is the dominant mechanism, and not pyrolysis, for these reactions.

Overall Mass Balances and Recommendations

The overall material balances for all catalysts and reactants studied are presented in Table 8.4. This table shows the amount of initial reactant, the total yield of products, as determined from GC quantitation, and the amount of coke, as determined by thermal gravimetric adsorption (TGA). The amount of unreacted material is not available as the Quatra C was designed to evaluate the smaller molecular weight cracked compounds and not the initial starting material. In fact, only in the oleic acid reactions is the reactant peak seen in the GC/MS ion trace. It is, however, chromatographically overloaded and quantitation is of little value.

Results from this study can be used to make some general comparisons between acylglycerides versus crude petroleum cracking. Typical riser reactors operate at ~1,000°F and with a catalyst to oil ratio (wt/wt) of 2. The conditions for the Quatra C for these reactions were 752°F and a catalyst to oil ratio (wt/wt) of 20. At these conditions, faujasite produced significant amounts of methylnaphthalene. Methylnaphthalene is a

poor component for diesel because it acts as a "wax" and precipitates out of solution. Also, in both the faujasite and silica-alumina reactions, significant amounts of gaseous products were formed. In an industrial environment, refineries are designed to handle only a few percent (in overall product composition) in gaseous products [68]. Therefore, taking equipment issues into consideration and the poor use of feedstock carbons, it is suggested that faujasite is not an ideal catalyst for lipid cracking, at least at the process conditions stated above.

Silica-alumina catalyst, on the other hand, showed promising results for lipid cracking. Although the gaseous fraction is high, lower amounts of methylnaphthalene were produced. Also, the sizeable amounts of dienes will be ideal for diesel fuel usage, or an additional reaction step will convert the dienes to aromatics for gasoline [68, 72, 73].

All catalysts studied produced significant amounts of coke. The mass percent of coke obtained from these experiments is consistent with that reported by Idem, et al. (1997) [6], ranging from 12 – 18 wt% of initial reactant. During normal petroleum refining operations, riser reactors produce only 4 to 5 wt% coke. Therefore, existing equipment is designed to handle lower coking yields than what is presented here for the cracking of lipids. At high coking loads, catalyst regeneration will not be 100% [68]. As coking is autocatalytic, less than 100% regeneration will lead to complete fouling of the catalyst within a short time [23, 24]. As can be seen from Figures 8.6 and 8.7, decreasing the reaction temperature from 400°C to 350°C decreases the overall product yields for reactions on faujasite and silica-alumina, respectively. This is especially remarkable for

the production of alkyl-substituted naphthalenes which are solids at room temperature and will have large effects on both fuel processing and fuel properties.

Table 8.4. Overall Mass Balances for Acylglycerides Reacted on Multiple Catalysts

Reactant	mg Reactant	µg Total Product	µg Coke	Products (wt % of Reactant)	Coke (wt % of Reactant)
H-ZSM-5 (Si/Al=23)					
Oleic Acid	2.07	916	255	44	12
Monoolein	2.53	148	332	6	13
Diolein	2.67	539	237	20	9
Triolein	2.15	444	398	21	18
Faujasite (Y)					
Monoolein	2.64	327	350	12	13
Diolein	2.44	398	406	16	17
Triolein	1.85	433	225	23	12
Silica-Alumina					
Monoolein	2.88	297	260	10	9
Diolein	2.18	532	286	24	13
Triolein	1.96	535	255	27	12

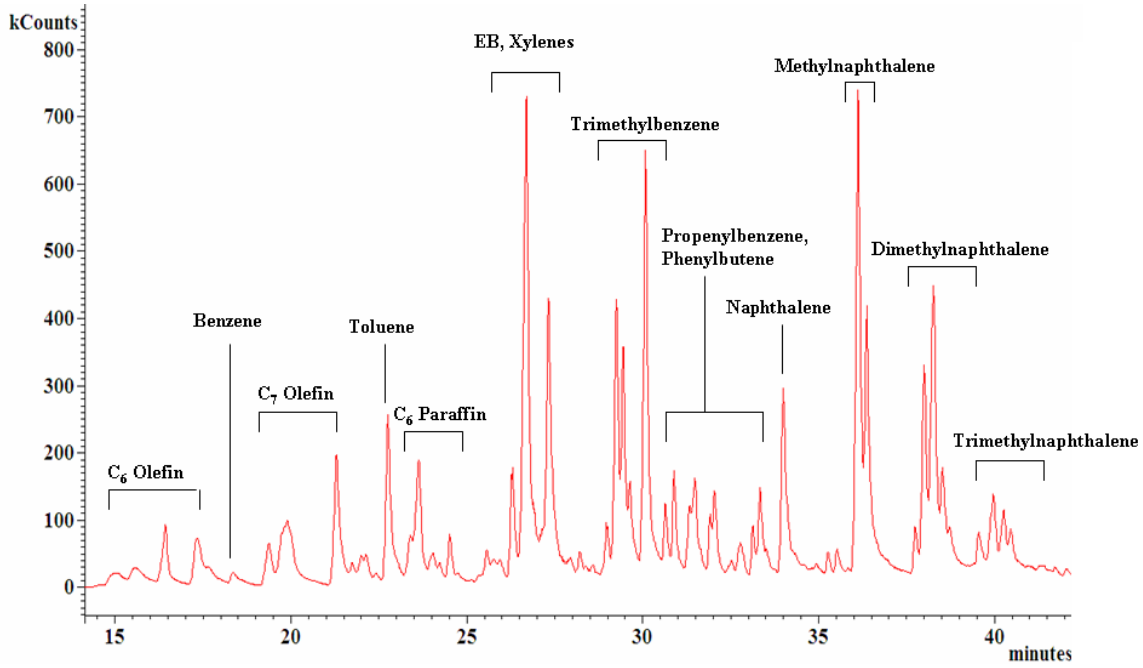

Figure 8.1. Total Ion Chromatogram for Triolein Cracking on Faujasite Catalyst.

NOTE: Reaction conditions: T = 400°C, Catalyst/oil = 20

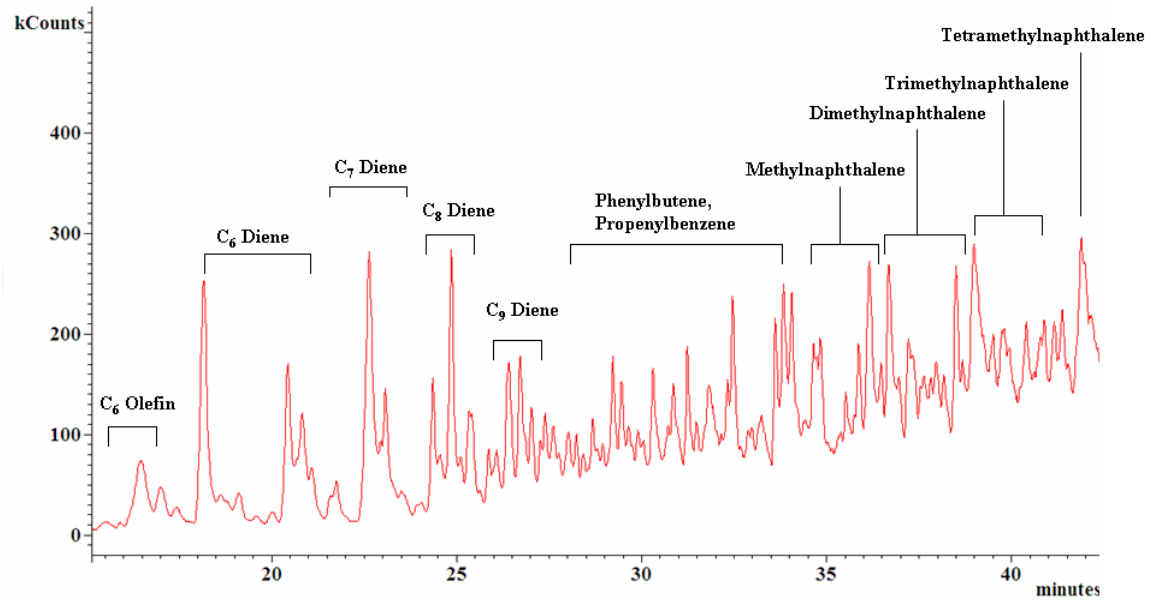

Figure 8.2. Total Ion Chromatogram for Triolein Cracking on Silica-Alumina Catalyst.

NOTE: Reaction conditions: T = 400°C, Catalyst/oil = 20

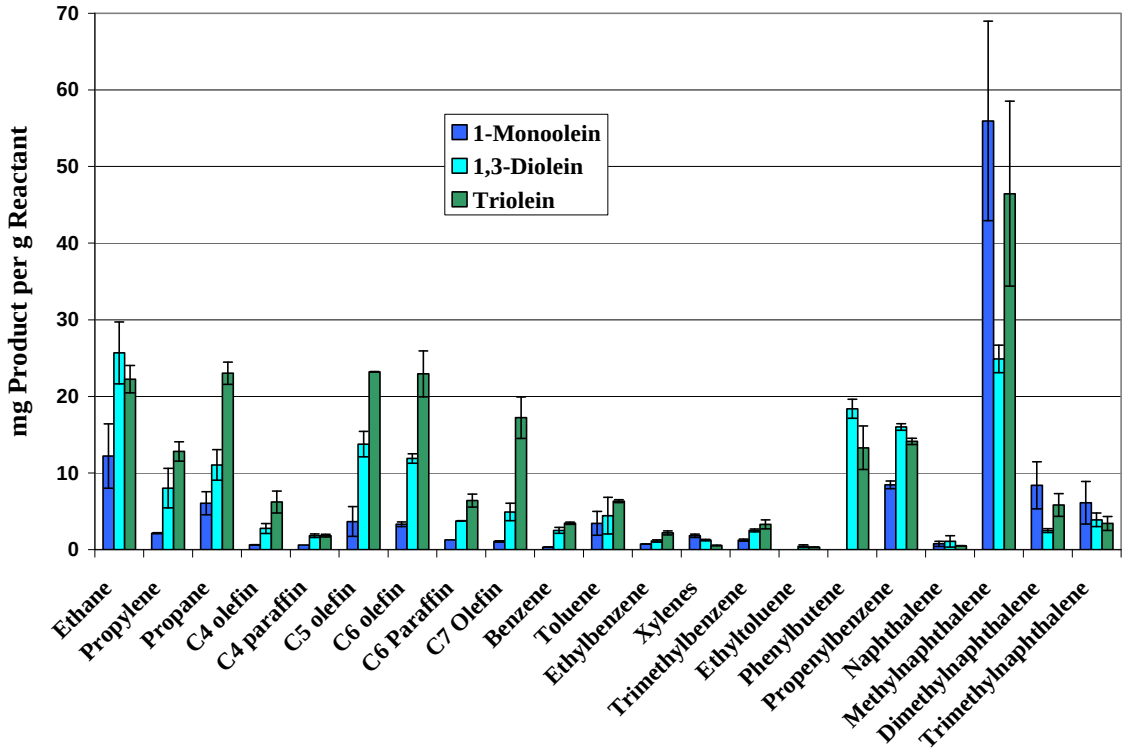

Figure 8.3. Product Yield for Lipid Cracking on Y Zeolite Catalyst.

NOTE: Reaction T = 400°C

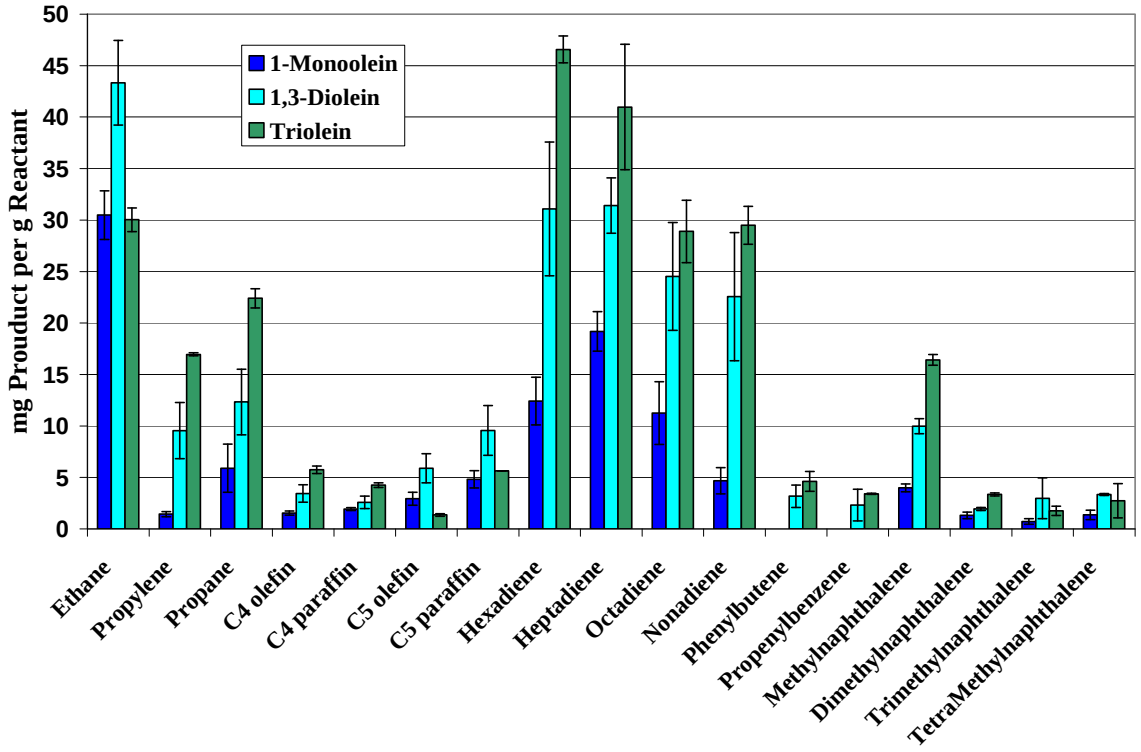

Figure 8.4. Product Yield for Lipid Cracking on Silica-Alumina Catalyst.

NOTE: Reaction T = 400°C

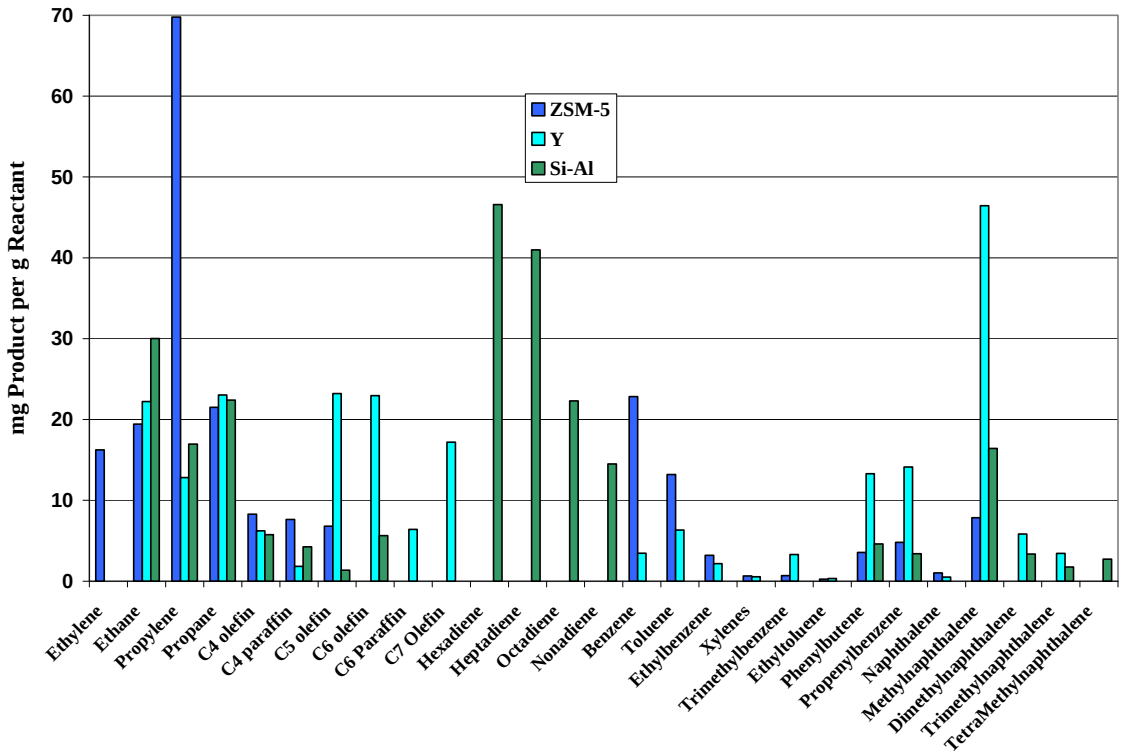

Figure 8.5. Comparison on Product Yields for Triolein Cracking on Selected Catalysts.

NOTE: Reaction T = 400°C

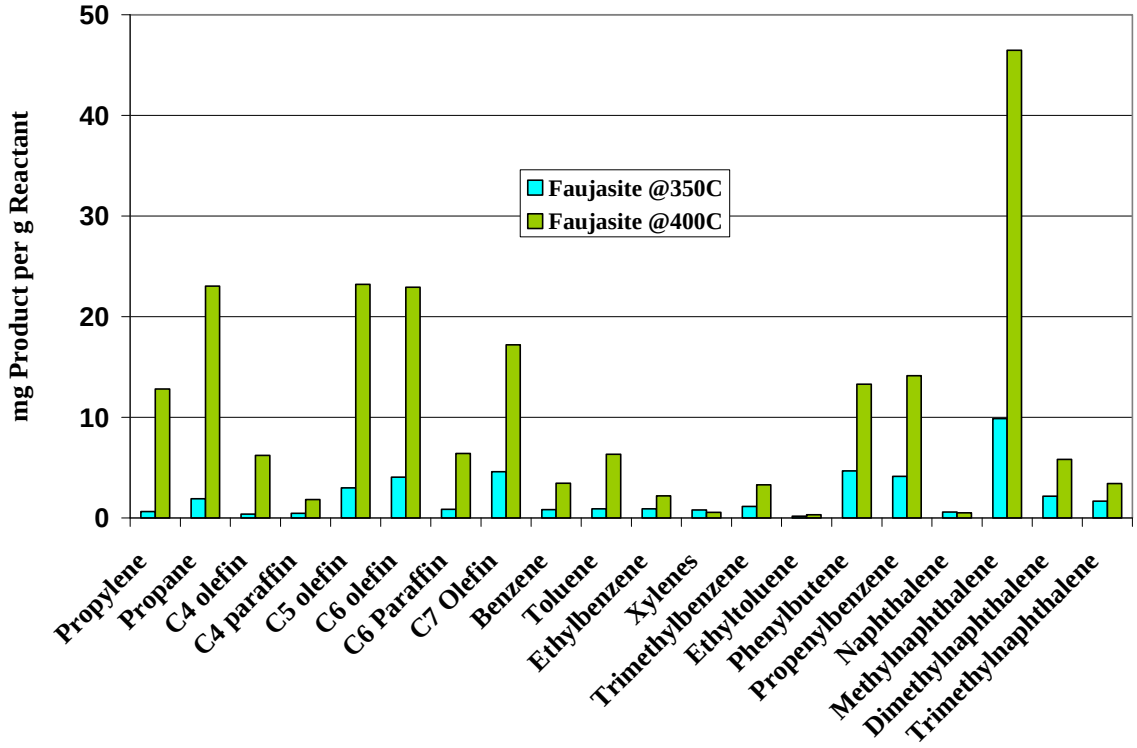

Figure 8.6. Product Comparison for Triolein Cracking on Faujasite at Different Temperatures.

NOTE: Catalyst/oil = 2

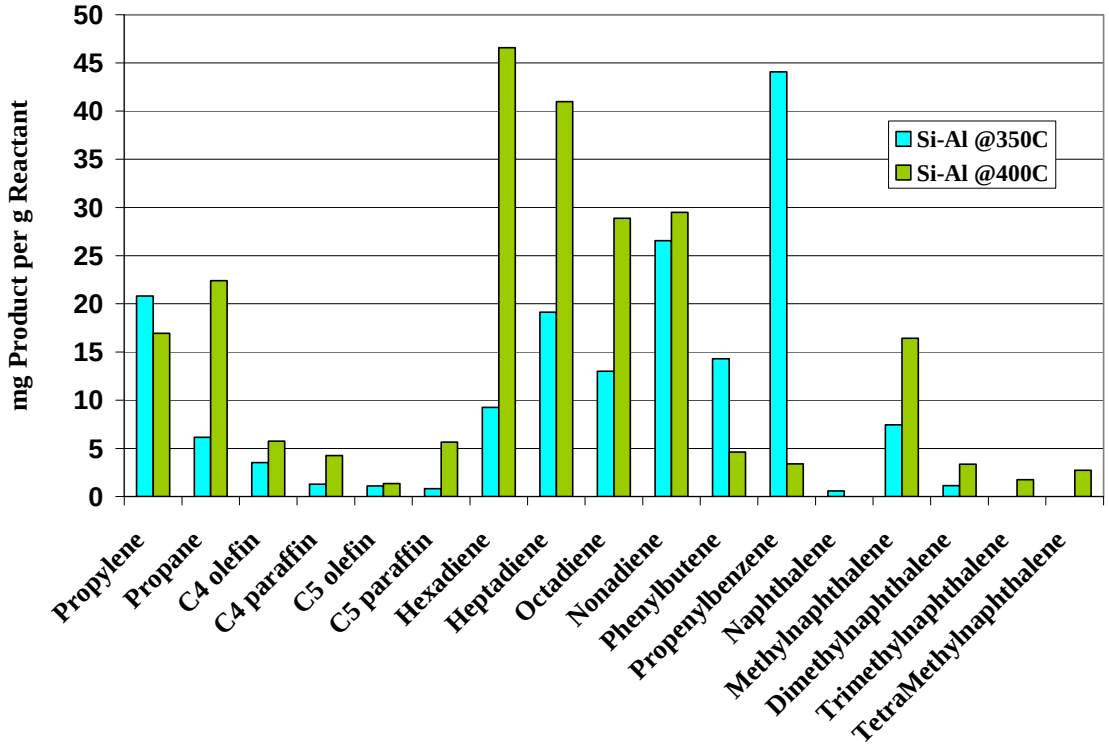

Figure 8.7. Product Comparison for Triolein Cracking on Silica-Alumina at Different Temperatures.

NOTE: Catalyst/oil = 20

CHAPTER IX

CONCLUSIONS AND ENGINEERING SIGNIFICANCE

Initial work began with the elucidation of the cracking mechanism using a homogeneous catalytic approach. Use of triflic acid as the homogeneous catalyst demonstrated the capability of lipid cracking without the interferences of solid-liquid interactions, high temperature pyrolysis, or reactant/product diffusion limitations. The heterogeneous work formulated the cracking products and mechanism as applied to a highly acidic, benchmark catalyst and two commercial cracking catalysts.

Conclusions

- Homogeneous results indicated that cracking of unsaturated lipids begins at the double bond. No reaction was seen using a saturated lipid and triflic acid under the mild conditions of the reaction setup.
- The unsaturated acylglycerides had the same cracking pattern with regards to the amounts of product formed. Products yields were heavy with light hydrocarbon gases (especially propylene) and included the formation of aromatic compounds.
- All acylglycerides studied showed the formation of propenylbenzene from cracking on H-ZSM-5 catalyst. Propenylbenzene yield decreased

from monoolein to diolein to triolein. The product composition (wt %) of propenylbenzene decreased with increased catalyst to oil ratios of 5, 10, and 20:1.

- Additional cracking experiments using toluene and m-xylene indicated that transalkylation of the aromatic compound was the governing mechanism for the formation of multi-substituted alkyl-aromatics.
- Additional cracking experiments using propenylbenzene and phenylbutene indicated that mono-aromatic compounds with longer substituted side chains were more likely to form light hydrocarbon gases along with multi-substituted alkyl-aromatics than toluene and xylenes.
- The proposed cracking mechanism includes the cracking of the unsaturated fatty acid side chains outside the catalyst pores as the *ab initio* step. Additional steps include cyclization and aromatization to form mono- and di-aromatic compounds.
- The additional experiments using perceived aromatic intermediates which were conducted to develop the cracking mechanism indicated that isomers of propenylbenzene and phenylbutene were the secondary cracking products. Tertiary products (paraffins, olefins, and aromatics) were then produced by additional reactions of propenylbenzene and phenylbutene.
- Product analysis using a ^{13}C labeled triolein as the reactant in the Quatra C was inconclusive in determining the plight of the glycerol carbons.
- Catalytic cracking of unsaturated acylglycerides on Faujasite indicated a shift in product formation as compared to H-ZSM-5. Faujasite reactions yielded fewer light hydrocarbon gases and more aromatics.

- Catalytic cracking of unsaturated acylglycerides on silica-alumina catalyst indicated the formation of $C_6 - C_9$ dienes. There was also significant amounts of ethane and fewer amounts of aromatic formation as compared to the H-ZSM-5 results.
- Lowering of reaction temperatures from 400 to 350°C resulted in a decrease in conversions for both Faujasite and silica-alumina catalysts. The lower temperature reactions did yield higher amounts of propenylbenzene. This is perhaps due to lower conversions and also further evidence that propenylbenzene is a reaction intermediate.

Engineering Significance

This work sought to advance a renewable feedstock to permit the potential displacement of petroleum by lipids. One advantage of using lipid feedstocks is the reduction of greenhouse gases by preventing the emission of exogenous carbon dioxide into the atmosphere, as is seen by petroleum. Another advantage of lipid cracking as a motor fuel is the utilization of petroleum refining, which is a rather mature technology with preexisting reactors, distillation columns, and American Society of Testing and Materials (ASTM) standards.

Typical riser reactors use a combination of catalysts and process conditions that yield a mixture of products while regenerating spent catalyst. Market demands and feedstock properties will dictate the specific combination of catalysts and process conditions. However, some process conditions can be stated at this point. One, it is apparent from this study that unsaturated lipids crack more readily than petroleum

feedstocks. This is evident from lipid cracking experiments on ZSM-5 where large amounts of hydrocarbon gases were produced.

As this study has shown, faujasite promotes the production of aromatic compounds that are typically found in gasoline and silica-alumina favors the production aliphatic compounds found in diesel. Therefore, a mixture of these two catalysts in an FCC would produce a blended fuel that can be separated by downstream processes such as distillation.

From this study, catalyst beds with an operating temperature of 350°C are ideal for the cracking of lipids to produce gasoline and diesel fuels. It is important to keep the catalyst to oil ratio low (<5) to ensure low coking and high selectivity towards longer chain aliphatics. Also, low catalyst to oil ratios will lower the production of alkyl-substituted naphthalenes, which could become precipitates in a fuel mixture.

Future work on lipid cracking should extent into the development of ideal catalysts for oxygenated fuels. This work has concentrated on a bench-mark catalyst and two industrial catalysts. An interesting path might be in the incorporation of a bi-functional catalyst, such as Pt-Y, into the catalyst stream, whereby deoxygenation may occur before cracking along the fatty acid side chains. It is important to consider the thermal stabilities of catalysts as the de-coking step operates at much higher temperatures than the cracking steps. That is the reason of continued work with both faujasite and silica-alumina catalysts.

Albeit a complete economic analysis of green fuels from lipids is beyond the scope of this work, a few ancillary thoughts should be mentioned here. Production of

green fuels via lipid cracking would utilize the current petroleum refining processes and practices. Therefore, there would appear to be little changes to the production costs in producing green fuels versus traditional crude petroleum.

The substantial differences arise in the cost of feedstock lipids. As long as lipid feedstocks are derived from row-crop plant oils, feedstock costs will be dependent upon farming practices and weather related issues. Therefore, cultivated lipids, either from oleaginous yeasts, algae, or municipal waste sludges, must be explored to maintain a steady supply of lipids to the refiners.

BIBLIOGRAPHY

[1] National Biodiesel Board, http://www.biodiesel.org

[2] U.S. Department of Energy, http://www.eia.doe.gov/oiaf/aeo/index.html

[3] Ma, F. and Hanna, M.A. (1999) Biodiesel Production: A Review, Bioresource Technology, V70, N1, pp. 1 – 15.

[4] Prasad, Y.S. and Bakhshi (1986) Catalytic Conversion of Canola Oil to Fuels and Chemical Feedstocks Part I. Effect of Process Conditions on the Performance of HZSM-5 Catalyst, Canadian Journal of Chemical Engineering, V 64, pp. 278 – 284.

[5] Prasad, Y.S. and Bakhshi (1986) Catalytic Conversion of Canola Oil to Fuels and Chemical Feedstocks Part I. Effect of Co-feeding Steam on the Performance of HZSM-5 Catalyst, Canadian Journal of Chemical Engineering, V 64, pp. 285 – 292.

[6] Idem, R.O., Katikaneni, S.P.R., Bakhshi, N.N. (1997) Catalytic conversion of canola oil to fuels and chemicals: roles of catalyst, acidity, basicity, and shape selectivity on product distribution, Fuel Processing Tech. V51, pp. 101 – 125.

[7] Adjaye, J.D., Katikaneni, S.P.R., Bakhshi, N.N. (1996) Catalytic conversion of a biofuel to hydrocarbons: effect of mixtures of HZSM5 and silica-alumina catalysts on product distribution, Fuel Processing Tech. V48, pp. 115 – 143.

[8] Katikaneni, S.P.R., Adjaye, J.D., and Bakhshi, N.N. (1997) Conversion of Canola Oil to Various Hydrocarbons Over Pt/HZSM-5 Bifunctional Catalyst, Canadian Journal of Chemical Engineering, V 75, pp. 391 – 400.

[9] Katikaneni, S.P.R., Adjaye, J.D., and Bakhshi, N.N. (1995) Studies on the Catalytic Conversion of Canola Oil to Hydrocarbons: Influence of Hybrid Catalysts and Steam, Energy and Fuels, V 9, pp. 599 – 609.

[10] Leng, T.Y., Mohamed, A.R., and Bhatia, S. (1999) Catalytic Conversion of Palm Oil to Fuels and Chemicals, Canadian Journal of Chemical Engineering, V 77, N1, pp. 156 – 162.

[11] Ooi, Y.S., Farouq, T., Zakaria, R., Mohamed, A.R., and Bhatia, S. (2003) Biofuel Production from Catalytic Cracking of Palm Oil, Energy Sources, V 25, pp. 859 – 869.

[12] Twaiq, F.A., Zabidi, N.A.M., and Bhatia, S. (1999) Catalytic Conversion of Palm Oil to Hydrocarbons: Performance of Various Zeolite Catalysts, Industrial Engineering and Chemistry Research, V 38, pp. 3230 – 3237.

[13] Twaiq, F.A.A., Mohamad, A.R., and Bhatia, S. (2004) Performance of Composite Catalysts in Palm Oil Cracking for the Production of Liquid Fuels and Chemicals, Fuel Processing Technology, V 85, pp. 1283 – 1300.

[14] Ooi, Y.S., Zakaria, R., Mohamed, A.R., and Bhatia, S (2004) Hydrothermal Stability and Catalytic Activity of Mesoporous Aluminum-Containing SBA-15, Catalysis Communications, V 5, pp. 441 – 445.

[15] Ooi, Y.S., Zakaria, R., Mohamed, A.R., and Bhatia, S. (2005) Catalytic Conversion of Fatty Acids Mixture to Liquid Fuel and Chemicals Over Composite Microporous/Mesoporous Catalysts, Energy and Fuels, V 19, N 3, pp. 736 – 743.

[16] Twaiq, F.A., Zabidi, N.A.M., Mohamed, A.R., and Bhatia, S. (2003) Catalytic Conversion of Palm Oil Over Mesoporous Aluminosilicate, MCM-41 for the Production of Liquid Hydrocarbon Fuels, Fuel Processing Technology, V 84, pp. 105 – 120.

[17] Chen, N.Y., Degnan, T.J., and Smith, C.M. (1994) Molecular Transport and Reaction in Zeolites: Design and Application of Shape Selective Catalysts, Wiley-VCH.

[18] Chen, N.Y., Miale, J.N., and Reagan, W.J. (1978) Preparation of Zeolites. U.S. Patent # 4,112,056

[19] Wachter, W.A. () The Role of Next Nearest Neighbors in Zeolite Acidity and Activity, Theoretical Aspects of Heterogeneous Catalysis

[20] Gates, B. (1992) Catalytic Chemistry, Wiley and Sons.

[21] Derouane, E.G., Baltusis, L., Dessau, R.M., and Schmitt, K.D. (1985) Quantitation and Modification of Catalytic Sites In ZSM-5, Catalysis By Acids and Bases, pp. 135 – 146.

[22] Lunsford, J.H. (1990) Origin of Strong Acidity in Dealuminated Zeolite-Y, Fluid Catalytic Cracking II: Concepts in Catalyst Design, ACS Symposium Series, V 452, pp. 1 – 11.

[23] Derouane, E.G. (1985) Factors Affecting the Deactivation of Zeolites by Coking, Catalysis by Acids and Bases, Elsevier Science Publishers, pp. 221 – 240.

[24] Pachovsky, R.A., Best, D.A., and Wojciechowski, B.W. (1973) Applications of the Time-On-Stream Theory of Catalyst Decay, Industrial & Engineering Chemistry, Process Design and Development, V 12, N 3, pp. 254 – 261.

[25] Rollman, L.D. and Walsh, D.E. (1982) Constraints On Carbon Formation in Zeolite Catalysts, NATO Advanced Study Institutes Series, Series E: Applied Sciences, N 54, pp. 81 – 91.

[26] Wojciechowski, B.W. (1998) The Reaction Mechanism of Catalytic Cracking: Quantifying Activity, Selectivity, and Catalyst Decay, Catalysis Reviews – Science and Engineering, V 40, N 3, pp. 209 – 328.

[27] Olah, G.A., Prakash, G.K.S., and Sommer, J. (1985) Superacids, Wiley and Sons, New York.

[28] V. Kissin (2001) Chemical Mechanisms of Catalytic Cracking Over Solid Acidic Catalysts: Alkanes and Alkenes, Catalysis Reviews, V 43, N1 & 2, pp. 85 – 146.

[29] Y. Zhao, G.R. Bamwenda, W.A. Groten, B.W. Wojciechowski (1993) The Chain Mechanism in Catalytic Cracking – The Kinetics of 2-methylpentane Cracking, Journal of Catalysis, V 140, pp. 243 – 261.

[30] Buchanan, J.S., Santiesteban, J.G., and Haag, W.O. (1996) Mechanistic Considerations in Acid-Catalyzed Cracking of Olefins, Journal of Catalysis, V 158, pp. 279 – 287.

[31] Vedrine, J.C., Dejaifve, P., Garbowski, E.D., and Derouane, E.G. (1980) Aromatics Formation from Methanol and Light Olefins Conversion on H-ZSM-5 Zeolite: Mechanism and Intermediate Species, Catalysis By Zeolites, V, pp. 29 – 37.

[32] Benito, P.L., Gayubo, A.G., Aguayo, A.T., Olazar, M., and Bilbao, J. (1996) Effect of Si/Al Ratio and of Acidity of H-ZSM5 Zeolites o the Primary Products of Methanol to Gasoline Conversion, Journal of Chemical Technology and Biotechnology, V 66, pp. 183 – 191.

[33] Adjaye, J.D. and Bakhshi, N.N. (1995) Catalytic Conversion of a Biomass-Derived Oil to Fuels and Chemicals I: Model Compound Studies and Reaction Pathways, Biomass and Bioenergy, V 8, N 3, pp. 131 – 149.

[34] Chen, N.Y., Garwood, W.E., and Dwyer, F.G. (1989) Shape Selectivity Catalysis in Industrial Applications, Marcel Dekker, New York.

[35] Brown, W.H. (1995) Organic Chemistry, Saunders College Publishing, Fort Worth.

[36] Maki-Arvela, P, Kubickova, I., Snare, M., Eranen, K., and Murzin, D. (2007) Catalytic Deoxygenation of Fatty Acids and Their derivatives, Energy and Fuels, V 21, pp. 30 – 41.

[37] Kubickova, I., Snare, M., Eranen, K., Maki-Arvela, P., and Murzin, D. (2005) Hydrocarbons for Diesel Fuel via Decarboxylation of Vegetable Oils, Catalysis Today, V 106, pp. 197 – 200.

[38] Zhang, Z.C., Dery, M., Zhang, and Steichen, D. (2004) New Process for the Production of Branched-Chain Fatty Acids, Journal of Surfactants and Detergents, V 7, N3, pp. 211 – 215.

[39] Occelli, M.L. (1987) Recent Trends in Fluid Catalytic Cracking Technology, Fluid Catalytic Cracking: Role in Modern Refining, ACS Symposium Series V375, pp. 1 – 16.

[40] Otterstedt, J.E., Gevert, B., and sterte, J. (1987) Catalytic Cracking of Heavy Oils, Fluid Catalytic Cracking: Role in Modern Refining, ACS Symposium Series V375, pp. 266 – 278.

[41] Schipper, P.H., Dwyer, F.G., Sparrell, P.T., Mizrahi, S., and Herbst, J.A. (1987) Zeolite ZSM-5 in Fluid Catalytic Cracking: Performance, Benefits, and Applications, Fluid Catalytic Cracking: Role in Modern Refining, ACS Symposium Series V375, pp. 64 – 84.

[42] Kokotailo, G.T., Fyfe, C.A., Feng, Y., and Grondey, H. (1990) Characterization of Zeolite-Cracking Catalysts, Fluid Catalytic Cracking II: Concepts in Catalyst Design, ACS Symposium Series, V 452, pp. 27 – 44.

[43] Pappal, D.A. and Schipper, P.H. (1990) Increasing Motor Octanes by Using ZSM-5 in Catalytic Cracking: Riser Pilot Plant Gasoline Composition Analyses, Fluid Catalytic Cracking II: Concepts in Catalyst Design, ACS Symposium Series, V 452, pp. 45 – 55.

[44] Rawlence, D.J. and Dwyer, J. (1990) Modification of Fluid Catalytic Cracking Catalysis by the Addition of ZSM-5: Gasoline Over-Cracking Studies, Fluid Catalytic Cracking II: Concepts in Catalyst Design, ACS Symposium Series, V 452, pp. 56 – 78.

[45] Downard, K. (2004) Mass Spectrometry: A Foundation Course, Royal Society of Chemistry, Cambridge, UK.

[46] Harrison, A.G. (1992) Chemical Ionization Mass Spectrometry, 2nd Edition, CRC Press, Boca Raton, FL.

[47] Moneti, G., Pieraccini, G., Dani, F.R., Catinella, S., and Traldi, P. (1996) Acetonitrile as an Effective Reactant Species for Positive-ion Chemical Ionization of Hydrocarbons by Ion-Trap Mass Spectrometry, Rapid Communications in

Mass Spectrometry, V 10, pp. 167 – 170.

[48] Petris, G. Fornarini, S., Crestoni, M.E., Troiani, A., and Mayer, P.M. (2005) What Ion is Generated When Ionizing Acetonitrile?, Journal of Physical Chemistry A: Letters, V 109, pp. 4425 – 4427.

[49] March, R.E. (1997) An Introduction to Quadrupole Ion Trap Mass Spectrometry, Journal of Mass Spectrometry, V 32, pp. 351 – 369.

[50] March R.E. and Todd, J.F.J, (1995) Practical Aspects of Ion Trap Mass Spectrometry: Fundamentals of Ion Trap Mass Spectrometry, CRC press, V1.

[51] March R.E. and Todd, J.F.J, (1995) Practical Aspects of Ion Trap Mass Spectrometry: Chemical, Environmental, and Biomedical Applications, CRC press, V3.

[52] Wells, G. and Huston, C. (1995) Field-Modulated Selective Ion Storage in a Quadrupole Ion Trap, Journal of the American Society of Mass Spectrometry, V 6 pp. 928 – 935.

[53] Wells, G. and Huston, C. (1995) High-Resolution Selected Ion Monitoring in a Quadrupole Ion Trap Mass Spectrometer, Anal Chem 67(20) pp. 3650 – 3655.

[54] Guan, S. and Marshall, A.G. (1993) Stored Waveform Inverse Fourier Transform Axial Excitation/Ejection for Quadrupole Ion Trap Mass Spectrometry, Analytical Chemistry V65, N 9, pp. 1288 – 1294.

[55] Bowers, L.D. and Borts, D.J. (1997) Evaluation of Selected Ion Storage Ion-Trap Mass Spectrometry for Detecting Urinary Anabolic Agents, Clinical Chemistry V43, N 6, pp. 1033 – 1039.

[56] D. Firestone (1999) Physical and Chemical Characteristics of Oils, Fats, and Waxes, American Oil Chemists' Society, V67.

[57] Allen, C.A.W., Watts, K.C., Ackman, R.G., Pegg, M.J. (1999) Predicting the Viscosity of Biodiesel Fuels from Their Fatty Acid Ester Composition, Fuel, V78, pp. 1319 – 1326.

[58] Hussein, H.S., Mackie, R.I., Merchen, N.R., Baker, D.H., Parsons, C.M. (1996) Effects of Oleaginous Yeast on Growth Performance, Fatty Acid Composition of Muscles, and Energy Utilization by Poultry, Bioresource Technology, V55, pp. 125-130.

[59] Canakci, M.,Van Gerpen, J. (2001) Biodiesel Production from Oils and Fats with High Free Fatty Acids, Trans of the American Society of Agricultural Engineering, V 44, N 6, pp. 1429 – 1436.

[60] Dufreche, S., Hernandez, R., French, T., Sparks, D., Zappi, M., Alley, E. (2007) Extraction of Lipids from Municipal Wastewater Plant Microorganisms for Production of Biodiesel, Journal of the American Oil Chemists' Society, V84, N2, pp. 181 – 187.

[61] Christopher, R.A. (2005) Carborane acids. New "Strong Yet Gentle" Acids for Organic and Inorganic Chemistry, Chemical Communications Royal Society of Chemistry.

[62] Serrano, D.P., Aguado, J., Escola, J.M., Rodriquez, J.M., Miguel, S.G. (2005) An Investigation Into the Catalytic Cracking of LDPE Using Py-GC/MS, Journal of Analytical and Applied Pyrolysis, V 74, pp. 370 – 378.

[63] Buelna, G., Jarek, R.L., Thornberg, S.M., Nenoff, T.M. (2003) Real-Time Study on Cumene Formation Based on RGA/MS Analysis, Journal of Molecular Catalysis A: Chemical, V198, pp. 289 – 295.

[64] Borade, R.B., Hedge, S.G., Kulkarni, S.B., and Ratnasamy, P. (1984) Active Centers Over HZSM5 Zeolites for Paraffin Cracking, Applied Catalysis, V 13, pp. 27 – 38.

[65] Nayak,V.K. and Moffat, J.B. (1989) Catalytic Activity and Product Distribution In Cracking of n-Hexane Over Heteropoly Oxometalates and ZSM-5 Zeolite, Applied Catalysis, V47, N 1, pp. 97 – 113.

[66] Santilli, D.S. (1990) Mechanism of Hexane Cracking in ZSM-5, Applied Catalysis, V 60, 137 – 141.

[67] Babitz, S.M., Williams, B.A., Miller, J.T., Snurr, R.Q., Haag, W.O., and Kung, H.H. (1997) Monomolecular Cracking of n-Hexane on Y, MOR, and ZSM-5 Zeolites, Applied Catalysis A: General, V 179, pp. 71 – 86.

[68] Sadeghbeigi, R. (2000) Fluid Catalytic Cracking Handbook: Design, Operation, and Troubleshooting of FCC Facilities,Gulf Publishing Co., Houston, TX.

[69] Dean, J.A. (1992) Lange's Handbook of Chemistry,14th Ed., McGraw Hill, New York.

[70] Perry, R.H. and Green, D.W. (1997) Perry's Chemical Engineers' Handbook, McGraw Hill, New York.

[71] Olson, D.H. and Haag, W.O. (1984) Structure-Selectivity in Xylene Isomerization and Selective Toluene Disproportionation, Catalytic Materials: Relationship Between Structure and Reactivity, pp. 275 – 307.

[72] Hilt, G. and Galbiati, F. (2006) Rhodium- or Copper-Catalyzed CH-Insertion of Carbenoids into Dihydro-aromatic Compounds and Acyclic 1,4-dienes,

Synthesis, V 21, pp. 3589 – 3596.

[73] Isaquliants, G.V., Gitis, K.M., Kondratjev, D.A., and Minachev, K.M. (1984) On the Formation of Hydrocarbon Chains in the Aromatization of Aliphatic Olefins and Dienes Over High-Silica Zeolites, Studies in Surface Science and Catalysis, pp. 225 – 232.

APPENDIX A

RAW DATA FOR HETEROGENEOUS CATALYSIS USING QUATRA C

Table A.1. Cracking of Oleic Acid on H-ZSM-5 (cat/oil=5)

Product	Area Count (Run #1)	Area Count (Run#2)	Average, ug Product/ mg reactant	St. Dev.
Methane	357691	637808	1.77	0.133
Ethylene	268220	583477	1.48	0.317
Ethane	907971	1152612	3.81	0.625
Propylene	3694781	5466358	16.64	0.941
Propane	4449945	7216780	20.97	0.176
C4 olefin	4180177	7529555	20.79	1.716
C4 paraffin	1677905	2316097	7.31	0.771
C5 olefin	1813647	2640672	8.11	0.550
C5 paraffin	856903	1566383	4.30	0.399
C6 olefin	932522	1251041	4.01	0.503
Benzene	857386	1561909	3.47	0.314
Toluene	2881034	5703313	10.09	1.502
Propenylbenzene	2490791	4377661	9.43	0.614
Xylenes	419666	648859	1.31	0.033
Phenylbutene	1923335	2272260	6.03	1.290
Ethyltoluene	696585	877718	2.04	0.345
Trimethylbenzene	925011	1468247	17.07	0.116
Naphthalene	75831	95960	1.26	0.209
Methylnaphthalene	297103	362416	13.83	2.652
Dimethylnaphthalene	427343	624620	4.66	0.303

Table A.2. Cracking of Oleic Acid on H-ZSM-5 (cat/oil=10)

Product	Area Count (Run #1)	Area Count (Run#2)	Average, ug Product/ mg reactant	St. Dev.
Methane	762458	748269	3.54	0.047
Ethylene	565002	552145	2.62	0.043
Ethane	887679	1055122	4.55	0.555
Propylene	6261430	5328538	27.14	3.090
Propane	8221779	7545160	36.93	2.241
C4 olefin	9418453	8554069	42.09	2.863
C4 paraffin	1283407	1786066	7.19	1.665
C5 olefin	1490210	1156400	6.20	1.106
C5 paraffin	2120610	1900648	9.42	0.729
C6 olefin	931468	975327	4.47	0.145
Benzene	2160472	1804488	7.51	0.953
Toluene	7018279	6269687	20.83	1.659
Propenylbenzene	958996	674589	2.95	0.726
Xylenes	829801	547492	2.19	0.636
Phenylbutene	1741811	1873575	6.53	0.336
Ethylbenzene	150340	200723	0.66	0.135
Ethyltoluene	397964	292172	1.13	0.245
Trimethylbenzene	4659214	4388578	83.87	3.548
Naphthalene	1565878	1448317	27.94	1.541
Methylnaphthalene	453678	411674	22.87	1.570
Dimethylnaphthalene	776379	731969	8.60	0.358

Table A.3. Cracking of Oleic Acid on H-ZSM-5 (cat/oil=20)

Product	Area Count (Run #1)	Area Count (Run#2)	Average, ug Product/ mg reactant	St. Dev.
Methane	1092678	1072029	5.07	0.0684
Ethylene	892901	788528	3.94	0.3457
Ethane	2076018	2125138	9.84	0.1627
Propylene	8005451	7676293	36.73	1.0902
Propane	12510555	9496855	51.54	9.9821
C4 olefin	13851119	12175252	60.96	5.5509
C4 paraffin	2014667	2165831	9.79	0.5007
C5 olefin	1534288	1412898	6.90	0.4021
C5 paraffin	3086812	2646203	13.43	1.4594
C6 olefin	1228915	1008881	5.24	0.7288
Benzene	3123921	3098518	11.78	0.0680
Toluene	9527766	9768167	30.24	0.5329
Propenylbenzene	751565	679381	2.58	0.1843
Xylenes	2365283	2453226	7.67	0.1980
Phenylbutene	582547	541501	2.03	0.1048
Ethylbenzene	140771	178340	0.60	0.1006
Ethyltoluene	765123	899943	2.73	0.3126
Trimethylbenzene	6319328	6339292	117.34	0.2617
Naphthalene	2059924	2101001	38.57	0.5385
Methylnaphthalene	565460	607305	30.99	1.5636
Dimethylnaphthalene	397664	408588	4.60	0.0881

Table A.4. Cracking of Monoolein on H-ZSM-5 (cat/oil=5)

Product	Area Count (Run #1)	Area Count (Run#2)	Average, ug Product/ mg reactant	St. Dev.
Ethane	2375955	4054479	12.41	0.978
Propylene	821593	1125124	3.84	0.294
Propane	2859832	2106172	11.98	2.995
C4 olefin	1231814	2139673	6.49	0.593
C4 paraffin	506195	793919	2.53	0.049
C5 olefin	141905	251766	0.76	0.080
Benzene	1813211	2723201	7.17	0.082
Toluene	1805585	3173125	6.41	0.638
Ethylbenzene	184418	324936	0.75	0.077
Xylenes	32156	72860	0.13	0.037
Trimethylbenzene	49731	95728	0.21	0.035
Ethyltoluene	167585	289515	0.62	0.054
Phenylbutene	108088	129821	1.88	0.318
Propenylbenzene	313465	805371	8.21	2.956
Naphthalene	148479	108521	0.44	0.218

Table A.5. Cracking of Monoolein on H-ZSM-5 (cat/oil=10)

Product	Area Count (Run #1)	Area Count (Run#2)	Average, ug Product/ mg reactant	St. Dev.
Ethane	5559346	3054430	16.944	3.728
Propylene	418978	781929	2.175	0.819
Propane	464663	867712	2.413	0.910
C4 olefin	155270	175037	0.604	0.018
C4 paraffin	181224	170609	0.646	0.063
C5 olefin	166773	125567	0.539	0.136
Benzene	1275300	692032	2.949	1.383
Toluene	249310	110119	0.447	0.266
Ethylbenzene	69771	26989	0.139	0.093
Xylenes	189567	87642	0.350	0.199
Trimethylbenzene	244696	199715	0.630	0.125
Ethyltoluene	155698	117170	0.352	0.089
Phenylbutene	85196	53055	1.012	0.385
Propenylbenzene	997219	446742	4.992	1.746
Naphthalene	58441	57212	0.171	0.012
Methylnaphthalene	61013	44822	2.201	0.594

Table A.6. Cracking of Monoolein on H-ZSM-5 (cat/oil=20)

Product	Area Count (Run #1)	Area Count (Run#2)	Average, ug Product/ mg reactant	St. Dev.
CO	142669	239334	2.2	0.516
CO2	142031	174941	8.2	0.808
Ethane	2662835	5173760	14.7	2.991
Propylene	2063312	1958530	8.1	2.398
Propane	966802	1412254	4.6	0.014
C4 olefin	281338	580936	1.6	0.395
C4 paraffin	200940	477418	1.3	0.426
C5 olefin	107246	123617	0.5	0.074
Benzene	1694388	3697733	8.1	2.294
Toluene	1075080	3103232	5.1	2.370
Ethylbenzene	205909	356136	0.8	0.100
Xylenes	50908	230063	0.3	0.244
Trimethylbenzene	32155	230188	0.3	0.325
Ethyltoluene	165336	114808	0.4	0.202
Phenylbutene	21144	173647	1.3	1.301
Propenylbenzene	161549	527676	4.9	2.665
Naphthalene	87470	455531	0.8	0.611
Methylnaphthalene	43322	176946	4.4	2.957

Table A.7. Cracking of Diolein on H-ZSM-5 (cat/oil=5)

Product	Area Count (Run #1)	Area Count (Run#2)	Average, ug Product/ mg reactant	St. Dev.
CO	150334	193960	2.19	0.547
CO2	1028407	583297	17.56	3.135
Ethylene	2757000	2821967	12.85	1.102
Ethane	4862283	4984650	22.68	1.970
Propylene	8220995	8455879	38.41	3.426
Propane	4252853	4376296	19.88	1.779
C4 olefin	1769931	1898120	8.46	1.003
C4 paraffin	1463409	1530791	6.90	0.697
C5 olefin	1603687	1723462	7.67	0.921
Benzene	4633832	4725487	17.43	1.449
Toluene	4053643	4122938	12.60	1.024
Ethylbenzene	299183	314468	1.09	0.114
Xylenes	198529	216100	0.65	0.084
Trimethylbenzene	108494	129990	0.42	0.083
Ethyltoluene	324928	358023	1.10	0.152
Phenylbutene	247334	256149	4.59	0.432
Propenylbenzene	1713045	1756638	31.63	2.753
Naphthalene	184938	345831	1.00	0.492

Table A.8. Cracking of Diolein on H-ZSM-5 (cat/oil=10)

Product	Area Count (Run #1)	Area Count (Run#2)	Average, ug Product/ mg reactant	St. Dev.
CO2	595805	694736	13.32	3.743
Ethylene	4172165	3426858	14.72	1.219
Ethane	6723216	5727890	24.19	2.626
Propylene	11617454	11424250	45.27	9.447
Propane	5310360	4596821	19.27	2.308
C4 olefin	2028787	1814568	7.50	1.069
C4 paraffin	1868929	1566379	6.67	0.647
C5 olefin	1736114	1563346	6.44	0.949
Benzene	7153689	6184007	20.98	2.492
Toluene	5471946	4739784	13.30	1.598
Ethylbenzene	1644717	263890	2.57	2.324
Xylenes	266302	247021	0.68	0.115
Trimethylbenzene		129045	0.45	
Ethyltoluene	413459	405674	1.13	0.233
Phenylbutene	336201	318087	5.07	0.923
Propenylbenzene	1644717	1507979	24.38	3.901
Naphthalene	243084	111991	0.53	0.171

Table A.9. Cracking of Diolein on H-ZSM-5 (cat/oil=20)

Product	Area Count (Run #1)	Area Count (Run#2)	Average, ug Product/ mg reactant	St. Dev.
CO	304972	252807	3.50	0.585
CO2	1033191	1152400	21.31	0.421
Ethylene	6111974	6305723	28.11	0.340
Ethane	10336863	9355501	44.64	4.666
Propylene	5898579	6809343	28.72	1.933
Propane	10129691	9591371	44.68	3.249
C4 olefin	1575414	1818872	7.67	0.517
C4 paraffin	1280434	1539934	6.37	0.613
C5 olefin	1905109	1483180	7.69	1.613
Benzene	11985410	12737442	45.23	0.401
Toluene	7484981	8144234	23.66	0.604
Ethylbenzene	479036	502821	1.71	0.0002
Xylenes	627671	781801	2.16	0.261
Trimethylbenzene	306541	351967	1.15	0.073
Ethyltoluene	348755	505152	1.35	0.304
Phenylbutene	908982	935976	16.53	0.223
Propenylbenzene	1218743	1201330	21.69	0.961
Naphthalene	834404	305520	2.11	1.441
Methylnaphthalene	263497	332922	15.19	1.988

Table A.10. Cracking of Triolein on H-ZSM-5 (cat/oil=5)

Product	Area Count (Run #1)	Area Count (Run#2)	Average, ug Product/ mg reactant	St. Dev.
Ethylene	1178831	1226804	5.50	1.777
Ethane	1279787	950415	4.92	0.443
Propylene	6032999	6409892	28.53	9.606
Propane	2485585	2748698	12.05	4.378
C4 olefin	1070398	1239256	5.34	2.102
C4 paraffin	739485	866520	3.72	1.492
C5 olefin	1004438	1135137	4.94	1.864
Benzene	1945236	2080257	7.47	2.547
Toluene	1725371	1895386	5.58	2.001
Trimethylbenzene	79494	91733	0.31	0.119
Ethyltoluene	88001	100557	0.30	0.117
Phenylbutene	93149	104892	1.81	0.678
Propenylbenzene	748531	850105	14.61	5.563

Table A.11. Cracking of Triolein on H-ZSM-5 (cat/oil=10)

Product	Area Count (Run #1)	Area Count (Run#2)	Average, ug Product/ mg reactant	St. Dev.
Ethylene	4043115	3691386	15.50	2.785
Ethane	5150341	4023825	18.14	1.277
Propylene	11402583	10470687	43.85	8.055
Propane	5615070	5497773	22.40	5.109
C4 olefin	2228650	1931107	8.30	1.188
C4 paraffin	2020150	1679171	7.35	0.839
C5 olefin	1671392	1520874	6.39	1.134
Benzene	6353028	5232232	18.60	2.001
Toluene	4426656	4182135	11.58	2.355
Ethylbenzene	310354	226773	0.81	0.019
Xylenes	1092292	962764	2.79	0.433
Trimethylbenzene	204878	189747	0.61	0.116
Ethyltoluene	202080	180325	0.54	0.088
Phenylbutene	242112	167996	3.18	0.043
Propenylbenzene	247647	188785	3.41	0.181
Naphthalene	263939	218622	0.78	0.087
Methylnaphthalene	133668	138416	6.22	1.657

Table A.12. Cracking of Triolein on H-ZSM-5 (cat/oil=20)

Product	Area Count (Run #1)	Area Count (Run#2)	Average, ug Product/ mg reactant	St. Dev.
CO	38899	29190	0.38	0.021
CO2	143193	155057	8.27	1.469
Ethylene	3647318	3706451	16.26	2.855
Ethane	4784452	4091348	19.42	1.059
Propylene	16220848	11532671	69.77	8.787
Propane	5514410	4355243	21.50	0.036
C4 olefin	2065514	1721252	8.27	0.300
C4 paraffin	2057797	1467435	7.63	0.564
C5 olefin	1615690	1478641	6.80	0.696
Benzene	7362681	5616761	22.82	0.598
Toluene	5121069	3953226	13.21	0.236
Ethylbenzene	913579	958347	3.20	0.632
Xylenes	232865	202719	0.65	0.044
Trimethylbenzene	178671	208172	0.66	0.179
Ethyltoluene	76346	79465	0.24	0.046
Phenylbutene	232272	180629	3.56	0.045
Propenylbenzene	294913	259368	4.81	0.357
Naphthalene	292345	277069	1.01	0.129
Methylnaphthalene	145951	167022	7.86	2.025

Table A.13. Cracking of Triolein on Faujasite (cat/oil=20)

Product	Area Count (Run #1)	Area Count (Run#2)	Average, ug Product/ mg reactant	St. Dev.
CO	63156	50292	0.76	0.0060
CO2	600394	180416	12.95	2.4495
Methane	25170	27770	0.14	0.0312
Ethylene	218933	131579	0.87	0.1725
Ethane	4612527	4113328	22.24	1.7822
Propylene	2622288	2399248	12.82	1.2587
Propane	5287657	3850771	23.02	1.4494
C4 olefin	1141732	1267003	6.22	1.4463
C4 paraffin	429174	299943	1.83	0.1686
C5 olefin	5107165	4060704	23.21	0.0210
C6 olefin	5510712	3644947	22.94	2.9981
C6 Paraffin	1540339	1018264	6.41	0.8403
C7 Olefin	3362924	3348191	17.21	2.7100
Benzene	907965	768641	3.44	0.1496
Toluene	2038743	1689755	6.33	0.1802
Ethylbenzene	571603	538283	2.19	0.2591
Xylenes	181623	141887	0.56	0.0074
Trimethylbenzene	822578	844243	3.30	0.5895
Ethyltoluene	92257	84983	0.32	0.0326
Phenylbutene	627445	677302	13.30	2.8421
Propenylbenzene	768612	637882	14.13	0.4153
Naphthalene	140810	107616	0.51	0.0147
Methylnaphthalene	739128	853300	46.46	12.0701
Dimethylnaphthalene	431692	494322	5.83	1.4810
Trimethylnaphthalene	250364	292644	3.42	0.9175

Table A.14. Cracking of Triolein on Silica-Alumina (cat/oil=20)

Product	Area Count (Run #1)	Area Count (Run#2)	Average, ug Product/ mg reactant	St. Dev.
Ethane	6300757	6255107	30.03	1.146
Propylene	3677204	3415945	16.95	0.149
Propane	4970846	4406792	22.39	0.937
C4 olefin	1294209	1113591	5.75	0.362
C4 paraffin	951747	831353	4.26	0.223
C5 olefin	310565	254049	1.35	0.133
C5 paraffin	1213479	1143566	5.63	0.008
Hexadiene	5432605	5317412	46.57	1.311
Heptadiene	3289783	3820529	40.98	6.086
Octadiene	2457831	1991732	28.89	3.039
Nonadiene	2206541	1899519	29.49	1.846
Phenylbutene	213941	270975	4.61	0.962
Propenylbenzene	183303	176145	3.40	0.051
Methylnaphthalene	306837	301761	16.42	0.517
Dimethylnaphthalene	306535	270951	3.36	0.147
Trimethylnaphthalene	126788	172375	1.75	0.451
TetraMethylnaphthalene	346966	129386	2.73	1.671

Table A.15. Calibration of Compounds from Standards.

Compound Name	Calibration Formula		
	y =	m	b
Propene	y =	213483.2	0
Propane	y =	213483.2	0
Butane	y =	213483.2	0
Pentane	y =	213483.2	0
3-methylpentane	y =	226000.0	0
Benzene	y =	99000.0	0
Trimethylpentane	y =	140000.0	0
Toluene	y =	119625.0	0
Ethylbenzene	y =	138500.0	0
m-xylene	y =	157000.0	0
o-xylene	y =	152500.0	0
Trimethylbenzene	y =	138500.0	0
Naphthalene	y =	132000.0	0
2-ethyltoluene	y =	10788.0	93208
Propenylbenzene/Phenylbutene	y =	26971.0	0
Methylnaphthalene	y =	9462.0	0
Dimethylnaphthalene	y =	43859.0	0
Hexadiene	y =	117840.0	0
Heptadiene	y =	8811	0
Octadiene	y =	78403	0
Nonadiene	y =	70950	0
CO	y =	76549.0	2692
CO2	y =	70903.0	-471643